ON THE BUCKLING AND VIBRATION BEHAVIOR OF A THIN TENSIONED SHEET WITH AN ELLIPTICAL HOLE

A THESIS

Presented to

The Faculty of the Division of Graduate

Studies and Research

by

Prosun Kumar Datta

In Partial Fulfillment

of the Requirements for the Degree

Doctor of Philosophy

in the School of Aerospace Engineering

Georgia Institute of Technology

June, 1972

In presenting the dissertation as a partial fulfillment of the requirements for an advanced degree from the Georgia Institute of Technology, I agree that the Library of the Institute shall make it available for inspection and circulation in accordance with its regulations governing materials of this type. I agree that permission to copy from, or to publish from, this dissertation may be granted by the professor under whose direction it was written, or, in his absence, by the Dean of the Graduate Division when such copying or publication is solely for scholarly purposes and does not involve potential financial gain. It is understood that any copying from, or publication of, this dissertation which involves potential financial gain will not be allowed without written permission.

7/25/68

ON THE BUCKLING AND VIBRATION BEHAVIOR OF A
THIN TENSIONED SHEET WITH AN ELLIPTICAL HOLE

Approved:

Chairman

Date approved by Chairman: April 24, 1972

ACKNOWLEDGMENT

I wish to express my sincere appreciation to Dr. Robert L. Carlson, my thesis advisor, for his advice, interest and encouragement during the course of this research work. It was through his guidance and our many hours of discussion that led to the successful completion of this work. His guidance throughout my graduate academic career has been invaluable and is greatly appreciated.

I would also like to thank the other members of my reading committee, Dr. C. V. Smith, Dr. G. A. Pierce, Dr. J.T.S. Wang and Dr. D. J. McGill for their constructive criticism, scrutiny and suggestions during the course of this work. My fellow graduate students also contributed with a helping hand or a responsive mind to this work.

This work has been supported by the U. S. Army Research Office-Durham under Contract No. DAHC04 68C 0004.

To Mrs. Ruth Shaw, I express my deepest appreciation for her patience and skill in typing the final manuscript.

Finally, I am grateful to my parents. Their love and encouragement beyond all else are responsible for my academic career and the successful completion of this work.

TABLE OF CONTENTS

LIST OF TABLES

LIST OF FIGURES

Figure | Page

NOMENCLATURE

A	Lamé parameter
A_{MN}	coefficients in the deflection function
a	semi-major axis of the ellipse
a_i	coefficients in the space function f(x)
B	Lamé parameter
b	semi-minor axis of the ellipse
D	plate bending rigidity
E	Young's modulus
F	Airy's stress function
$F(\alpha,\beta)$	a function of α and β
$f(x)$	a function of x
$f_i(\xi)$	a function of ξ
$g_j(\eta)$	a function of η
H	slot half length
2 h	distance between the foci of the elliptic hole
i	indicial integer in the deflection function
j	indicial integer in the deflection function
k	dimensionless proportionality factor
K_α	local curvature of the deflected surface in α-direction
K_β	local curvature of the deflected surface in β-direction
$K_{\alpha\beta}$	torsion of the surface

L	crack length
$L(w_{MN})$	operator on the quantity w_{MN}
ℓ	direction cosine, $\cos(x,n)$
M	indicial integer in the deflection function
M_α	bending moment per unit length along constant β curves
M_β	bending moment per unit length along constant α curves
$M_{\alpha\beta}$	twisting moment per unit length
m	direction cosine, $\cos(y,n)$
N	indicial integer in the deflection function
N_x	in-plane force per unit lengh in x-direction
N_y	in-plane force per unit length in y-direction
N_{xy}	shear force per unit length
N_α	in-plane force per unit length in α-direction
N_β	in-plane force per unit length in β-direction
$N_{\alpha\beta}$	shear force per unit length
n	normal to the edge of a prismatic element
P	applied tensile stress at the infinity
P_1	smallest buckling load
q	transverse force per unit area
R	slot end radius
S	shear stress component on edge of a prismatic element
t	sheet thickness
$W(\xi,\eta,\tau)$	deflection function which is the function of space variables and time

$\ddot{W}$	differentiation of W twice with respect to time
w	displacement function in z-direction
$w_{MN}(\alpha,\beta)$	a deflection function which is function of space variables α, β
x	Cartesian coordinate
$\bar{X}$	x-direction component of stress acting on edge of a prismatic element
x'	transformed Cartesian coordinate
y	Cartesian coordinate
$\bar{Y}$	y-direction component of stress acting on edge of a prismatic element
y'	transformed Cartesian coordinate
z	coordinate direction normal to x, y plane
z_1	lower limit of integration on z
z_2	upper limit of integration on z
α	curvilinear coordinate
α_1	lower limit of integration on α
α_2	upper limit of integration of α
β	curvilinear coordinate
β_1	lower limit of integration on β
β_2	upper limit of integration on β
ξ	elliptic coordinate
ξ_0	value of ξ on the boundary of an elliptic hole
ξ_1	lower limit of integration on ξ
ξ_2	upper limit of integration on ξ

η	elliptic coordinate
η_1	lower limit of integration on η
η_2	upper limit of integration on η
θ	angle between tangent to ξ-curve and the x-axis
γ	angle between the direction of the tension applied at infinity with the major axis of the elliptic hole
ρ	mass density of the plate
ν	Poisson's ratio
ω	natural frequency of vibration
τ	time
$\psi(z)$	complex potential function
$\chi(z)$	complex potential function
Φ	complex number
$\varphi_i(x)$	set of functions in the function space
$\varphi_{ij}(\alpha,\beta)$	space function which is function of space variables, α,β
λ	nondimensional load parameter
Ω	nondimensional frequency parameter
δ	variation
σ	normal stress component on edge of a prismatic element
σ_x	midsurface normal stress in x-direction
σ_y	midsurface normal stress in y-direction
σ_{xy}	midsurface shearing stress
$\sigma_{x'}$	midsurface normal stress in x'-direction

$\sigma_{y'}$	midsurface normal stress in y'-direction
$\sigma_{x'y'}$	midsurface shear stress
σ_{α}	midsurface normal stress in α-direction
σ_{β}	midsurface normal stress in β-direction
$\sigma_{\alpha\beta}$	midsurface shearing stress
σ_{b}	critical applied traction stress for a cracked specimen
σ_{cr}	critical applied tensile stress for a slotted specimen
$\Delta\epsilon$	twice the bending strain
$\partial/\partial x$	$(\ )_{,x}$ partial differentiation with respect to independent variable x

SUMMARY

The out-of-plane deflection which can be developed in a thin, tensioned sheet containing a central opening is discussed. It is noted that this behavior is of practical importance because it can alter the stress concentration and fatigue properties.

The results of an experimental and analytical study of the buckling and vibration behavior of tensioned sheets with an elliptical opening are presented. Data from buckling and vibration experiments for several opening shapes ranging between a crack and a circle are presented. A generalized Galerkin method for solving the governing differential equations is used and the results obtained are presented in terms of buckling loads and natural frequencies.

The experimental buckling stress estimates correlate well with the analytical results. The data from the vibration experiments indicate that the load vs frequency behavior is dependent on the size of the test specimen and the opening shape. The analytical results display a load vs frequency behavior which is experimentally observed for a narrow elliptical hole; i.e., for a small value of the ratio of minor axis to major axis. Some features of the analytical and experimental vibration results differ substantially however. The analysis indicates that the frequency decreases to zero as the applied load approaches the buckling load. The experimental results do not exhibit this behavior. The sources of this difference in behavior are discussed.

CHAPTER I

INTRODUCTION

The Cutout Problem in Structural Elements

For thousands of years man has built structures which included openings in the walls. Usually, his designs made use of previous experience and included an amount of reinforcement necessary to ensure the integrity of the building or vehicle for what were considered to be reasonable service conditions. Under these circumstances the design problems were not difficult and the need for optimum solutions was not particularly urgent.

With the advent of flight vehicles with skins which were made from thin sheet, monocoque or semi-monocoque construction, the need for the development of design procedures which allowed for the incorporation of openings in both a safe and an efficient manner became apparent. The consequences of failure to solve the indicated design problem could not be ignored.

If the opening or cutout problem is extended to include both those present by design and those incurred by accident, it is found that a variety of modes of static and dynamic behavior are possible. The responses which may be observed are of interest not just as peculiar occurrences in a particular type of structure, but as events which can lead to a failure in the structure.

The mode of static behavior which is of interest in this investigation is buckling. The occurrence of buckling introduces a distortion of the surface of the element and results in a change in the stress distribution. Both of these possibilities can have undesirable effects on the performance of the vehicle of which the element is a part.

The dynamic behavior studied here involves the effect of initial stress on transverse vibration properties of sheet elements with openings. In the extreme case of a crack, the presence of excitation at a resonant frequency can lead to crack propagation. For other opening shapes the cyclic character of vibration can be expected to nucleate cracks at stress concentration sites. These nucleated cracks can then introduce crack propagation problems.

In the sections that follow a brief review of work related to the subject problem will be presented. Both the static problem and the dynamic problem will be discussed.

The Static Problem

The importance of cutout problems in structures, particularly in flight vehicles, has been mentioned in the previous section. In these types of structures the skin carries all or some of the in-plane loads as well as pressure type loads. Failures in these structures are often caused by the development of fatigue cracks which propagate from a cutout or some other form of discontinuity.

In this section the buckling behavior of loaded sheets with cutouts will be discussed. When a thin sheet containing a central opening is subjected to a unidirectional tensile load, a region adjacent to the internal free edge perpendicular to the direction of loading is in compression. The presence of this compressive zone may create the necessity for considering the possibility of buckling at some critical value of load.

One extreme of a cutout is a crack. Buckling of the cracked sheet under tensile loading is of considerable interest to structural engineers. In a cyclic load environment a crack which is initially very short can increase in length through crack propagation until a point is reached where buckling of the free edge can develop. If buckling does occur, the crack propagation behavior can be expected to be modified.

The result of a semi-empirical analysis of the associated buckling problem has been used by a number of workers [1-6]. The buckling load has been expressed as

$$\sigma_b = kE\left(\frac{t}{L}\right)^2$$

where σ_b is the applied traction stress necessary to cause buckling, E is Young's modulus, t is the sheet thickness, and L is the crack length. A value of k of about 10 has been suggested by Mansfield [1]. Experimentally, k has been observed to vary from about 2 to about 7 [5]. The value of k appears to depend on material properties, the model geometry (specimen width, etc.) and very likely the manner in which the critical stress was defined in each experimental investigation.

A precise specification of the stress at which buckling takes place has been avoided in most of the work that has been published. Dixon and Strannigan [2] have studied the problem of a sheet with a tensile load applied perpendicular to the crack direction and have chosen to select an upper and lower bound for buckling from plots of average stress versus bending strain at the buckled edge. These bounds can differ substantially in magnitude.

Analytically, it is quite difficult to predict the actual buckling load. Some of the difficulties which are encountered in an analysis of the problem are: (1) a nonuniform prebuckle elastic-plastic stress state, and (2) an undefined boundary of the buckled region. Up to the present time, the only mathematical treatment of the cracked sheet problem is due to P. G. Cherepanov [3,4]. Cherepanov's solution was for a membrane (that is, a plate with zero flexural regidity) however, so he did not actually treat the buckling problem. Concerning a finite flexural rigidity Cherepanov comments, ". . . the problem of buckling for a plate with a finite fluxural rigidity at this time presents apparently insurmountable difficulties of a mathematical and even more fundamental nature." By limiting his analysis to a membrane, Cherepanov was able to obtain a solution that described the boundary of a "buckled" region. The buckled region in this case is developed by the requirement that a membrane cannot support a compressive stress. He was able to obtain a result in closed form for his model.

Recently, Carlson, et al., [5] obtained buckling loads for the cracked sheet experimentally using an extension of the Southwell method.

The problem of incipient buckling of cracked plates which are loaded in uniaxial tension has been the subject of several other studies [2,6,7] and these have been reviewed in Reference 5.

Zielsdorff [8] in his Ph.D. dissertation considered the problem of the buckling of cutouts in a tensioned sheet. The cutout considered in his investigation was defined as the slot which is constructed by putting semi-circular ends on a rectangle. Based on his experimental results he developed an empirical expression for the static buckling stress of cutouts in a tensioned field.

The objective of the present work is to determine analytically the buckling stress of a tensioned sheet with an elliptic hole and then to confirm that result experimentally on selected specimens. By varying the semi-major and semi-minor axes, this problem covers the shapes which range between a circle and the crack. This opening shape is easier to analyze than the shape considered by Zielsdorff. The elliptic coordinate system which is the natural system of the elliptic hole can be used to obtain a solution to the buckling problem. To obtain the static stress distribution Zielsdorff used a truncated infinite series for the mapping function of the hole. The accuracy depends on the number of terms in the series. In the case of an elliptic hole, the mapping function is exact and relatively simple. Hence, the stress distribution in the field can be obtained more simply and more accurately.

The Dynamic Problem

The existence of a compressive zone adjacent to the free edge of the opening of a tensioned sheet has been discussed in the previous section. The presence of this compressive zone can also be expected to have an effect on the character of the modes of vibration. An additional aim of this investigation is to study this effect. As noted earlier, one important case of the cutout shape is the crack and the practical importance of this problem cannot be questioned.

A number of dynamic effects are important. Among them are the dynamic effects associated with the crack propagation. Another important dynamic problem is the associated vibration behavior of the structural element having initial stress. As these two problems are directly associated with the importance of the present research, it is appropriate to review briefly the research progress in the literature.

The effects which are noted here primarily focus on the propagation phase of the crack extension. When the stress becomes sufficiently large at the tip of a crack, the crack propagates and the propagation depends on the material properties and the nature of the stress field around the crack. If the rate of flow of available energy at the crack tip is sufficient for the formation of the new crack surface and associated plastic work, the crack can extend without any change in external conditions. The energy absorption rate for a given material is defined as its fracture toughness.

The analyses of moving cracks have mainly been centered on two crack models: (1) a crack of constant length traversing with a constant speed in a uniform stress field, (2) a crack whose length is symmetrically increasing with constant speed, or a semi-infinite crack extending with constant speed.

Natural cracks are of the second type. Griffith [9] in his static analysis of crack extension used the surface energy of the material as a basis for his determination of the maximum stable crack length. Yoffe [10] solved a dynamic steady state problem in which a crack of fixed length moves at constant speed through a stretched elastic sheet. She found that for higher crack speeds the stress field near the tip might lead to a branching of the crack.

Another steady state problem, one in which a semi-infinite crack extends at constant speed through an elastic sheet, was solved by Craggs [11]. Several criteria, including those of Griffith and Yoffe, were used by Craggs in seeking an upper bound for the crack speed.

Problems referred to above are steady state in character. A transient problem in which a semi-infinite crack suddenly appears in a stretched elastic plate has been solved by Maue [12]. This problem has also been discussed by Ang [13] and by Baker [14].

A review of the analyses made of dynamic effects indicates that it has been necessary, because of the difficulty of the problem, to adopt relatively simple crack extension models. It is not clear at this time to what extent these models possess features and properties of real cracks. Thorough comparisons of analytical results with experimental results have yet to be made, and this is an area in which more work needs to be done. With reference to experimental work, it may be noted that Wells and Post [15] have made a dynamic, photoelastic analysis of a moving crack. Photoelastic material properties differ substantially, however, from metals.

The dynamic effects described in the preceding section were associated with the motion accompanying crack extension. Other important dynamic effects are possible. For example, induced, transverse vibration of the crack edge surfaces can be expected to influence the character of crack extension. Under a static in-plane load, the occurrence of such oscillations introduces a fatigue type environment at the crack tip. The response characteristics of such behavior may be described as the vibration behavior of structural elements with initial stress.

The vibration behavior of structures with initial stress has been studied by a number of investigators. Saint Venant [16] studied the influence of initial stress on the vibration behavior of beams and plates. M. A. Biot [17] and Goodier [18] discussed the effect of initial axial stress on torsional vibration. Biot [19] later studied the influence of initial stress on elastic wave propagation. In the latter studies Biot and Goodier derived equations of motion for bodies under initial stress by linearizing non-linear equations of motion.

In the last decade, a number of papers have been published on the effect of initial stress on vibration characteristics [16-30]. Among those who have made recent contributions, the work of G. Herrmann is quite extensive. Herrmann has presented results both on the derivation of the governing equations and on solutions to specific problems.

The dynamic problem of interest in the present investigation involves tensioned sheets with cutouts. A review of the literature reveals that some studies of this type have been made by Clarkson and his co-workers [31-40]. They investigated the dynamic behavior of cracked plates subjected to a tensile load. The driving force used to induce oscillations in these studies was noise generated by a siren. It is appropriate to give a summary of the related work done by Clarkson and his co-workers on the propagation of fatigue cracks in a tensioned plate subjected to acoustic loads. To study this type of effect, they conducted experiments on a simple sheet model in which a crack had already been initiated. In this environment the crack propagated in a direction normal to the tensile stress.

The natural frequency of vibration in Clarkson's work was found to depend on the overall tension of the plate and on the crack length. Since the rate of crack propagation was expected to depend on the vibration characteristics of the plate, the investigation was concerned with the basic features of plate vibration; i.e., mode shapes at resonant frequency, and the load-frequency behavior. The effects of initial stress, over-all noise level and the thickness of the plate on the rate of crack propagation were also observed.

Although the work of Clarkson and his co-workers is extensive on cracked sheets, the corresponding problem for other opening shapes remains to be studied. One of the objectives of the work described in this report is to study the vibration behavior of tensioned sheets with a variety of hole shapes.

The Fracture Problem

Although buckling or vibration which can precede or lead to crack extension are of primary interest in this investigation, the ultimate concern in service applications is failure through the fracture of a structural element. The status of fracture research will, therefore, briefly be summarized here to provide an enlarged perspective for the new results which are presented in this report.

The problem of crack initiation and crack propagation in structural elements has attracted the attention of investigators for many years. The growth of microscopic cracks in the material of a structure and the sudden failure of the structure can occur without warning. The potential danger and the resulting consequences of failure have served as a strong motivation for the development of both design techniques which isolate failure and prevent it from becoming complete, and crack detection devices.

The Griffith-Irwin fracture mechanics theory [41-43] of crack extension is used as a basis for most of the current work on the fracture problem. Griffith's theory was based on a study of crack extension in an ideally brittle solid. He based his work on an analysis of the transformation of stored strain energy to surface energy which is developed by the formation of new surfaces during crack extension. Irwin [42-45] and Orowan [46-47] recognized that for metals the plastic deformation which occurs during crack extension invalidates the use of Griffith's theory. They observed that the energy supplied to the fracture process is absorbed both in the creation of new surfaces and in plastic deformation in layers adjacent to the crack surfaces. Irwin used analytical results obtained by Westergaard [48] as a basis for modifying Griffith's theory and the result is often described in the fracture mechanics literature as the Griffith-Irwin theory.

In the preceding discussion the applied load is assumed to be static in character; i.e., it does not vary with time. Cases in which the applied load is cyclic or varying with time can lead to fracture through fatigue. Fatigue in structures is a complex phenomenon. It may occur at relatively low stress levels, and can cause cracks which can propagate and produce catastrophic failure. Fatigue damage is irreversible in metals because it is associated with rupture of atomic bonds and results in the formation of cracks. The complexity of fatigue mechanism makes it very difficult to make predictions about its progress. Much, however, has been gained by studying the details of the fatigue process in metals. It has been observed that during fatigue in a structural metal the process may be divided into distinct stages. In the initial stage of the fatigue process in metals, microscopic slip bands are formed within the individual grains of the material. Minute cracks, which eventually join to produce major cracks, develop within the slip bands. The final phase of the fatigue process occurs when the propagation of major cracks results in catastrophic failure.

The final phases of the fatigue process are of primary concern to the engineers in the design, analysis, and inspection of structures. Fatigue cracks developed must be contained within the structure without producing catastrophic failure, and this requires a thorough knowledge of the response of structures and materials to fatigue loading environments.

A rational, analytic application of fracture mechanics to crack propagation caused by sinusoidal loading has been proposed by Paris, et al.,[49-51]. The relations proposed suggest that the local stress intensity determines the rate of growth of the crack. Unfortunately, each load cycle of a loading history can affect the crack propagation during subsequent load cycles. In other words, there is an interaction effect between load cycles; i.e., at a given time, the material has a memory of previous cycles. Since the proposed relation suggests that the rate of propagation depends only on the current stress state, it does not include history effects.

From the preceding discussion it may be concluded that due to history effects it may be questionable to predict the crack rate under variable amplitude loading by use of growth rate data from constant amplitude loading. In addition, it is certainly clear that if a sheet with a hole or a crack has buckled or is undergoing local vibration at a resonant frequency, the crack nucleation and crack extension behavior are going to be affected. This would be expected to be true under either a fixed in-plane load or under cyclic loading, because if out-of-plane deflection occurs, stresses will vary through the thickness of the sheet and the analysis suggested by Irwin [45] will not be applicable.

Objectives

The static, dynamic and fracture phenomena associated with the cutout problem were discussed in the preceding sections of this chapter. The primary objective of the present investigation is to study the buckling and vibration behavior of a thin sheet with an elliptical hole in a tensile field. The range of shapes included will vary between the circle and the crack. A common feature of these problems is the presence of a free edge with a compressive stress acting parallel to the edge.

The analysis of the problems of interest can be simplified to some degree by the choice of the cutout shape. Since, an elliptical hole is used, the analysis can be most effectively accomplished by use of elliptic coordinates. The analytical procedure to be adopted for solving the buckling and the vibration problems of thin sheet with an elliptical hole in a tensile field will be to solve Karman plate equations under the assumption that for sufficiently small deflections the Gaussian curvature can be neglected. For convenience these equations will be expressed in terms of elliptic coordinates and the solution will proceed as follows:

(1) The initial stress state will be determined. This computation can be carried out by application of the complex variable method.

(2) The equation corresponding to transverse equilibrium will then be a partial differential equation with known coefficients which are functions of position. The vibration problem will be restricted to the case of a simple harmonic motion so time can be eliminated.

(3) The equation from Step 2 will then be solved for both the buckling and vibration problems by the use of a generalized Galerkin procedure.

As the behavior of the localized zone adjacent to the elliptic hole is of interest, the deflection function can then be chosen such that the maximum deflection occurs near the free edge of the hole and decreases as the distance from the hole increases. In addition to an area integral over the field around the hole, appropriate line integrals along boundaries having natural boundary conditions will be included. For the buckling problem the buckling loads (eigenvalues) and the buckling modes (eigenfunctions) will be obtained. For the vibration problem the frequencies (eigenvalues) and the vibration modes (eigenfunctions) will be determined.

The usefulness of any analytical results depends upon the degree to which they describe actual behavior. Hence, the objective of the experimental work conducted is to study the buckling behavior and the vibration behavior of the localized zone adjacent to an elliptic hole in a thin sheet specimen in a tensile field. The shapes of holes included range between the extremes of the circle and the crack.

CHAPTER II

GOVERNING EQUATIONS

The Problem of In-Plane Loading

In the derivation of elementary bending theory of plates a basic assumption is that the middle surface does not undergo any stretching due to bending. This assumption is valid only in a particular case in which the deflection surface is a developable surface. For the case in which stretching of the midsurface due to bending of the plate occurs, the additional stress can be significant when the deflection is moderately large (of the order of the plate thickness). The governing differential equations for a thin plate experiencing moderately large deflection [24] were first formulated by T. von Karman in 1910. These equations, which commonly bear his name (the Karman equations), are expressions of the transverse equilibrium and of the in-plane compatibility of the plate. With the introduction of the Airy stress function, F, the in-plane compatibility equation for the case of constant plate thickness and non-in-plane body forces may be written in Cartesian coordinates as

$$\nabla^4 F = E\left[\left(\frac{\partial^2 w}{\partial x \partial y}\right)^2 - \frac{\partial^2 w}{\partial x^2}\ \frac{\partial^2 w}{\partial y^2}\right], \qquad (1)$$

where

$$\sigma_x = \frac{N_x}{t} = \frac{\partial^2 F}{\partial y^2} , \quad \sigma_y = \frac{N_y}{t} = \frac{\partial^2 F}{\partial x^2} , \quad \sigma_{xy} = \frac{N_{xy}}{t} = - \frac{\partial^2 F}{\partial x \partial y} ,$$

the quantities $\sigma_x, \sigma_y, \sigma_{xy}$ are the midsurface in-plane stresses, N_x, N_y, N_{xy} are the midsurface in-plane forces per unit length and w is the transverse deflection. For the same case the equation of motion in the transverse direction is

$$D\nabla^4 w = t \left[\frac{q}{t} + \frac{\partial^2 F}{\partial y^2} \frac{\partial^2 w}{\partial x^2} - 2 \frac{\partial^2 F}{\partial x \partial y} \frac{\partial^2 w}{\partial x \partial y} + \frac{\partial^2 F}{\partial x^2} \frac{\partial^2 w}{\partial y^2} \right] \tag{2}$$

where

$$D = \frac{Et^3}{12(1 - \nu^2)} ;$$

E is the Young's modulus, t is the plate thickness, ν is the Poisson's ratio and q is the applied transverse force. Equations (1) and (2) are coupled in w and F and must be solved simultaneously. Note, however, that if the Gaussian curvature (right side of Equation (1)) is zero, as is the case for bending into a developable surface, the equations are uncoupled.

The problems of interest in the present investigation involve non-uniform initial stress states in a multiply connected body. For the stress function formulation Equations (1) and (2) are not sufficient, and integral relations must be included to ensure single valued displacements. A derivation of these relations for the nonlinear, coupled problem has been given by Zielsdorff [8].

In the present work it is assumed that deflections are small enough to neglect the nonlinear effect of middle surface stretching due to bending. By this procedure, Equations (1) and (2) are uncoupled and the solution proceeds by first determining the stress distribution and then solving Equation (2).

Because of the geometry of the problem it is convenient to express Equation (2) in elliptic coordinates. To provide a more general development, however, the solution procedure will be developed first in terms of generalized orthogonal curvilinear coordinates.

The Problem in Curvilinear Coordinates

The problem of interest in the present investigation involves a sheet with an elliptic hole in a unidirectional tensile field. It is clear that an elliptic coordinate system would be most convenient in analyzing the problem. But before writing the governing equations in elliptic coordinates, the equations will first be presented in terms of generalized orthogonal curvilinear coordinate system. The resulting equation can then be converted into the special case of elliptic coordinates and the solution procedure follows.

The equation of motion in transverse direction in curvilinear coordinates may be written as [52,53],

$$D\nabla^2\nabla^2 w - N_\alpha K_\alpha - N_\beta K_\beta - 2\, N_{\alpha\beta} K_{\alpha\beta} - q = 0, \tag{3}$$

where, referring to Figure 1, α, β, z represent any orthogonal

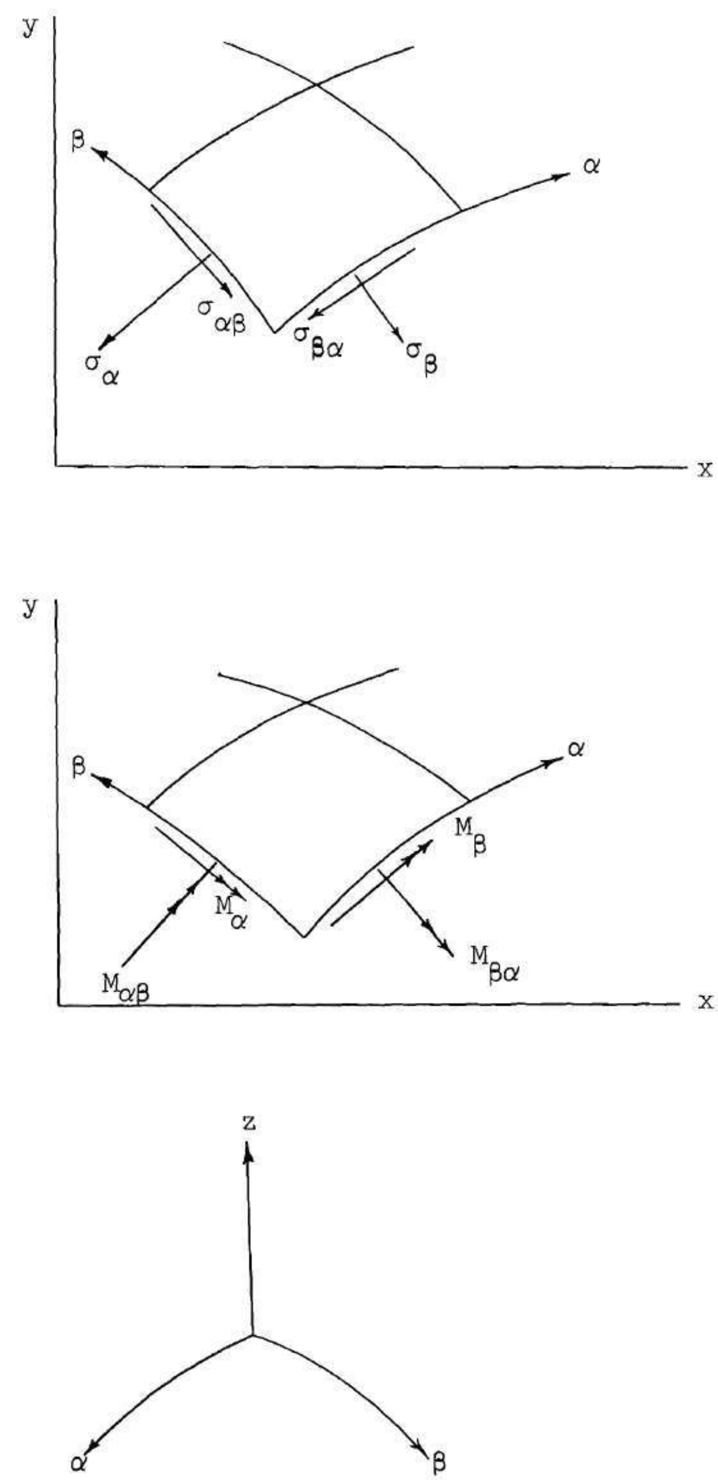

Figure 1. Orthogonal Curvilinear Coordinate Convention

curvilinear coordinate system. q is the applied transverse load. The quantities N_α, N_β and $N_{\alpha\beta}$ are in-plane forces per unit length and those are defined as,

$$N_\alpha = \int_{z_1}^{z_2} \sigma_\alpha dz; \quad N_\beta = \int_{z_1}^{z_2} \sigma_\beta dz; \quad N_{\alpha\beta} = \int_{z_1}^{z_2} \sigma_{\alpha\beta} dz,$$

while σ_α, σ_β and $\sigma_{\alpha\beta}$ are the in-plane stresses. K_α, K_β and $K_{\alpha\beta}$ are the local curvatures of the deformed surfaces, $z_1 = -t/2$ and $z_2 = t/2$. Also

$$\nabla^2 w = \frac{1}{AB}\left\{\frac{\partial}{\partial\alpha}\left[\frac{B}{A}\ \frac{\partial w}{\partial\alpha}\right] + \frac{\partial}{\partial\beta}\left[\frac{A}{B}\ \frac{\partial w}{\partial\beta}\right]\right\},$$

where, w is the transverse deflection and A, B are called the Lamé parameters. In this development it is assumed that the edges of the plate are along lines of constant α or constant β and if ds is the differential length along an edge, either $Ad\alpha = ds$ or $Bd\beta = ds$.

For both the buckling and vibration problems Equation (3) is homogeneous and the boundary conditions are homogeneous. The homogeneous boundary conditions in the curvilinear coordinate system are given [52,53] in the following tabulation:

Boundary Descriptions	Boundary Conditions
On α = Constant	
Clamped	$w = 0, \qquad w,_{\alpha} = 0$
Hinged	$w = 0, \qquad \frac{B}{A} M_{\alpha} = 0$
Free	$\frac{B}{A} M_{\alpha} = 0, \qquad N_{\alpha} \frac{B}{A} w,_{\alpha} + N_{\alpha\beta} w,_{\beta} + (M_{\alpha} \frac{B}{A}),_{\alpha} + M_{\alpha} \frac{B}{A^2} A,_{\alpha} - M_{\beta} \frac{B,_{\alpha}}{A} + 2(M_{\alpha\beta}),_{\beta} + 2 M_{\alpha\beta} \frac{A,_{\beta}}{A} = 0$
On β = Constant	
Clamped	$w = 0, \qquad w,_{\beta} = 0$
Hinged	$w = 0, \qquad \frac{A}{B} M_{\beta} = 0$
Free	$\frac{A}{B} M_{\beta} = 0, \qquad N_{\beta} \frac{A}{B} w,_{\beta} + N_{\alpha\beta} w,_{\alpha} + (M_{\beta} \frac{A}{B}),_{\beta} + M_{\beta} \frac{A}{B^2} B,_{\beta} - M_{\alpha} \frac{A,_{\beta}}{B} + 2(M_{\alpha\beta}),_{\alpha} + 2 M_{\alpha\beta} \frac{B,_{\alpha}}{B} = 0$

The corner condition is either $2 M_{\alpha\beta} = 0$ or $w = 0$.

In the boundary conditions noted above, there are no applied edge bending moments or shear forces. In the above relations, the quantities M_α, M_β and $M_{\alpha\beta}$ are defined as

$$M_\alpha = - D(K_\alpha + \nu K_\beta); \quad M_\beta = - D(K_\beta + \nu K_\alpha) \quad \text{and} \quad M_{\alpha\beta} = - D(1-\nu)K_{\alpha\beta} \; .$$

D is the plate bending rigidity and ν is the Poisson's ratio. The curvature relations in orthogonal curvilinear coordinate system are

$$K_\alpha = \left[\frac{1}{A}\frac{\partial}{\partial\alpha}\left(\frac{1}{A}\frac{\partial w}{\partial\alpha}\right) + \frac{1}{AB^2}\frac{\partial A}{\partial\beta}\frac{\partial w}{\partial\beta}\right] ,$$

$$K_\beta = \left[\frac{1}{B}\frac{\partial}{\partial\beta}\left(\frac{1}{B}\frac{\partial w}{\partial\beta}\right) + \frac{1}{A^2B}\frac{\partial B}{\partial\alpha}\frac{\partial w}{\partial\alpha}\right],$$

$$2\,K_{\alpha\beta} = \left[\frac{1}{A}\frac{\partial}{\partial\alpha}\left(\frac{1}{B}\frac{\partial w}{\partial\beta}\right) - \frac{1}{A^2B}\frac{\partial A}{\partial\beta}\frac{\partial w}{\partial\alpha} + \frac{1}{B}\frac{\partial}{\partial\beta}\left(\frac{1}{A}\frac{\partial w}{\partial\alpha}\right)\right.$$

$$\left. - \frac{1}{AB^2}\frac{\partial B}{\partial\alpha}\frac{\partial w}{\partial\beta}\right] .$$

In applied mechanics it is often necessary to find the solution of certain partial differential equations with known boundary conditions as in the present problems. Exact methods of solution are often very difficult, so a number of approximate methods of solution have been developed. For these particular problems, one method of solution utilizes the direct method of the calculus of variations through a Rayleigh-Ritz application of either the principle of stationery potential energy (for the static problem) or Hamilton's principle (for the dynamic problem). This is perhaps the most obvious approximate solution procedure, and therefore the most well-known. For this reason it has been considered worthwhile to demonstrate an alternative solution procedure*. The generalized Galerkin method is one such approximate method, and it will be used to obtain solutions to the present problems. The governing equation in the generalized Galerkin method may be written in the form [54,55]

$$\int_{\alpha_1}^{\alpha_2}\int_{\beta_1}^{\beta_2}\left(D\,\nabla^2\nabla^2 w - N_\alpha K_\alpha - N_\beta K_\beta - 2\,N_{\alpha\beta}\,K_{\alpha\beta} - q\right) AB\delta w\,d\alpha\,d\beta \tag{4}$$

$$- \int_{\beta_1}^{\beta_2}\left\{M_\alpha \frac{B}{A}\right\}\delta\left(\frac{\partial w}{\partial\alpha}\right)\Big|_{\alpha_1}^{\alpha_2} d\beta + \int_{\beta_1}^{\beta_2}\Big[\Big\{\left(M_\alpha \frac{B}{A}\right)_{,\alpha} + M_\alpha \frac{B}{A^2} A_{,\alpha} - M_\beta \frac{B_{,\alpha}}{A}$$

$$+ 2\left(M_{\alpha\beta}\right)_{,\beta} + 2\,M_{\alpha\beta}\frac{A_{,\beta}}{A} + N_\alpha \frac{B}{A}\;w_{,\alpha} + N_{\alpha\beta}\,w_{,\beta}\Big\}\,\delta w\,\Big|_{\alpha_1}^{\alpha_2}\Big]\,d\beta$$

$$- \int_{\alpha_1}^{\alpha_2}\left\{M_\beta \frac{A}{B}\,\delta\left(\frac{\partial w}{\partial\beta}\right)\right\}\Big|_{\beta_1}^{\beta_2} d\alpha + \int_{\alpha_1}^{\alpha_2}\Big[\Big\{\left(M_\beta \frac{A}{B}\right)_{,\beta} + M_\beta \frac{A}{B^2} B_{,\beta}$$

$$- M_\alpha \frac{A_{,\beta}}{B} + 2\left(M_{\alpha\beta}\right)_{,\alpha} + 2\,M_{\alpha\beta}\frac{B_{,\alpha}}{B} + N_\beta \frac{A}{B}\,w_{,\beta}$$

$$+ N_{\alpha\beta}\,w_{,\alpha}\Big\}\,\delta w\,\Big|_{\beta_1}^{\beta_2}\Big]\,d\alpha - 2\,M_{\alpha\beta}\,\delta w\,\Big|_{\alpha_1}^{\alpha_2}\,\Big|_{\beta_1}^{\beta_2} = 0$$

---

* The modified Galerkin solution technique used here is particularly useful in problems in which the governing equations can not be derived from a functional by the application of variational principle.

where δ represents the variation of the indicated quantities [54,55]. α_1, α_2, β_1 and β_2 are the limits of integration for an area element in the α and β coordinate plane. Equation (4) can be simplified for certain coordinate systems. For example, in an elliptic coordinate system if constant α curves are identified as the closed ellipses then for any continuous functions $F(\alpha,\beta)$ the integrands of such terms as

$$\int_{\alpha_1}^{\alpha_2} F(\alpha,\beta) \Big|_{\beta_1}^{\beta_2} d\alpha$$

are zero, because in completing a circuit around the closed curve, $F(\alpha,\beta_1) = F(\alpha,\beta_2)$; in fact on a constant α curve in the elliptic coordinate system $F(\alpha,\beta_1) = F(\alpha,\beta_1 + 2\pi)$. Then

$$\int_{\alpha_1}^{\alpha_2} \int_{\beta_1}^{\beta_2} \left(D \nabla^2\nabla^2 w - N_\alpha K_\alpha - N_\beta K_\beta - 2 N_{\alpha\beta} K_{\alpha\beta} - q\right) AB \, \delta w \, d\alpha \, d\beta \tag{5}$$

$$- \int_{\beta_1}^{\beta_2} \left\{M_\alpha \frac{B}{A} \delta \left(\frac{\partial w}{\partial \alpha}\right)\right\} \Big|_{\alpha_1}^{\alpha_2} d\beta + \int_{\beta_1}^{\beta_2} \left[\left\{\left(M_\alpha \frac{B}{A}\right)_{,\alpha} + M_\alpha \frac{B}{A^2} A_{,\alpha} - M_\beta \frac{B_{,\alpha}}{A}\right.\right.$$

$$\left.\left. + 2(M_{\alpha\beta})_{,\beta} + 2 M_{\alpha\beta} \frac{A_{,\beta}}{A} + N_\alpha \frac{B}{A} w_{,\alpha} + N_{\alpha\beta} w_{,\beta}\right\} \delta w \Big|_{\alpha_1}^{\alpha_2} \right] d\beta = 0$$

To obtain an approximate solution a function may be selected of the form

$$w_{MN}(\alpha,\beta) = \sum_{i=1}^{M} \sum_{j=1}^{N} \varphi_{ij}(\alpha,\beta)\, A_{ij}$$

where the φ_{ij}'s satisfy the geometric boundary conditions. Taking a variation on $w_{MN}(\alpha,\beta)$ gives

$$\delta w_{MN}(\alpha,\beta) = \sum_{i=1}^{M} \sum_{j=1}^{N} \varphi_{ij}(\alpha,\beta)\, \delta A_{ij}$$

The δA_{ij}'s are arbitrary and the φ_{ij}'s are independent of each other. Substituting the deflection function into Equation (5), the following set of M x N equations, homogeneous and linear in the A_{ij}'s is obtained.

$$\int_{\alpha_1}^{\alpha_2}\int_{\beta_1}^{\beta_2} L(w_{MN})\, \varphi_{ij}\, AB\, d\alpha\, d\beta - \int_{\beta_1}^{\beta_2} \left\{ M_\alpha \frac{B}{A} \frac{\partial \varphi_{ij}}{\partial \alpha} \right\} \Bigg|_{\alpha_1}^{\alpha_2} d\beta \tag{6}$$

$$+ \int_{\beta_1}^{\beta_2} \Bigg[\Bigg\{ \left(M_\alpha \frac{B}{A} \right)_{,\alpha} + M_\alpha \frac{B}{A^2} A_{,\alpha} - M_\beta \frac{B_{,\alpha}}{A} + 2(M_{\alpha\beta})_{,\beta} + 2\, M_{\alpha\beta} \frac{A_{,\beta}}{A}$$

$$+ N_\alpha \frac{B}{A} w_{,\alpha} + N_{\alpha\beta}\, w_{,\beta} \Bigg\} \varphi_{ij} \Bigg|_{\alpha_1}^{\alpha_2} \Bigg] d\beta = 0$$

where, $i = 1, 2, \ldots, M$

$j = 1, 2, \ldots, N$

In these equations,

$$L(w_{MN}) = D\,\nabla^2\nabla^2\, w_{MN} - N_\alpha\,(K_\alpha)_{MN} - N_\beta\,(K_\beta)_{MN} - 2N_{\alpha\beta}(K_{\alpha\beta})_{MN} - (q)_{MN}$$

and

$$M_\alpha = -D\left[(K_\alpha)_{MN} + \nu(K_\beta)_{MN}\right], \text{ etc.}$$

and $(K_\alpha)_{MN}$, etc. involve derivatives of the dependent variable $w_{MN}(\alpha,\beta)$. In Equation (6), the buckling problem will correspond to the case where $q = 0$. The vibration problem will correspond to the case where q is the transverse inertial force of vibration. The details of the solution procedure are described in Chapter III.

CHAPTER III

SOLUTION TO THE SUBJECT PROBLEM

Statement of the Problem

In the previous chapter, the Karman plate equations and derivation of the Galerkin method in generalized orthogonal curvilinear coordinate systems were presented. The problem under consideration is the buckling and vibration behavior of a thin sheet with an elliptic hole in a tensile field. The analytical procedure is to uncouple the Karman plate equations in the curvilinear coordinate system under the assumption that for sufficiently small deflections the stretching of the midsurface due to bending can be neglected. Since the plate transverse equilibrium equation contains the in-plane stresses, the first step is to determine the in-plane stress distribution in the field around the hole. The equation corresponding to transverse equilibrium is then a partial differential equation with coefficients which are known functions of position and time. In the vibration problem, if the motion is considered to be simple harmonic for the linearized problem, then time can be eliminated, and the inertia term appears as a transverse load. For the buckling problem, the inertia term is not present. The equations for the above problems can then be solved by the generalized Galerkin method.

The behavior of interest is in a localized zone adjacent to the hole, and for convenience the plate is considered to be very large compared to the hole dimensions. The deflection function can be chosen such that the maximum deflection occurs near the free edge of the hole and goes to zero as the distance from the hole becomes unbounded. In addition to the integral over the field around the hole, the appropriate line integrals along the boundary of the hole must be included. Since the edge of the hole is free of traction, the integrands of the line integrals are those associated with natural boundary conditions.

Since the shape of the hole in the present problem is elliptic, the curvilinear coordinate system is taken as elliptic. The formulation of the stress distribution problem in the elliptic coordinate system is presented in the subsequent section.

The Stress Distribution in an Infinite Plate with an Elliptic Hole

Kolosoff's Equations

In the previous section, the features of the problem in the present investigation were discussed. This section will examine the stress distribution portion of the problem.

The stress distribution in an infinite plate having an internal hole can be determined efficiently by use of the complex variable formulation of elasticity [56-61]. The development proceeds with the determination of the complex potential functions of Kolosoff's equations. The stress solution can be expressed either in terms of components in a Cartesian coordinate system or, if more convenient, in an orthogonal curvilinear coordinate system. The Kolosoff's equations in Cartesian coordinates are written as:

$$\sigma_x + \sigma_y = 2\,\psi'(z) + 2\,\bar{\psi}'(\bar{z}) = 4\ \mathrm{Re}\ \psi'(z) \tag{1}$$

$$\sigma_y - \sigma_x + 2\,i\sigma_{xy} = 2[\bar{z}\,\psi''(z) + \chi''(z)], \tag{2}$$

where $$z = x + iy,$$

and $\psi(z)$, $\chi(z)$ are complex potential functions which must be determined for each problem.

In the curvilinear coordinate system of Figure 2,

σ_ξ = the normal stress component on a curve of ξ = constant,

σ_η = the normal stress component on a curve of η = constant,

$\sigma_{\eta\xi} = \sigma_{\xi\eta}$ = the shear stress components.

It is shown in elementary strength of materials that if $\bar{X}$ and $\bar{Y}$ are the components of stress acting on the side BC of the prismatic element OBC, Figure 3, then from the equilibrium of the prismatic element,

$$\bar{X} = \ell\,\sigma_x + m\sigma_{xy},$$

$$\bar{Y} = m\sigma_y + \ell\,\sigma_{xy},$$

where $$\ell = \cos\theta,$$

and $$m = \sin\theta.$$

Also, $$\sigma = \sigma_x \cos^2\theta + \sigma_y \sin^2\theta + 2\,\sigma_{xy} \sin\theta\cos\theta\ ,$$

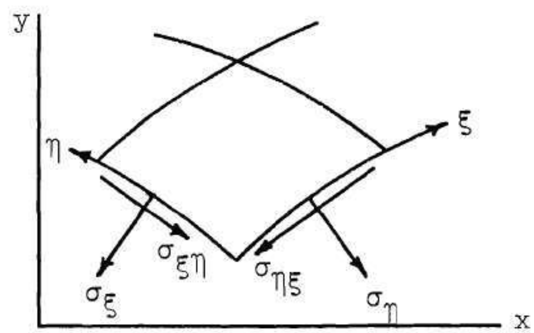

Figure 2. Stress Nomenclature

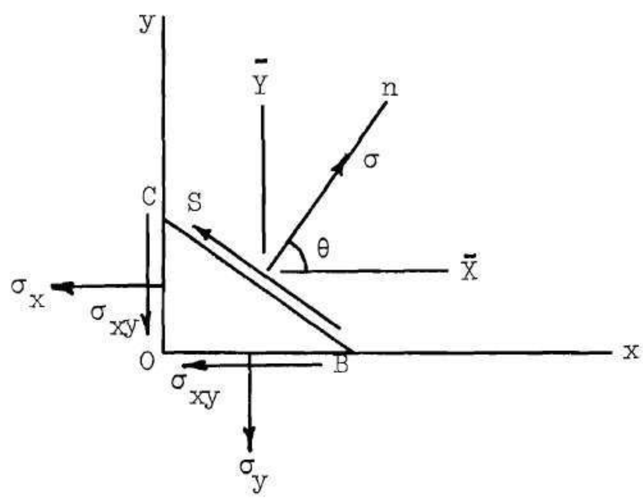

Figure 3. Stress Acting on a Prismatic Element

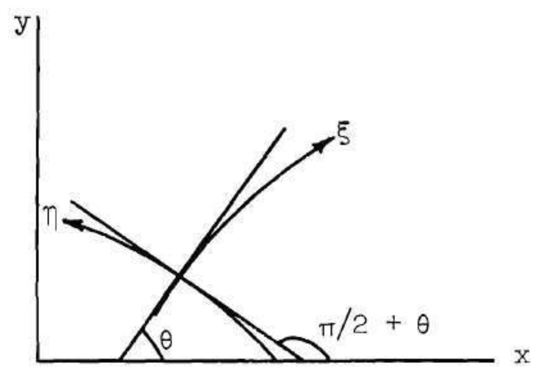

Figure 4. Curvilinear Coordinates

and $$S = \sigma_{xy} \cos 2\,\theta + (\sigma_y - \sigma_x) \sin\theta \cos\theta,$$

where, σ and S are the normal and shearing components of stress on the plane BC. Using the above,

$$\sigma_\xi = \tfrac{1}{2}(\sigma_x + \sigma_y) + \tfrac{1}{2}(\sigma_x - \sigma_y) \cos 2\,\theta + \sigma_{xy} \sin 2\,\theta,$$

$$\sigma_{\xi\eta} = -\tfrac{1}{2}(\sigma_x - \sigma_y) \sin 2\,\theta + \sigma_{xy} \cos 2\,\theta.$$

Replacing θ by $\pi/2 + \theta$,

$$\sigma_\eta = \tfrac{1}{2}(\sigma_x + \sigma_y) - \tfrac{1}{2}(\sigma_x - \sigma_y) \cos 2\,\theta - \sigma_{xy} \sin 2\,\theta,$$

From these the following relations are obtained:

$$\sigma_\xi + \sigma_\eta = \sigma_x + \sigma_y, \tag{3}$$

$$\sigma_\eta - \sigma_\xi + 2\,i\sigma_{\xi\eta} = e^{2i\theta}(\sigma_y - \sigma_x + 2\,i\sigma_{xy}), \tag{4}$$

where θ is the angle indicated in Figure 4 . Finally, Kolsoff's equations in the curvilinear coordinate system may be written in the form

$$\sigma_\xi + \sigma_\eta = 2\,[\psi'(z) + \bar{\psi}'(\bar{z})] = 4 \operatorname{Re} \psi'(z) \tag{5}$$

$$\sigma_\eta - \sigma_\xi + 2\,i\sigma_{\xi\eta} = 2\,e^{2i\theta}[\bar{z}\psi''(z) + \chi''(z)]. \tag{6}$$

The Elliptic Coordinate System

In the previous section, Kolosoff's equations in both the Cartesian and the curvilinear coordinate systems have been described. Since the natural boundary of the hole in the present problem is elliptic, it will be convenient to solve the problem in the elliptic coordinate system. The curvilinear coordinate system $\xi - \eta$ of the previous section will be interpreted here as an elliptic coordinate system (Figure 5).

Define, $$z = h \cosh \Phi ,$$

where $z = x + iy$ and $\Phi = \xi + i\eta$.

Substituting and equating real and imaginary parts, we get,

$$x = h \cosh \xi \cos \eta , \tag{7}$$

and $$y = h \sinh \xi \sin \eta .$$

Eliminating η from Equation (7) yields

$$\frac{x^2}{h^2 \cosh^2 \xi} + \frac{y^2}{h^2 \sinh^2 \xi} = 1 .$$

If ξ is constant, this is the equation of an ellipse with semiaxes

$$a = h \cosh \xi \quad \text{and} \quad b = h \sinh \xi$$

with foci at $x = \pm h$. For different values of ξ we obtain different

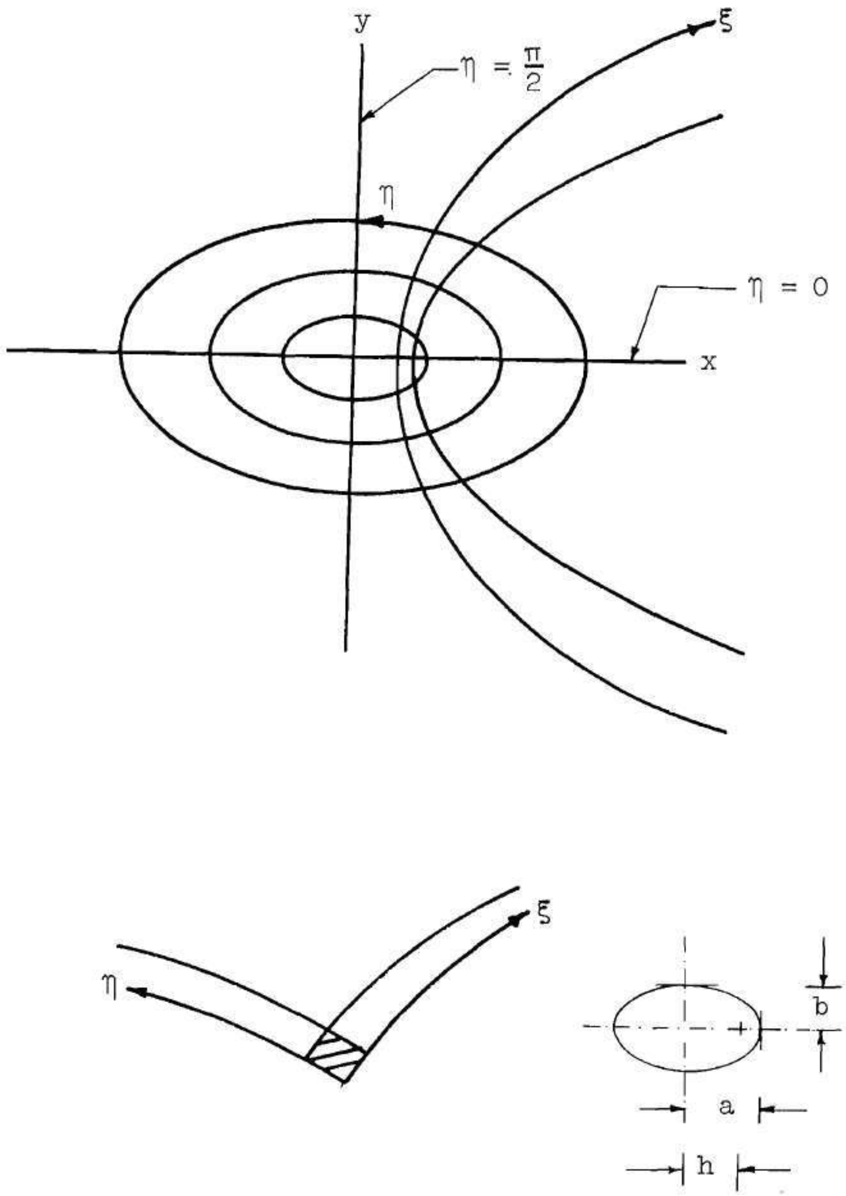

Figure 5. Elliptic Coordinate System

ellipses with the same foci; that is, a family of confocal ellipses. It may be noted that on any of these ellipses ξ is constant and η varies through from zero to 2π.

By eliminating ξ from Equation (7),

$$\frac{x^2}{h^2\cos^2\eta} - \frac{y^2}{h^2\sin^2\eta} = 1.$$

For a constant value of η this represents a hyperbola having the same foci as the ellipse. The above equation represents a family of confocal hyperbolas, on any of which η is constant and ξ varies. The coordinate system thus generated is called elliptic.

The coordinate ξ is constant and equal to ξ_o on an ellipse of semiaxes $h \cosh \xi_o$, $h \sinh \xi_o$. If the semiaxes are given as a and b, then h and ξ_o can be found from

$$h \cosh \xi_o = a \quad \text{and} \quad h \sinh \xi_o = b.$$

It follows that if one member of the family of ellipses is given, the whole family of ellipses and also the family of hyperbolas are defined. If ξ_o is very small the corresponding ellipse is very slender, and in the limit $\xi_o \to 0$, it becomes a line of length 2h joining the foci. Taking larger and larger positive values of ξ_o, the ellipse becomes larger and larger, approaching a circle.

Elliptic Hole in a Plate Under Simple Tension

The problem of interest may be represented as an infinite plate in a state of simple tensile stress, P, in a direction at an angle γ above the positive x-axis (Figure 6). An elliptic hole, with its major axis along the x-axis is positioned as shown. The case of an elliptic hole with major axis perpendicular to the applied tension ($\gamma = \pi/2$) describes the problem of interest. Let ox', oy' be Cartesian axes obtained by rotating ox through the angle γ so as to bring it parallel to the tension P. Then by Equations (3) and (4)

$$\sigma_{x'} + \sigma_{y'} = \sigma_x + \sigma_y ,$$

and
$$\sigma_{y'} - \sigma_{x'} + 2\, i\sigma_{x'y'} = e^{2i\gamma}(\sigma_y - \sigma_x + 2\, i\sigma_{xy}) .$$

Since at infinity

$$\sigma_{x'} = P \quad \text{and} \quad \sigma_{y'} = \sigma_{x'y'} = 0 ,$$

we have

$$\sigma_x + \sigma_y = P \quad \text{and} \quad \sigma_y - \sigma_x + 2\, i\sigma_{xy} = -\, P\, e^{-2i\gamma}$$

at infinity. Then by Equations (1) and (2),

$$4\, \mathrm{Re}\, \psi'(z) = P \quad \text{and} \quad 2[\bar{z}\, \psi''(z) + \chi''(z)] = -\, P\, e^{-2i\gamma}$$

at infinity.

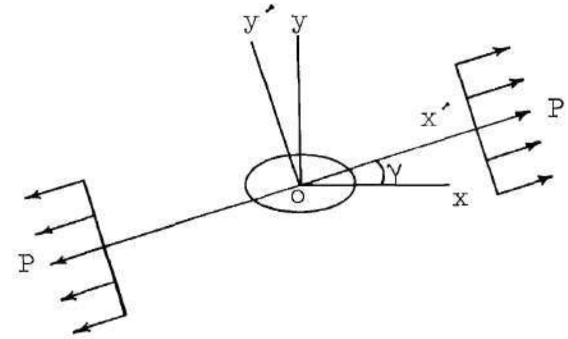

Figure 6. Elliptic Hole in an Infinite Plate Under Uniform Tensile Stress

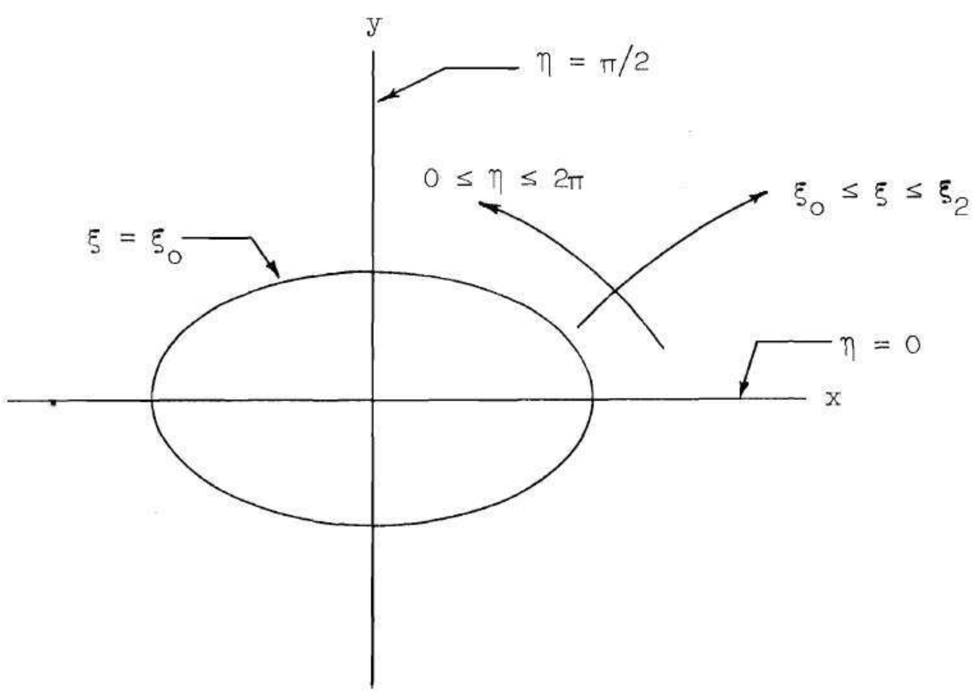

Figure 7. Elliptic Coordinate Nomenclature

At the boundary of the hole $\xi = \xi_o$, we must have $\sigma_\xi = \sigma_{\xi\eta} = 0$. All these boundary conditions can be satisfied by taking $\psi(z)$ and $\chi(z)$ in the forms

$$4\,\psi(z) = Ah \cosh \Phi + Bh \sinh \Phi,$$

and $$4\,\chi(z) = Ch^2\Phi + Dh^2\cosh 2\Phi + Eh^2\sinh 2\Phi ,$$

where A, B, C, D, E are constants to be determined. The constants are [61]

$$A = P\, e^{2\xi_o} \cos 2\gamma ,$$

$$B = P(1 - e^{2\xi_o - 2i\gamma}) ,$$

$$C = - P(\cosh 2\xi_o - \cos 2\gamma) ,$$

$$D = - \tfrac{1}{2} Pe^{2\xi_o} \cosh 2(\xi_o + i\gamma) ,$$

and $$E = \tfrac{1}{2} Pe^{2\xi_o} \sinh 2(\xi_o + i\gamma) .$$

The complex potential functions are consequently,

$$4\psi(z) = Ph[e^{2\xi_o}\cos 2\gamma \cosh \Phi + (1 - e^{2\xi_o + 2i\gamma}) \sinh\Phi] , \tag{8}$$

and

$$4\chi(z) = - Ph^2[(\cosh 2\xi_o - \cos 2\gamma)\Phi + \tfrac{1}{2}e^{2\xi_o} \cosh 2(\Phi - \xi_o - i\gamma)] \tag{9}$$

where

$$z = h \cosh \Phi, \quad \Phi = \xi + i\eta \quad \text{and} \quad \frac{dz}{d\Phi} = h \sinh \Phi.$$

In the present case, $\gamma = \pi/2$, hence

$$4\psi(z) = Ph[-e^{2\xi_o} \cosh \Phi + (1 + e^{2\xi_o}) \sinh \Phi] , \tag{10}$$

and

$$4\chi(z) = - Ph^2[(\cosh 2\xi_o + 1)\Phi + \tfrac{1}{2}e^{2\xi_o} \cosh (2\Phi - 2\xi_o - i\pi)] , \tag{11}$$

where $\xi = \xi_o$ is the boundary of the elliptic hole where $\sigma_\xi = \sigma_{\xi\eta} = 0$.

For a given elliptical hole a and b are known. From this h can be computed as $h = \sqrt{a^2 - b^2}$. Also ξ_o can be determined from the relation $\tanh \xi_o = b/a$.

The stress components in elliptic coordinates are obtained by inserting Equations (10) and (11) into Kolosoff's Equations (5) and (6) and separating the real and imaginary parts. The results can be written as

$$\sigma_\xi(\xi,\eta) = Pf_1(\xi,\eta), \tag{12}$$

$$\sigma_\eta(\xi,\eta) = Pf_2(\xi,\eta),$$

and

$$\sigma_{\xi\eta}(\xi,\eta) = Pf_3(\xi,\eta) .$$

In these expressions P represents the uniform tensile stress applied at infinity, and the nondimensional spatial functions f_1, f_2 and f_3 are given in Appendix A. It should also be noted that the elliptic coordinates ξ and η are nondimensional.

The Buckling and Vibration Problems

The analysis for determining the in-plane stress distribution in the field around the elliptic hole in an infinite plate under tension has been presented in the previous section. The equations governing the buckling and the vibration behavior of the tensioned sheet will be developed in this section. The generalized Galerkin method in a curvilinear orthogonal coordinate system as described in Chapter II will be used for the development. The elliptic coordinate system will be applied as a special case of the curvilinear coordinate system.

Referring to the Figure 5, let $\alpha = \xi$ and let $\beta = \eta$. In this system a constant value of ξ corresponds to an ellipse. Here ξ, η are consequently the coordinates of the elliptic coordinate system shown in Figure 5 .

From Equation (6) of Chapter II, the governing equations are

$$\int_{\xi_1}^{\xi_2}\int_{\eta_1}^{\eta_2} L(w_{MN})\varphi_{ij}\, AB\, d\xi\, d\eta - \int_{\eta_1}^{\eta_2}\left\{M_\xi \frac{B}{A}\frac{\partial\varphi_{ij}}{\partial\xi}\right\}\Bigg|_{\xi_1}^{\xi_2} d\eta + \int_{\eta_1}^{\eta_2}\Bigg[\Bigg\{\left(M_\xi \frac{B}{A}\right)_{,\xi} \tag{13}$$

$$+ M_\xi \frac{B}{A^2}A_{,\xi} - M_\eta \frac{B_{,\xi}}{A} + 2(M_{\xi\eta})_{,\eta} + 2M_{\xi\eta}\frac{A_{,\eta}}{A}$$

$$+ N_\xi \frac{B}{A} w_{,\xi} + N_{\xi\eta}\, w_{,\eta}\Bigg\}\varphi_{ij}\Bigg|_{\xi_1}^{\xi_2}\Bigg] d\eta = 0,$$

where

$$i = 1, 2, \ldots, M,$$

$$j = 1, 2, \ldots, N,$$

$$L(w_{MN}) = D\nabla^2\nabla^2 w_{MN} - N_\xi (K_\xi)_{MN} - N_\eta (K_\eta)_{MN} - 2N_{\xi\eta}(K_{\xi\eta})_{MN} - (q)_{MN} ,$$

$$M_\xi = - D[(K_\xi)_{MN} + \nu(K_\eta)_{MN}], \text{ etc.}$$

$(q)_{MN}$ is zero in the buckling problem and it is the inertial load in the vibration problem. $(K_\xi)_{MN}$, etc. involve derivatives of the dependent variable $w_{MN}(\xi,\eta)$. In addition,

$$A = B = \frac{h}{\sqrt{2}} (\cosh 2\xi - \cos 2\eta)^{\frac{1}{2}},$$

$$\nabla^2 w = \frac{2}{h^2(\cosh 2\xi - \cos 2\eta)} \left(\frac{\partial^2}{\partial\xi^2} + \frac{\partial^2}{\partial\eta^2}\right) w ,$$

$$\nabla^2\nabla^2 w = \frac{4}{h^4 \ell_2{}^2} \Bigg[\left(\frac{\partial^4 w}{\partial\xi^4} + 2\frac{\partial^4 w}{\partial\xi^2\partial\eta^2} + \frac{\partial^4 w}{\partial\eta^4}\right) + 2\left(\frac{\partial^2 w}{\partial\xi^2} + \frac{\partial^2 w}{\partial\eta^2}\right)\left(\frac{\cosh 4\xi - \cos 4\eta}{\ell_2{}^2}\right)$$

$$- 4\left(\frac{\partial^3 w}{\partial\xi^3} + \frac{\partial^3 w}{\partial\xi\partial\eta^2}\right)\frac{\sinh 2\xi}{\ell_2} - 4\left(\frac{\partial^3 w}{\partial\eta^3} + \frac{\partial^3 w}{\partial\eta\partial\xi^2}\right)\frac{\sin 2\eta}{\ell_2}\Bigg] ,$$

where

$$\ell_2 = \left(\cosh 2\xi - \cos 2\eta\right).$$

Also,

$$K_\xi = \frac{2\left[\sin 2\eta \dfrac{\partial w}{\partial \eta} - \sinh 2\xi \dfrac{\partial w}{\partial \xi} + \dfrac{\partial^2 w}{\partial \xi^2}(\cosh 2\xi - \cos 2\eta)\right]}{h^2(\cosh 2\xi - \cos 2\eta)^2},$$

$$K_\eta = \frac{2\left[-\sin 2\eta \dfrac{\partial w}{\partial \eta} + \sinh 2\xi \dfrac{\partial w}{\partial \xi} + \dfrac{\partial^2 w}{\partial \eta^2}(\cosh 2\xi - \cos 2\eta)\right]}{h^2(\cosh 2\xi - \cos 2\eta)^2},$$

and

$$K_{\xi\eta} = \frac{-2\left[\sinh 2\xi \dfrac{\partial w}{\partial \eta} + \sin 2\eta \dfrac{\partial w}{\partial \xi} - \dfrac{\partial^2 w}{\partial \xi \partial \eta}(\cosh 2\xi - \cos 2\eta)\right]}{h^2(\cosh 2\xi - \cos 2\eta)^2}.$$

The moment-curvature relations are

$$M_\xi = \frac{-2D}{h^2(\cosh 2\xi - \cos 2\eta)}\left[\frac{\partial^2 w}{\partial \xi^2} + \nu \frac{\partial^2 w}{\partial \eta^2} - \frac{(1-\nu)\sinh 2\xi}{(\cosh 2\xi - \cos 2\eta)}\frac{\partial w}{\partial \xi} + \frac{(1-\nu)\sin 2\eta}{(\cosh 2\xi - \cos 2\eta)}\frac{\partial w}{\partial \eta}\right],$$

$$M_\eta = \frac{-2D}{h^2(\cosh 2\xi - \cos 2\eta)}\left[\nu \frac{\partial^2 w}{\partial \xi^2} + \frac{\partial^2 w}{\partial \eta^2} + \frac{(1-\nu)\sinh 2\xi}{(\cosh 2\xi - \cos 2\eta)}\frac{\partial w}{\partial \xi} - \frac{(1-\nu)\sin 2\eta}{(\cosh 2\xi - \cos 2\eta)}\frac{\partial w}{\partial \eta}\right],$$

and

$$M_{\xi\eta} = M_{\eta\xi} = \frac{2D(1-\nu)}{h^2(\cosh 2\xi - \cos 2\eta)^2}\left[\frac{\partial w}{\partial \xi}\sin 2\eta + \frac{\partial w}{\partial \eta}\sinh 2\xi - \frac{\partial^2 w}{\partial\xi\partial\eta}(\cosh 2\xi - \cos 2\eta)\right] .$$

Equation (13) represents a set of M x N independent, linear and homogeneous equations in A_{ij}.

If simple harmonic motion is assumed in the vibration problem then the deflection function W can be written as

$$W(\xi,\eta,\tau) = w(\xi,\eta)e^{i\omega\tau} .$$

The inertial load is then

$$q = -\frac{\rho t\ddot{W}}{e^{i\omega\tau}} = \rho\tau\omega^2 w ,$$

where τ is time,

ρ is mass density of the plate,

t is plate thickness,

$\ddot{W}$ represents the second derivative of W with respect to time,

and ω is the natural frequency of vibration of the plate.

It was noted earlier that the deflection function, $w(\xi,\eta)$, can be chosen such that the maximum deflection occurs near the free edge of the hole and goes to zero as the distance from the hole becomes unbounded. A detailed discussion of $w(\xi,\eta)$, which is a function of the space variables only, will be presented in a subsequent section.

Referring to Figure 7 and Equation (13), ξ varies from $\xi_1 = \xi_o$ (edge of the elliptic hole) to an outer boundary at $\xi = \xi_2$. Due to the symmetry of the elliptic hole about both the x-and y-axis, only one quadrant of the coordinate space needs to be considered. Hence, η will range from $\eta_1 = 0$ to $\eta_2 = \pi/2$. In the numerical integration, the upper limit ξ_2 of the area integral can be taken as some finite number which is large compared to the dimension of the elliptic hole. It is finally possible to write Equation (13) as

$$\int_{\xi_o}^{\xi_2}\int_0^{\pi/2} L(w_{MN})\varphi_{ij}\, AB\, d\xi\, d\eta - \int_0^{\pi/2}\left\{M_\xi \frac{B}{A}\frac{\partial\varphi_{ij}}{\partial\xi}\right\}\Bigg|_{\xi_o}^{\xi_2} d\eta \tag{14}$$

$$+ \int_0^{\pi/2}\Bigg[\Bigg\{\left(M_\xi \frac{B}{A}\right)_{,\xi} + M_\xi \frac{B}{A^2} A_{,\xi} - M_\eta \frac{B_{,\xi}}{A} + 2(M_{\xi\eta})_{,\eta} + 2\, M_{\xi\eta}\frac{A_{,n}}{A}$$

$$+ N_\xi \frac{B}{A} w_{,\xi} + N_{\xi\eta}\, w_{,\eta}\Bigg\}\varphi_{ij}\Bigg|_{\xi_o}^{\xi_2}\Bigg] d\eta = 0,$$

where

$$L(w_{MN}) = D\nabla^2\nabla^2 w_{MN} - N_\xi(K_\xi)_{MN} - N_\eta(K_\eta)_{MN} - 2N_{\xi\eta}(K_{\xi\eta})_{MN} - \rho t\omega^2\, w_{MN}.$$

Note that, on $\xi = \xi_o$ (edge of the elliptic hole), $N_\xi = 0$ and $N_{\xi\eta} = 0$. As mentioned earlier,

$$w_{MN}(\xi,\eta) = \sum_{i=1}^{M} \sum_{j=1}^{N} A_{ij}\, \varphi_{ij}\, (\xi,\eta).$$

After substituting the above w_{MN} and selecting a form for $\varphi_{ij}(\xi,\eta)$, the indicated integrations in Equation (14) can be performed. The final form of Equation (14) represents a set of M x N independent, linear and homogenous equations in the A_{ij}'s. The above equations can be conveniently written in a matrix notation as

$$\left[\left[B_1\right] - \lambda \left[B_2\right] - \Omega \left[B_3\right] \right] \left\{A_1\right\} = 0 , \qquad (15)$$

where

$\left\{A_1\right\}$ is a column matrix which contains the A_{ij}'s and is of the order (M x N) x 1,

$\left[B_1\right]$, $\left[B_2\right]$ and $\left[B_3\right]$ are square matrices of the order (M x N) x (M x N),

In Equation (15) $\lambda = P\, t\, h^2/D$, so that λ is defined as a nondimensional load parameter. In this definition

P is applied uniform tensile stress,

D is flexural rigidity of the plate.

In addition Ω is defined as the nondimensional frequency parameter $\Omega = \rho\, t\, \omega^2\, h^4/D$.

The Buckling Problem

Equation (15) includes as special cases the buckling and vibration problems. For the case of buckling, the inertia term represented by the nondimensional frequency parameter, Ω , is absent. The equation governing the static buckling problem is then

$$\left[\left[B_1\right] - \lambda \left[B_2\right] \right] \left\{A_1\right\} = 0, \tag{16}$$

or,

$$\left[B_1\right] \left\{A_1\right\} = \lambda \left[B_2\right] \left\{A_1\right\} . \tag{17}$$

Equation (17) can be written as

$$\left[B_1\right]^{-1} \left[B_2\right] \left\{A_1\right\} = \frac{1}{\lambda} \left\{A_1\right\} ,$$

or

$$\left[B_4\right] \left\{A_1\right\} = \frac{1}{\lambda} \left\{A_1\right\} . \tag{18}$$

Equation (18) represents an eigenvalue problem, where the elements of $\left\{A_1\right\}$ are the eigenvectors and the λ's are eigenvalues. Equation (18) can be solved for the eigenvalues and corresponding eigenvectors by matrix iteration [66]. The first iteration of Equation (18) will converge to the largest value of λ^{-1} which corresponds to the lowest buckling load. The corresponding eigenvectors (mode shape) are also obtained as $\left\{A_1\right\}$.

The Vibration Problem

Equation (15) can also be used for the vibration problem of the present investigation. The aim is to obtain the natural frequency of the free vibration for different values of tensile load. For a given value of λ , Equation (15) can be written as

$$\left[B_5\right]\left\{A_1\right\} = \Omega\left[B_3\right]\left\{A_1\right\} , \tag{19}$$

where

$\left[B_5\right]$ is a square matrix = $\left[\left[B_1\right] - \lambda\left[B_2\right]\right]$ of the order $(M \times N) \times (M \times N)$.

Equation (19) can be written as

$$\left[B_5\right]^{-1}\left[B_3\right]\left\{A_1\right\} = \frac{1}{\Omega}\left\{A_1\right\} ,$$

or

$$\left[B_6\right]\left\{A_1\right\} = \frac{1}{\Omega}\left\{A_1\right\} . \tag{20}$$

For a given value of λ (corresponding to the applied tension) Equation (20) is an eigenvalue problem. Matrix iteration can again be employed to obtain the eigenvalues (frequencies of vibration) and the eigenvectors (mode shapes). The first iteration of Equation (20) will converge to the largest value of Ω^{-1} which corresponds the lowest natural frequency. The corresponding eigenvectors can then be obtained as $\left\{A_1\right\}$. In this manner the natural frequency of vibration and the corresponding mode shape can be obtained for different values of λ. Note that the value of λ corresponding to the lowest eigenvalue for buckling causes Ω in Equation (15) to be zero.

The Deflection Function

The choice of a deflection function is usually made to satisfy the geometric boundary conditions. The natural boundary conditions are generally more difficult to satisfy and often functions which are selected do not satisfy them. In some approximate methods of solution, only geometric boundary conditions need to be satisfied. Naturally, the solution constructed improves if the approximate functions also satisfy the natural boundary conditions.

In the problem of interest here it is desirable to be able to represent the solution by a sum of linearly independent functions which are given. Developments of this type are discussed in references [62-65]. It is known that a set of orthonormal functions $\varphi_i(x)$ can be used to represent a function $f(x)$ as

$$f(x) = \sum_{i=1}^{n} a_i \, \varphi_i(x),$$

where the coefficients a_i are constants. The mathematical problem here is to establish how good this representation is. If a good representation is desired, then it is necessary for the orthonormal set to be complete. The orthonormal set is said to be complete if for each function $f(x)$ over $x_1 \leq x \leq x_2$ and $\varepsilon > 0$, there exist an index n

such that [64]

$$\int_{x_1}^{x_2} \left| f(x) - \sum_{i=1}^{n} a_i \varphi_i(x) \right|^2 dx < \epsilon .$$

For a complete orthonormal system of functions, it has been shown that [63-64]

$$a_i = \int_{x_i}^{x_2} f \varphi_i(x) \, dx.$$

In some instances it is necessary to use sets which have not been orthonormalized. The concept of conpleteness can also be used in this case. According to Courant and Hilbert [63],

> The concept of completeness of a linearly independent system of functions retains its meaning even if the system is not orthonormal. In general, we call a system of functions complete if every piecewise continuous function can be approximated in the mean arbitrarily closely by a linear combination of functions of the system. The completeness of such a system is preserved under the process of orthogonalization.

The above discussion on the nature of the approximate functions refers to one dimensional function space. Without loss of generality, the same discussion can be extended to two or many dimensional function space.

In the subsequent discussion the two dimensional plate deflection function is the solution function. Let $w(\xi,\eta)$ be the deflection function which is continuous in ξ, η in a given region. Then $w(\xi,\eta)$ can be approximated in the function space as a linear combination of φ_{ij}'s. Hence,

$$w_{MN}(\xi,\eta) = \sum_{i=1}^{M} \sum_{j=1}^{N} A_{ij}\varphi_{ij}(\xi,\eta), \tag{21}$$

in the given interval. Here, the φ_{ij}'s are a set of linearly independent functions in the function space in the given interval and the A_{ij}'s are the expansion coefficients. Let $\varphi_{ij}(\xi,\eta)$ be expressed in the form

$$\varphi_{ij}(\xi,\eta) = f_i(\xi)g_j(\eta),$$

with $i = 1, 2, \ldots, M$ and $j = 1, 2, \ldots, N$. In the development to follow both the $f_i(\xi)$ and the $g_j(\eta)$ are chosen to form linearly independent sets.

If M and N are taken as infinite, an exact representation of $w(\xi,\eta)$ in the form of Equation (21) is obtained if the φ_{ij}'s form a complete set in the function space of the relevant interval. For practical engineering problems, however, M and N usually are taken as finite numbers. In the use of a representation such as Equation (21), the knowledge that the φ_{ij}'s form a complete set is useful because one can then be confident that if a sufficient number of terms are used, a good representation can be expected.

It is known that completeness can often be difficult to demonstrate. Also, since the existence of completeness does not, in itself, ensure that convergence will be rapid, an alternate procedure for evaluating computational results is desirable. For example, a procedure for obtaining upper and lower bounds might be developed. Correlation with experimental results can also provide a basis for evaluating the compuational results. In the investigation described here, an experimental program was conducted to provide data for evaluating the analytical results.

The selection of sets of approximation functions was influenced by the factors discussed above. In particular, it was found convenient to select a set of $g_j(\eta)$'s which both possess the property of orthogonality on the given interval and is known to be complete. For the $f_i(\xi)$ a linearly independent set which does not possess the orthogonality property was chosen. No attempt is made to prove completeness for this set. Note, however, that since the form of the nth function is known for both the f_i and the g_j, a systematic basis for developing a solution is established, and as many terms as desired can be used.

In the problem under investigation, the deflection function is approximated in the form of Equation (21),

$$w_{MN}(\xi,\eta) = \sum_{i=1}^{M} \sum_{j=1}^{N} A_{ij}\varphi_{ij}(\xi,\eta).$$

The $\varphi_{ij}(\xi,\eta)$ are chosen such that the maximum deflection occurs near the edge of the hole $(\xi = \xi_o)$ and the deflection and its derivatives tend to zero as ξ becomes unbounded. As mentioned earlier $\varphi_{ij}(\xi,\eta)$ can be represented in the form

$$\varphi_{ij}(\xi,\eta) = f_i(\xi)g_j(\eta),$$

with $i = 1, 2, \ldots, M$ and $j = 1,2,\ldots, N$. The form of $f_i(\xi)$ and $g_j(\eta)$ will be discussed separately.

A form is $f_i(\xi) = (\xi_o/\xi)^i$ with $i = 1,2,3,\ldots, M$, where $\xi = \xi_o$ represents the edge of the hole. Each term in the above form of $f_i(\xi)$ is linearly independent with respect to all others (Appendix B). $f_i(\xi)$ attains its maximum value at the free edge of the hole and tends to zero as ξ becomes unbounded. Convergence becomes very slow for the above form of $f_i(\xi)$ when the elliptical hole is narrow; i.e., when $\xi_o << 1$. The function is however satisfactory *when the ellipse approaches the circle.*

In order to eliminate the limitations associated with the above form of $f_i(\xi)$ other possibilities were considered. One which appeared to eliminate the difficulty cited above was examined and finally adopted. It has the form

$$f_i(\xi) = e^{-i\xi}$$

with $i = 1,2,3, \ldots, M$. This form of $f_i(\xi)$ again satisfies the requirement that the maximum value of $f_i(\xi)$ is obtained at the free edge of the hole $(\xi = \xi_o)$ and it goes to zero as ξ becomes unbounded. Again, each term in the above form of $f_i(\xi)$ can be shown to be linearly independent with respect to all others (Appendix B).

The forms of $g_j(\eta)$ selected are trigonometric sine and cosine terms. Different forms of $g_j(\eta)$ are listed below depending on the symmetry and antisymmetry about the x-y axes.

For symmetry about x-and y-axes,

$g_j(\eta) = \cos 2j\eta$ with $j = 0,1,2,3, \ldots , N$

For symmetry about x-axis and antisymmetry about y-axis,

$g_j(\eta) = \cos (2j + 1)\eta$ with $j = 0,1,2,3, \ldots , N$

For symmetry about y-axis and antisymmetry about x-axis,

$g_j(\eta) = \sin (2j + 1)\eta$ with $j = 0,1,2,3, \ldots , N$

For antisymmetry about x-and y-axis,

$g_j(\eta) = \sin 2j\eta$ with $j = 1,2,3, \ldots , N$

It should be noted that the terms $g_j(\eta)$ are linearly independent of one another. They also possess the property of orthogonality on the given interval and they are known to form a complete set when N is infinite.

CHAPTER IV

EXPERIMENTAL AND ANALYTICAL RESULTS

Introduction

In the previous chapter, the equations governing the buckling and vibration behavior of a thin tensioned sheet with an elliptic hole were described. The choice of approximate deflection functions for the problems was discussed, and the solution procedure of the resulting eigenvalue problems was described. This chapter will be devoted to a presentation of the experimental and analytical results obtained for the buckling and the vibration problems.

The Buckling Problem

Experimental Results

The usefulness of any analytical result depends upon the degree to which it describes the actual behavior. Hence, the experimental program was designed to provide data from which buckling loads could be estimated.

The use of a specimen whose width and length are much larger than the hole dimensions would be desirable. The stress distribution on such a specimen would very nearly be that determined for the corresponding infinite sheet. This latter distribution is available from the results of Chapter III. A review of the photoelastic results of Durelli [58] for finite width sheets with elliptic holes suggests that a hole length to sheet width ratio of 0.1 or less would be desirable if the infinite sheet analysis is used to compute the stresses.

The difficulties associated with applying uniform traction to very wide specimens and the need to be able to achieve loads up to the buckling load without exceeding the elastic limit at the stress concentration caused the ratio value of 0.1 to be impractical. After a consideration of these factors, a hole length to sheet width ratio of 0.25 was adopted for all the hole geometries. Durelli did not present results for the entire stress field. The results presented, however, suggest that the difference between the stress distribution in the infinite sheet and the finite sheet increases as the ratio of the minor axis to the major axis of the ellipse decreases. The approximate nature of the stress analysis applied must, therefore, be kept in mind when results for the buckling and vibration problem are evaluated.

The specimens were made from 0.025 inch thick sheet of aluminum alloy, Alclad 2024-T3. End plates made of 0.375 inch thick bar stock of 2024-T4 aluminum alloy were bonded on both faces of the sheet with a room temperature curing epoxy. Two dowel pins were used at each end to assure proper alignment of the end plates on the sheet. The elliptic holes were made in the specimens using a numerically controlled milling machine which produced hole contours which were within 0.005 inch of the specified dimensions. The major axis of the elliptic hole was three inches and the minor axis was adjusted to provide the hole shapes desired. A typical specimen is illustrated in Figure 8.

Each specimen was loaded in an Instron testing machine and the load increments were chosen to provide enough data to obtain a good

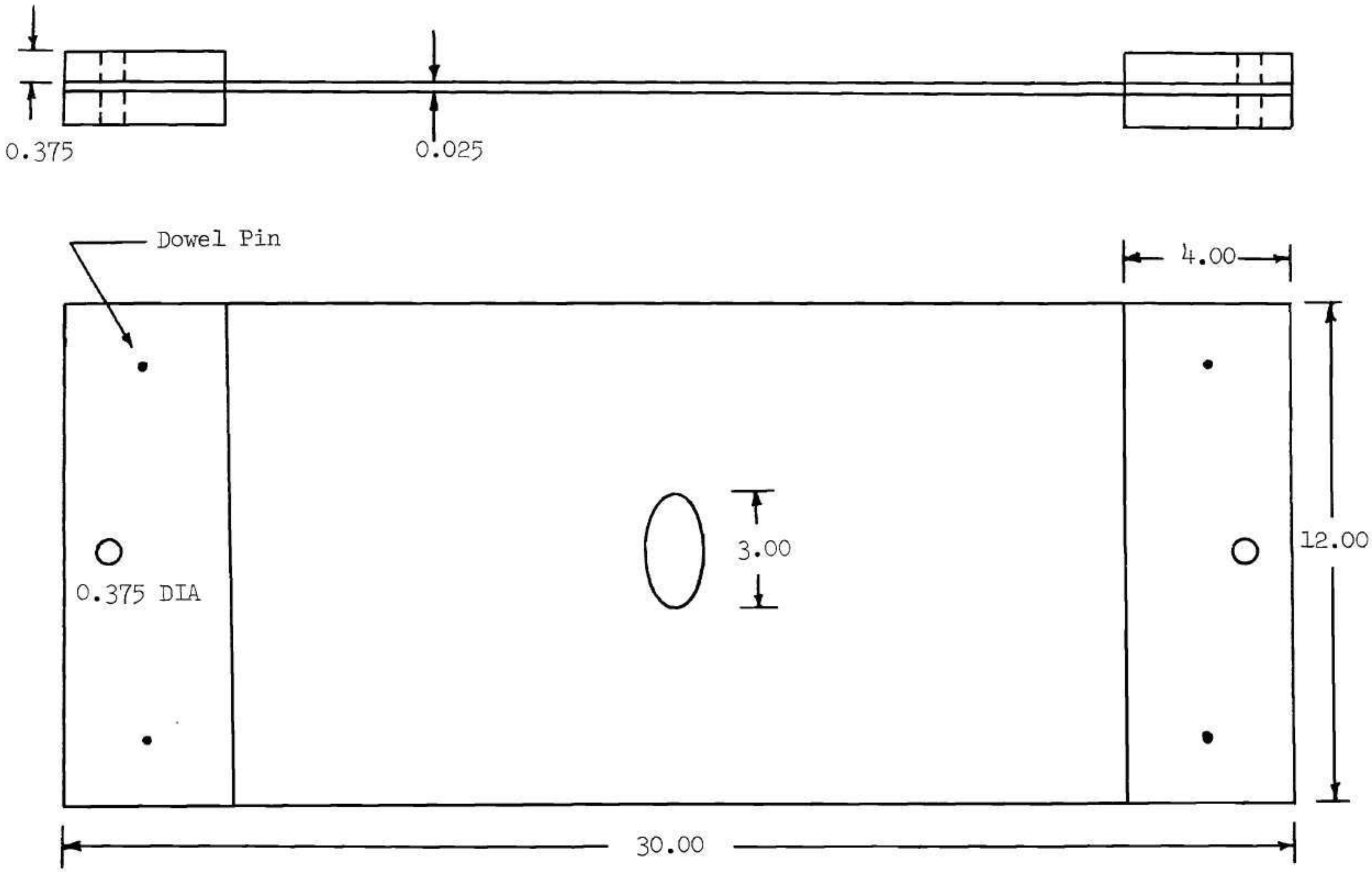

All dimensions in inches

Figure 8. Typical Plate Specimen

description of the response of the specimen to load. The proportional limit loads of the specimens were calculated from a knowledge of stress concentration factors and the material properties. Buckling load estimates were based on data obtained within the elastic range.

For analyzing the experimental results some measure of the lateral deflection of the free edge of the elliptic hole was required. Any quantity which provides a measure of the deflection is suitable. In the present case, a bending strain measurement was made because it was relatively easy to obtain. The bending strain is linearly proportional to the curvature which provides a local measurement of relative deflection. The bending strain was measured by use of electrical resistance strain gages which had a gage length of 0.25 inch. The gages were mounted back to back and centered on the specimen as close to the slot edge as practical. The strain sensitive direction was oriented prependicular to the direction of loading. The strain gage circuit was arranged to measure the difference of the two gage outputs. Actually, the difference of the two gages was twice the bending strain. The applied load and strain difference data for the different hole shapes considered are tabulated in Appendix C.

Estimation of the Buckling Loads from Experimental Data

One of the methods for estimating buckling loads from load vs deflection data is the Southwell method. If appropriate conditions are satisfied, the nonlinear, coupled governing equations can be replaced by a set of linear, uncoupled equations, and then a Southwell type deflection-load relationship can be derived. The applicability of the Southwell method of structural plate elements depends upon the degree to which the bent surface approaches a developable surface, the magnitude of the deflection, and the eigenvalue separation for the corresponding perfect plate problem [8,67]. If the amount of stiffening due to middle surface stretching is monitored in a plate experiment, the Southwell method can be applied. The final results can be given as a linear plot of w/λ versus w at a point on the plate, where w is the lateral deflection and λ is the load intensity.

In some instances the deflection behavior is erratic at small test loads. This type of behavior is common during the initial application of load in many structural experiments. To eliminate this behavior Lundquist [68] proposed a modified Southwell plot which tends to eliminate this erratic initial behavior.

A Lundquist type relation can be obtained in the same manner as the Southwell relation. The Southwell relation has the form

$$\lambda_1\left(\frac{w}{\lambda}\right) = w + c \quad ,$$

and the plotted variables are (w/λ) and w. In a modified form of the Lundquist type, the relation is

$$\left(\lambda_1 - \lambda_o\right)\left[\frac{w - w_o}{\lambda - \lambda_o}\right] = \left(w - w_o\right) + d \ .$$

In these equations c and d are measures of the initial imperfections. λ_1 is the first eigenvalue for the corresponding perfect plate problem [8,67]. In the latter relation the plotted variables are $(w - w_o)/(\lambda - \lambda_o)$ and $(w - w_o)$. λ_o and w_o are arbitrary initial values of load and deflection selected to eliminate the erratic initial behavior of the load vs deflection response.

If twice the bending strain is defined as $\Delta\varepsilon$, and P is the applied load, then the corresponding variables plotted are

$$\frac{\Delta\varepsilon - \Delta\varepsilon_o}{P - P_o} \quad \text{and} \quad (\Delta\varepsilon - \Delta\varepsilon_o) \; .$$

The inverse of the slope of the line obtained may then be identified as the magnitude of $(P_1 - P_o)$ where P_1 is the value corresponding to the smallest eigenvalue. A detailed discussion of the Southwell method and its applicability in plate stability problems is discussed by Carlson and Datta [67] and Zielsdorff in his Ph.D. thesis [8].

Lundquist plots of the data obtained for the four elliptical shapes tested are presented in Figures 9, 10, 11, and 12. It may be noted that the data points lie below the plotted lines for the larger values of strain difference in each plot. This behavior reflects stiffening (for a given $(\Delta\varepsilon - \Delta\varepsilon_o)$ the value of $(\Delta\varepsilon - \Delta\varepsilon_o)/(P - P_o)$ decreases) which accompanies middle surface stretching due to bending. This effect and its consequences will be discussed in Chapter V.

The experimentally determined buckling stress estimates for all of the hole shapes are presented in Table 1.

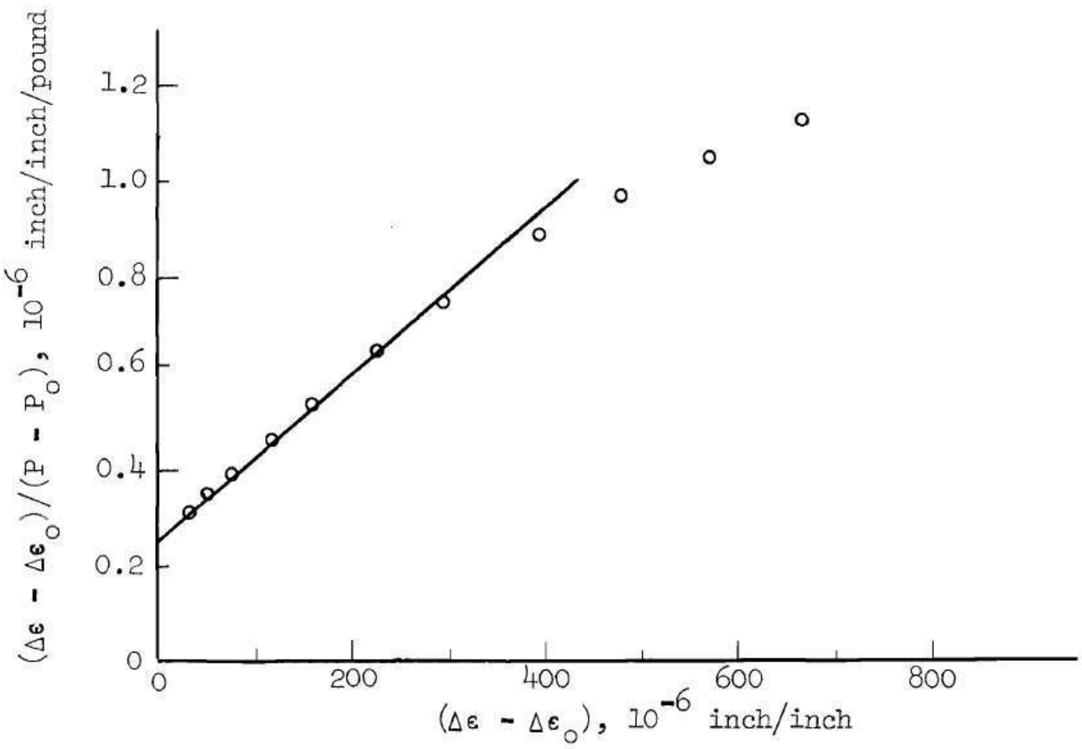

Figure 9. Lundquist Plot for b/a = 0.2

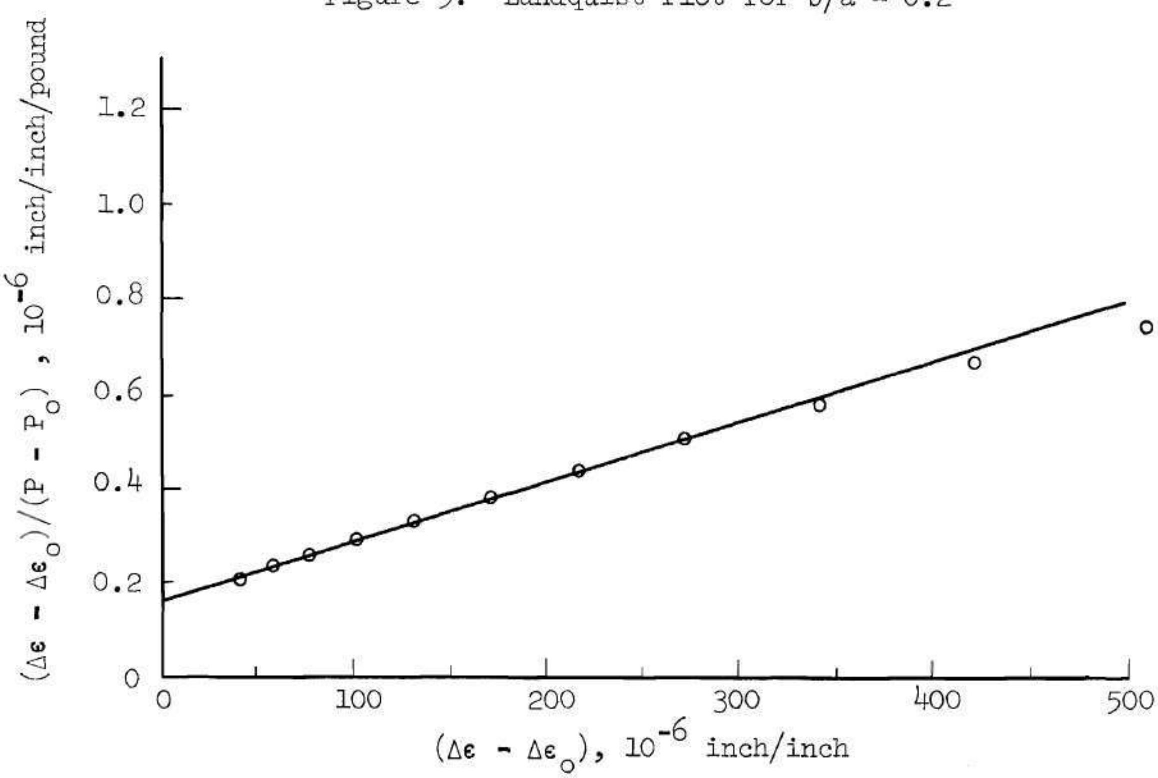

Figure 10. Lundquist Plot for b/a = 0.4

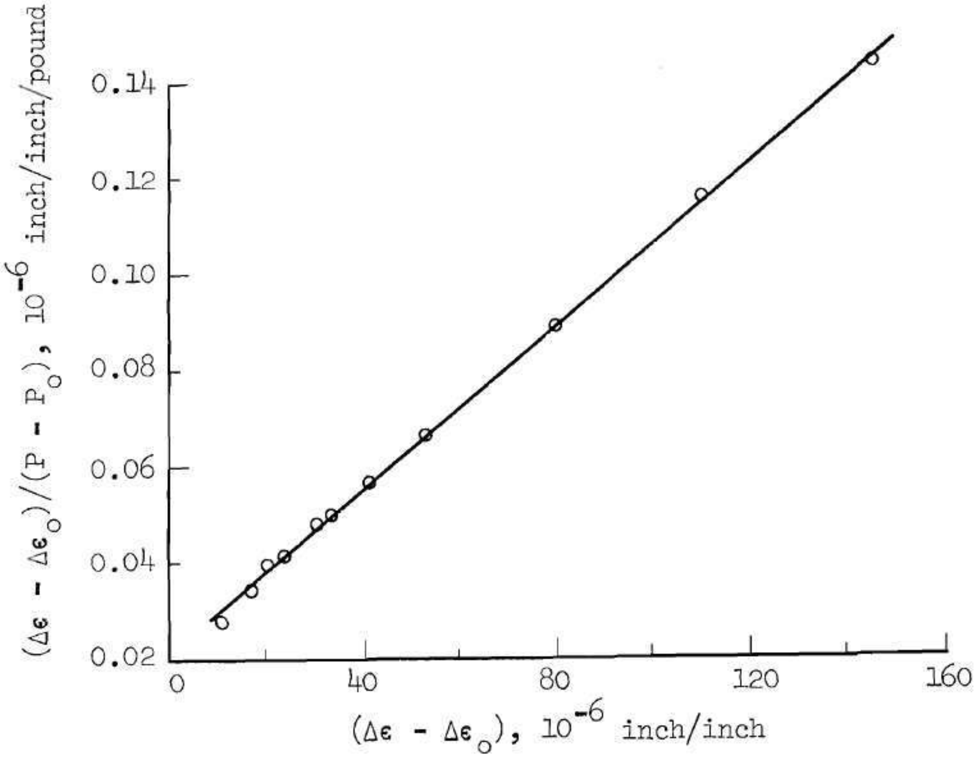

Figure 11. Lundquist Plot for b/a = 0.6

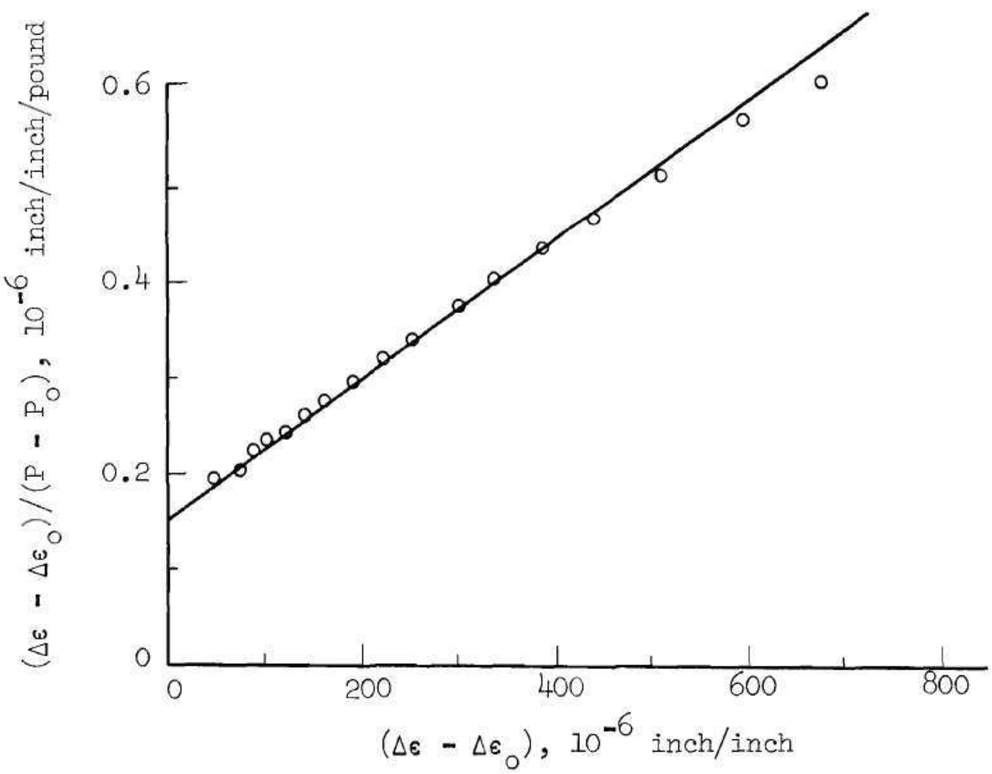

Figure 12. Lundquist Plot for b/a = 0.8

Table 1. Experimental Buckling Stress Estimates

b/a	0.2	0.4	0.6	0.8
Buckling Stress (psi)	3900	4600	5300	5800

Analytical Results

The equation governing the buckling behavior is presented as Equation (18) of the previous chapter and it may be written as

$$\left[B_4\right]\left\{A_1\right\} = \frac{1}{\lambda}\left\{A_1\right\} . \tag{1}$$

The matrix $\left[B_4\right]$ was derived earlier from matrices $\left[B_1\right]$ and $\left[B_2\right]$ whose elements are values computed from the area and line integrals in the formulation used to describe the problem.

The limits of integration chosen for the area and line integrals of Equation (18) of Chapter III were different for each value of the b/a ratio. In essence the analytical model used was an annular elliptic plate with an inner boundary at $\xi = \xi_o$ and an outer boundary at $\xi = \xi_2$. The tabulation below indicates the size of the annular plates for each b/a ratio. Note that the values for the axes give in inches the corresponding axes of the opening in the test specimens.

b/a	Major Axis*		Minor Axis	
	$\xi = \xi_o$	$\xi = \xi_2$	$\xi = \xi_o$	$\xi = \xi_2$
0.2000	3.000	132.1	0.600	132.0
0.4000	3.000	202.0	1.200	202.0
0.6000	3.000	396.0	1.800	396.0
0.8000	3.000	504.0	2.400	504.0

* $2a = 3.000$

The integration giving the values of the elements was performed numerically by use of the trapezoidal rule. Typically, the area was divided into 20,000 elements and the line integral was divided into 100 divisions. These divisions were within a quarter plane and for the model with $b/a = 0.2$, for example, the subdivisions are given below.

Area Integrals:

In range: $0 \le \eta \le \pi/2$, 100 divisions

In range: $\xi_1 \le \xi \le \xi_2$, 200 divisions

$\xi_1 = 0.2025$ at the inner boundary and $\xi_2 = 4.500$ at the outer boundary

Line Integrals:

In range: $0 \le \eta \le \pi/2$, 100 divisions

In Equation (1) the quantity λ is defined as the nondimensional load parameter which is obtained as the eigenvalue in the matrix iteration process. The lowest value of λ corresponds to the buckling load which is of primary interest. The elements of the column matrix

$\left\{A_1\right\}$ are the eigenvectors which correspond to the mode shape. In Chapter III λ is expressed as,

$$\lambda = P \frac{th^2}{D} \quad \text{or} \quad P = \lambda \frac{D}{th^2}, \tag{2}$$

Where P is the uniform, unidirectional buckling tensile stress.t is the plate thickness, E is Young's modulus, $D = Et^3/\ 12(1 - \nu^2)$, ν is Poisson's ratio, $h^2 = (a^2 - b^2)^*$, and a, b are the semi-major and semi-minor axis of the ellipse, respectively. For the computations and experiments, $t = 0.025$ inch, $E = 10.5 \times 10^6$ psi, and $\nu = 1/3$.

The buckling load was observed during experiments to have a mode shape which was symmetric with respect to both the semi-major and the semi-minor axes. It was, therefore, appropriate to take a deflection function which is symmetric about both axes in the analysis. The eigenvalue Equation (1) was solved by the matrix iteration process for the highest eigenvalue associated with the lowest critical load. The eigenvalues and the corresponding eigenvectors were determined for all of the hole shapes considered.

Equation (1) was also solved for a deflection function which is symmetric about y-axis and antisymmetric about the x-axis for one hole shape. The later case is discussed in Chapter V.

---

* Note that Equation (2) cannot be used for the circular opening because as $b \rightarrow a$, $h \rightarrow 0$ and $P \rightarrow \infty$.

The deflection function for the symmetric case is written as

$$w_{MN}(\xi,\eta) = \sum_{i=1}^{M} \sum_{j=0}^{N} A_{ij} e^{-i\xi} \cos 2j\eta, \tag{3}$$

where ξ, η are the nondimensional elliptic coordinates for the given system and the A_{ij}'s are the unknown coefficients of the deflection function.

It should be noted that the choice of w_{MN} in Equation (3) implies that natural boundary conditions (see Chapter II) are present on both the inner and outer boundaries of the annular plate. This, of course, corresponds to the case of zero moment and zero transverse effective shear on both edges.

Equation (2) can be used to compute the buckling stresses when the λ's are obtained. The values of the computed buckling stresses for the hole shapes with respect to the number of terms in the solution are shown in Figure 13. In Figure 13 a 6 term solution indicates, $M = 2$ and $N = 3$ in Equation (3), a 9 term solution indicates, $M = 3$ and $N = 3$ in Equation (3), a 12 term solution indicates, $M = 3$ and $N = 4$ in Equation (3), and a 15 term solution indicates, $M = 3$ and $N = 5$ in Equation (3). The convergence for the values of buckling stresses is good for the cases of $b/a = 0.2$ and 0.4. For the cases of $b/a = 0.6$ and 0.8 more terms would be required to obtain comparable results. Because a trend has been established and since the computational effort is great, the estimation was discontinued at 12 terms for $b/a = 0.6$ and at 15 terms for $b/a = 0.8$. All of the estimates computed are

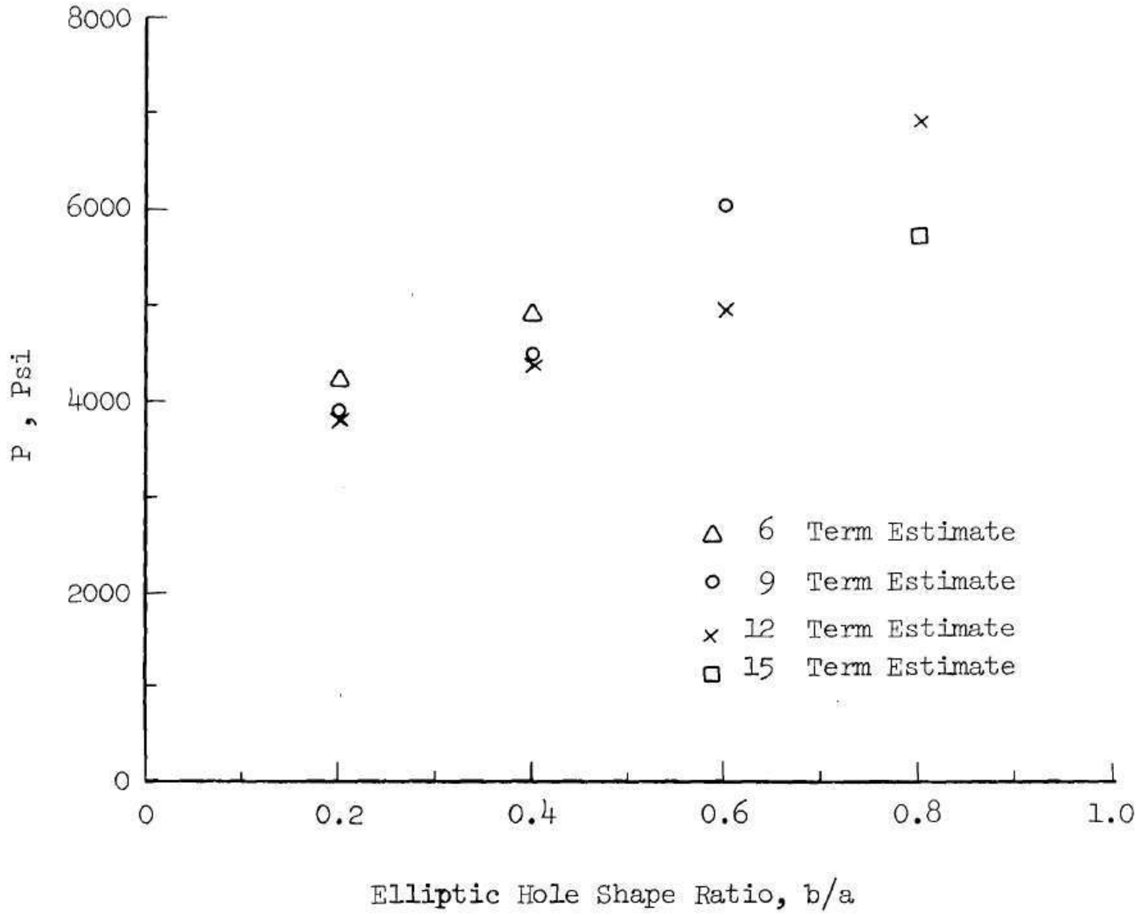

Figure 13. Analytical Buckling Stress Estimates for Different Hole Shapes

shown in Figure 13.

A discussion of the symmetric mode shapes which are associated with the eigenvalue estimate for the case of $b/a = 0.2$ is presented in Chapter V.

The Vibration Problem

Experimental Results

Experiments were conducted to find the natural frequency of vibration of the sheet specimen for different values of applied tensile stress. The tests were conducted in a specially built tensile testing machine. The test rig used is capable of applying a load of up to 5000 pounds to the specimen. Figure 14 shows the test machine. A hydraulic loading system was used to apply the load. The load was measured by reading the output of a calibrated load cell on a strain indicator.

The same type of test specimen used in the buckling experiments was used in the vibration experiments. A schematic diagram of the test facility is shown in Figure 15. In the test facility the loaded plate was excited by an electrodynamic shaker. An audio oscillator in conjunction with a power amplifier was used to generate the input signal. The electrodynamic shaker was connected to the lower end plate of the specimen on the vertical line of symmetry. This method of attachment eliminated problems which would occur if the connection was made directly to the sheet; i.e., changes in the effective mass of the sheet.

A load cell attached at the point of contact between the end plate and the shaker provided a signal for the input exciting force

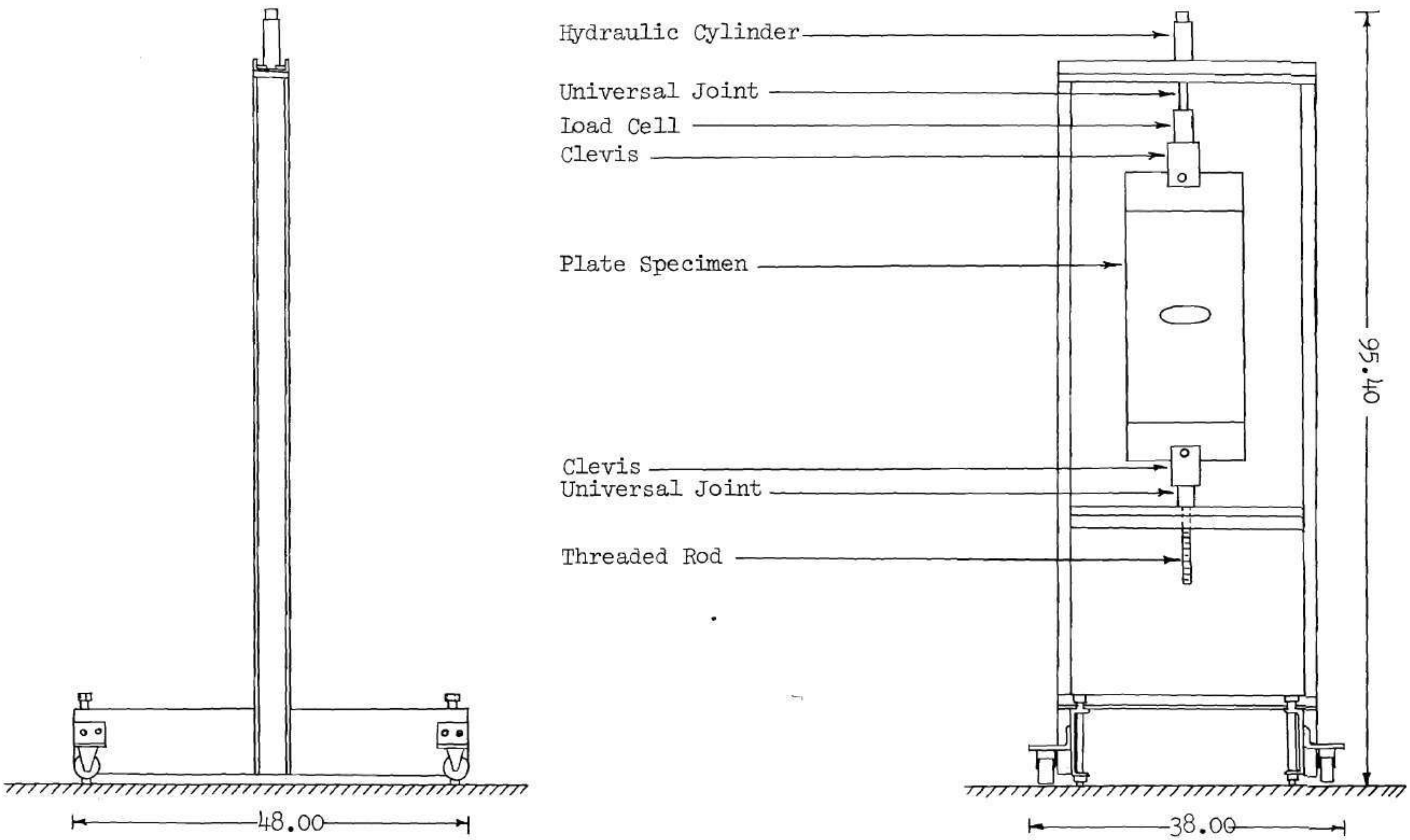

Figure 14. Test Stand

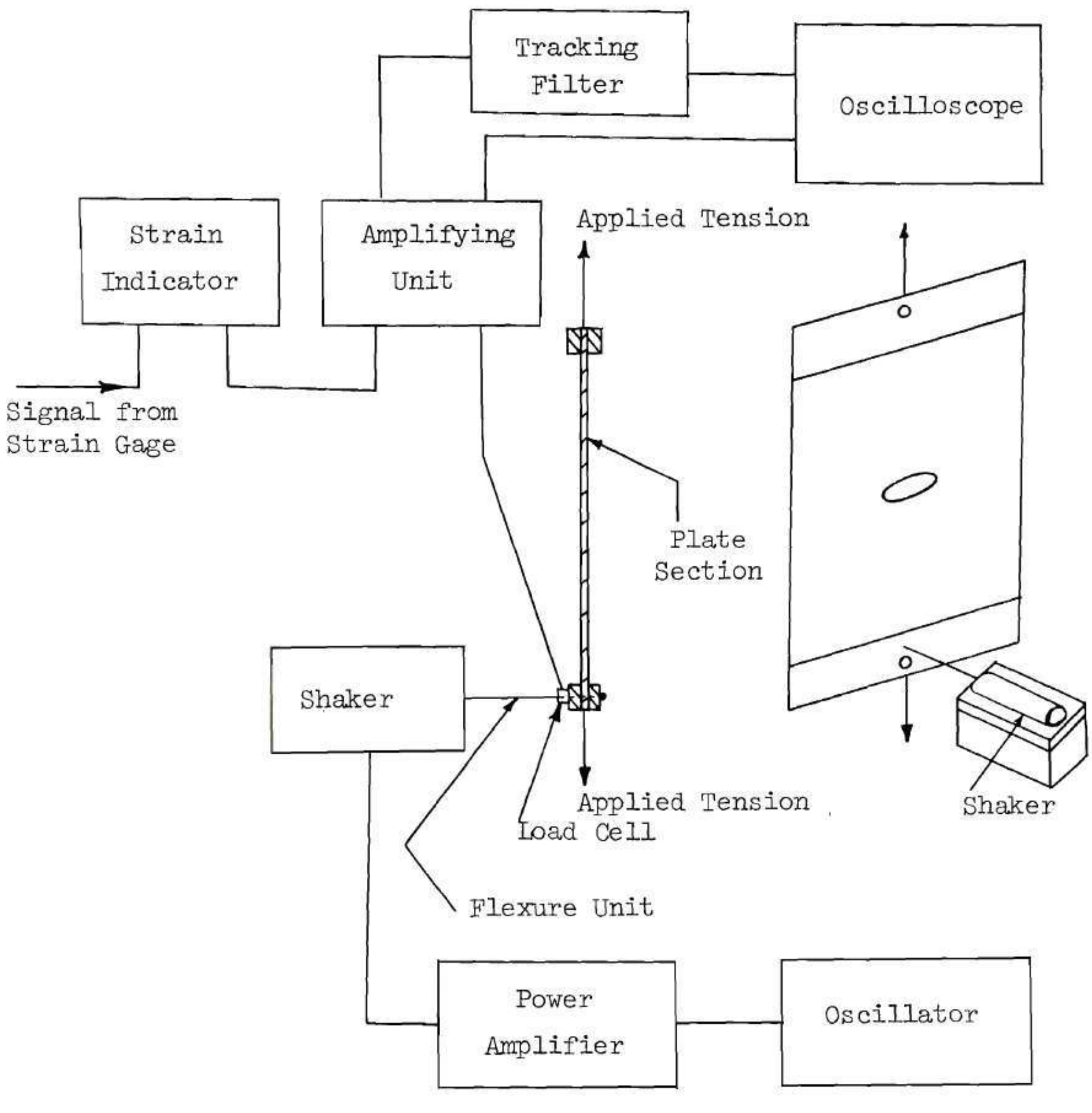

Figure 15. Schematic of Test Facility

from the shaker. The response of the free edge of the elliptic hole was measured by the use of strain gages. Two strain gages were mounted back to back as close to the slot edge as practical with their strain sensitive direction perpendicular to the line of loading. A bridge was connected such that the reading measured the difference of the two gage outputs. The difference of the two gage outputs provide a measure of the bending strain. To observe the dynamic bending strain, a BLH strain indicator was used to amplify the signal which was fed to an oscilloscope. A list of all of the instruments used in the vibration experiments is given in Table 2.

The natural frequency of vibration at different tensile stresses can be detected very accurately by use of an oscilloscope. The exciting force signal was amplified through a two-channel amplifier and was fed into the vertical input of the oscilloscope. The response (dynamic bending strain) signal from the strain indicator was amplified through the second channel of the two-channel amplifier and fed into a tracking filter. The filtering unit eliminated the noise from the main signal. The response signal was then fed into the horizontal input of the oscilloscope. The force vs response trace on the oscilloscope was an ellipse as shown in Figure 16. The change in sign of the in-phase component of response was used as an indication of transition through the natural frequency. The change is indicated in the diagram with $\omega = \omega_n$ corresponding to the natural frequency.

The data obtained are shown as frequency vs applied tensile stress plots in Figures 17 and 18 for different values of b/a ratio.

Table 2. Instrument Specifications

INSTRUMENT	MODEL	MANUFACTURER
Electrodynamic Shaker	PM-25 Exciter	M. B. Electronics
Load Cell	Model 912 Quartz Cell	Kistler Instrument Corp.
Power Amplifier	Model 2125MB	M. B. Electronics
Oscillator	209A Oscillator	Hewlett-Packard
Strain Indicator	BLH Strain Indicator Type 20	BLH, Inc.
Amplifying Unit	N400 Zero Drive Data Acquisition Amplifier Module	M. B. Electronics
Tracking Filter	Model SD101B Dynamic Analyzer	Spectral Dynamics Corp.
Oscilloscope	Type 502A Dual-Beam Oscilloscope	Tektronix, Inc.
Flexure Unit	- - - - - - -	Designed and made in laboratory

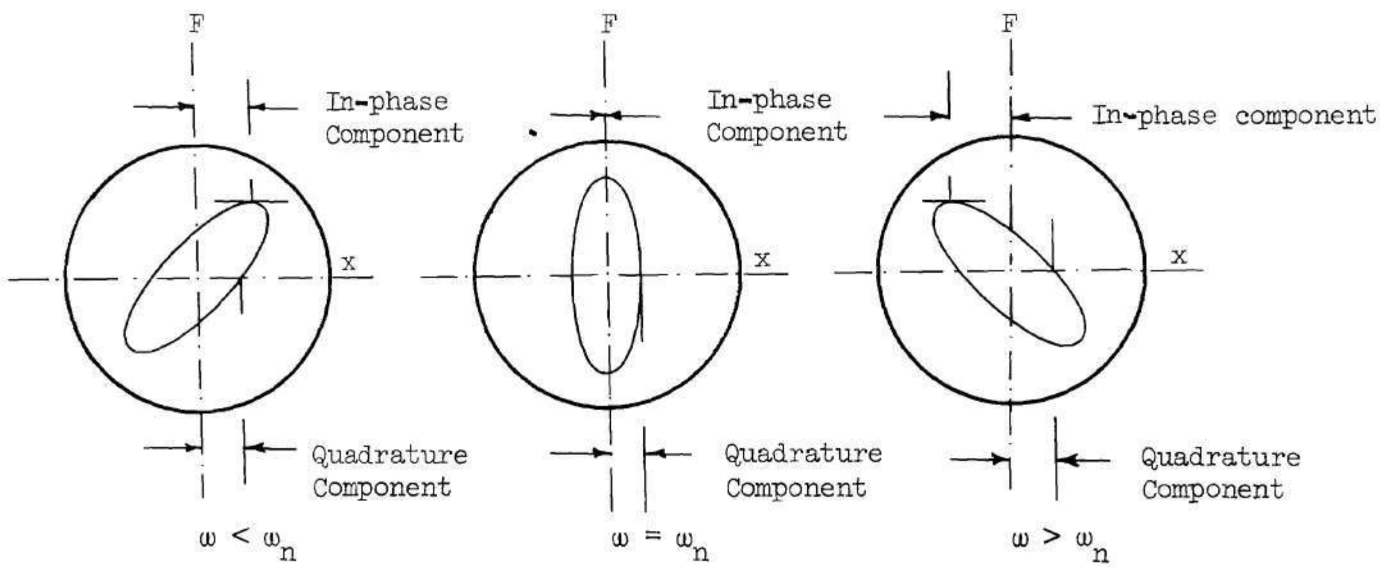

Figure 16. Force vs Response Plot on the Oscilloscope Screen

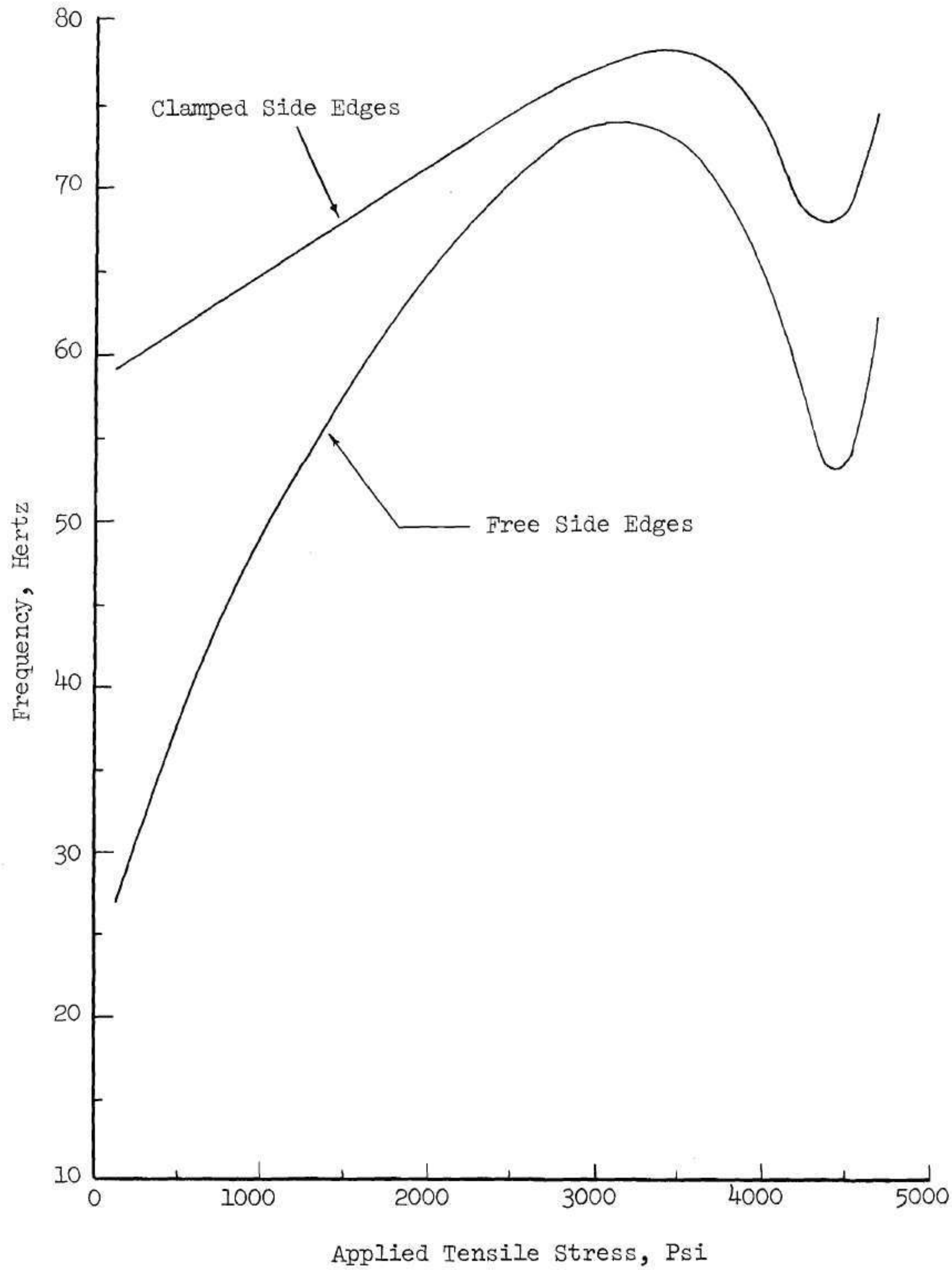

Figure 17. Experimental Stress vs Frequency Plot for b/a = 0.2

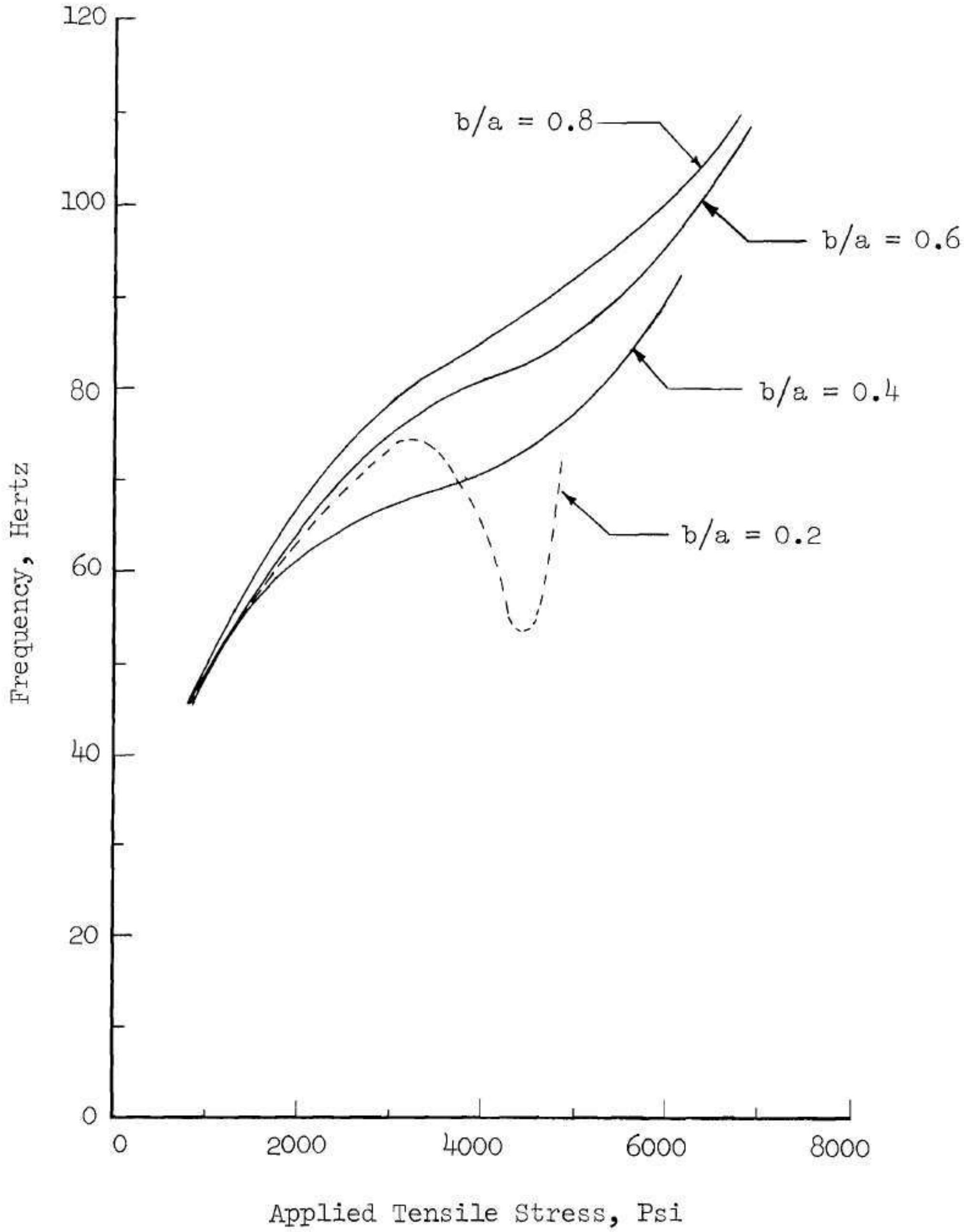

Figure 18. Experimental Stress vs Frequency Plot for All Hole Shapes

The curves shown in Figures 17 and 18 are based on a large number of data points which uniformly cover the indicated range of applied stress. No less than 35 data points were obtained for each curve and all points lie on the indicated curves. The upper curve shown in Figure 17 represents the case of the side edges clamped. This test was conducted to check the influence of constraint on the vibration behavior of the specimen. It may be noted that the constraint effect is substantial. This will be further discussed in Chapter V.

Analytical Results

The equation governing the vibration problem is presented as Equation (20) of the previous chapter and it may be written as

$$\left[B_6\right]\left\{A_1\right\} = \frac{1}{\Omega}\left\{A_1\right\} . \qquad (4)$$

The evaluation of the matrix $\left[B_6\right]$ was carried out according to the procedure used for the analysis of the buckling problem. Ω is defined as the nondimensional frequency parameter which is obtained as the eigenvalue in the matrix iteration process. The elements of the column matrix $\left\{A_1\right\}$ are the eigenvectors which correspond to the mode shape. Ω is expressed as,

$$\Omega = \frac{\rho t \omega^2 h^4}{D} \quad \text{or} \quad \omega^2 = \Omega \frac{D}{\rho t h^4} ,$$

where ω is the natural frequency of vibration, ρ is the mass density of the sheet material and the quantities D, t, h have been defined previously.

Because the experimentally observed mode shape was symmetric, a symmetric deflection function was used for the analysis. The analysis was carried out for the case of $b/a = 0.2$ with the same size annular plate as used for the corresponding buckling problem. A twelve term estimate was used to compute frequencies for different values of applied tensile stress. The results are shown in Figure 19. The corresponding experimental plot for $b/a = 0.2$ is also shown in Figure 19.

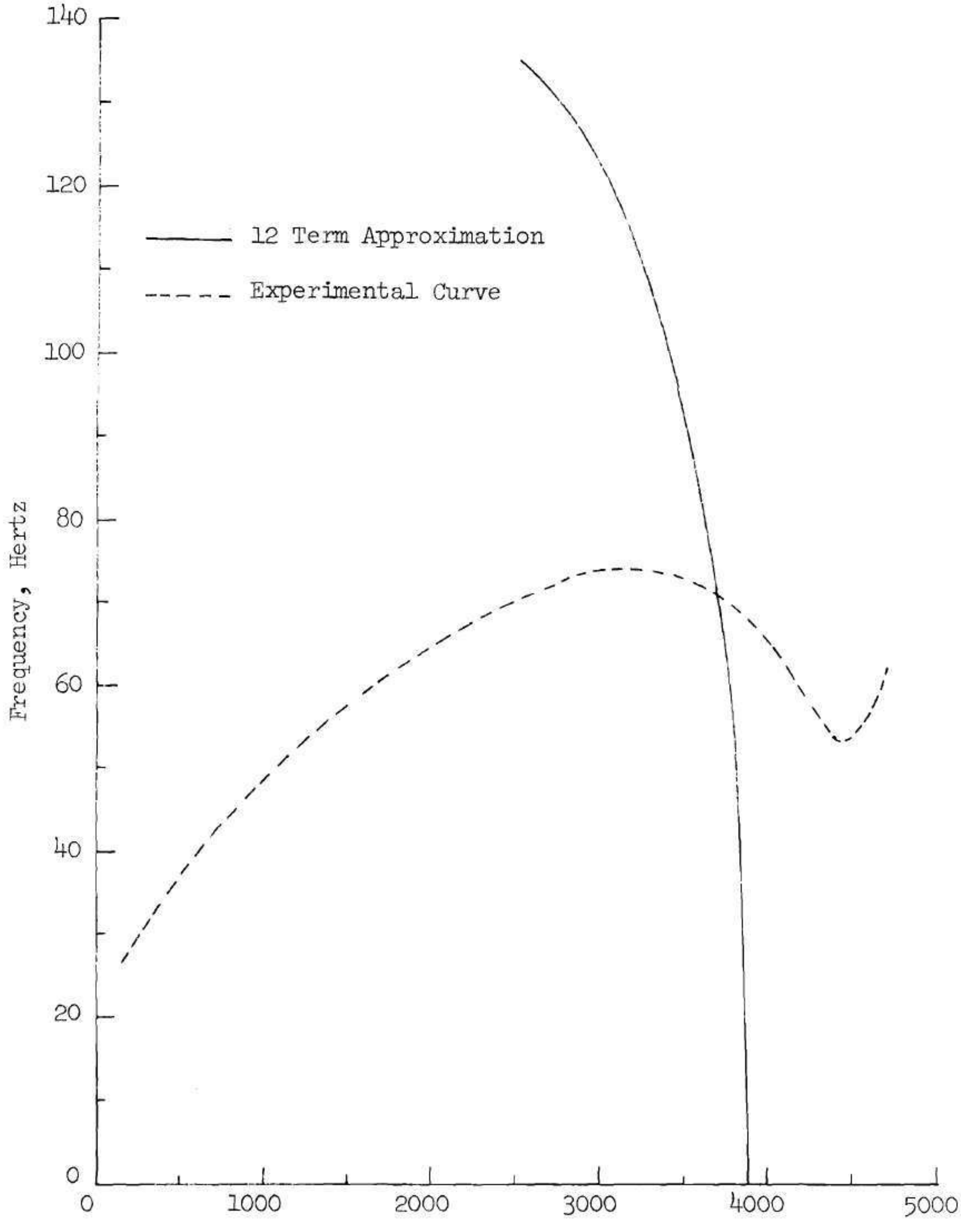

Figure 19. Analytical and Experimental Stress vs Frequency Plot for b/a = 0.2

CHAPTER V

DISCUSSION OF RESULTS

Introduction

The results of an experimental and analytical investigation of the buckling and vibration behavior of a thin tensioned sheet with an elliptic hole were presented in the previous chapter. The present chapter is devoted to the discussion of the results obtained for the buckling and the vibration problems.

The Buckling Problem

The buckling stress estimates which were determined experimentally and analytically were presented in the previous chapter. The different features of the results obtained for the buckling problem are discussed in this section.

Experimental Results

The buckling stress estimates of thin tensioned sheets with elliptic holes were computed from experimental data using the Lundquist method. The results were presented in Table of Chapter IV for all the elliptic hole shapes considered. As noted in Chapter IV, the applicability of the Southwell method depends on the validity of a linearization of the Karman plate equations [8,67]. The difference between the linearized behavior and the nonlinear behavior is illustrated in Figure 20. The behavior of a perfect model is described

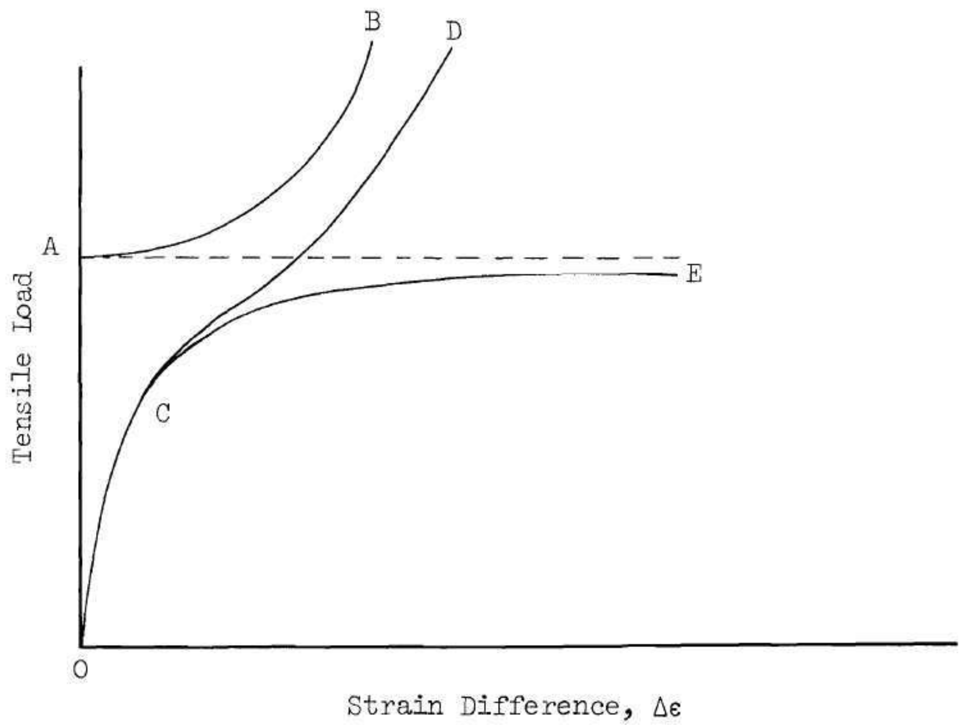

Figure 20. Load vs Strain Difference Plot

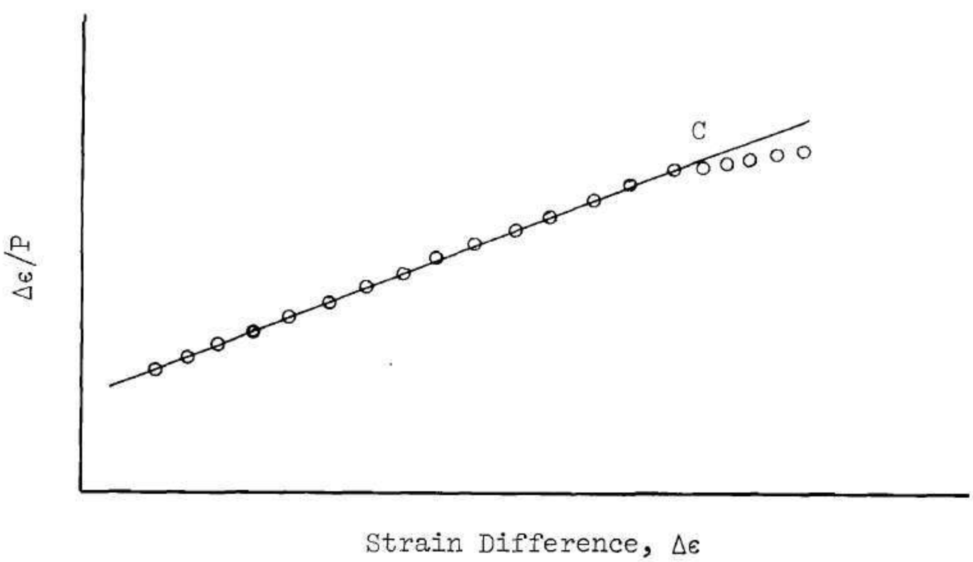

Figure 21. Typical Southwell Plot

by the curve O-A-B. The value of the buckling load at A is obtained from the solution of the linearized, homogeneous plate equations. The curve A-B is obtained from a solution of the coupled, nonlinear plate equations.

If the model is imperfect, the behavior deviates from that described above, and it may be depicted as shown by the curve O-C-D. If the equations governing the behavior of the imperfect model are linearized, a solution which gives a curve of the type O-C-E is obtained.

The Southwell method is based on the use of a curve which corresponds to the curve O-C-E. Since the real behavior deviates from this curve at C to move along C-D, it is clear that the load corresponding to C must be accepted as the load above which the Southwell method does not apply.

The deviation at Point C can be traced to the effect of the term in the nonlinear governing equations which describes the contribution of middle surface stretching due to bending. This effect can, in turn, be detected on a load vs midsurface strain diagram [8,67]. The load vs midsurface strain curve deviates from linearity above the load corresponding to point C of Figure 20.

The behavior illustrated in Figure 20 must be considered when applying the Southwell method to plate stability problems. To illustrate this, a typical Southwell plot is presented in Figure 21. The straight line of this plot corresponds to the curve O-C-E of Figure 20. Since the actual behavior which is depicted by the plotted points corresponds to the curve O-C-D of Figure 20, a deviation of the type shown at point C of Figure 21 must occur. This behavior was noted in all of the data presented in Figures 9, 10, 11 and 12 of Chapter IV. It should be noted that if data points for strain differences larger than the value corresponding to point C are used, the buckling load estimate will tend to be too large. The same type of error can occur with use of the Lundquist plot.

Other methods are available for the estimation of buckling stress from experimental data. They are described briefly in the discussion which follows.

The first method to be described here is an estimation of the buckling stress based on a plot of load vs $(\text{deflection})^2$. For a structural system, the load vs deflection relation can be developed in a Taylor's series expansion of $P(\delta)$ about $\delta = \delta_o$ as

$$P(\delta) = P(\delta_o) + (\delta - \delta_o)\, P'(\delta_o) + \frac{1}{2!}(\delta - \delta_o)^2\, P''(\delta_o) + \ldots \quad .$$

Where the primes denote differentiation with respect to δ. If P vs δ is a symmetric function and $\delta_o = 0$,

$$P = P_o + \frac{1}{2!}\delta^2 P_o'' + \frac{1}{4!}\delta^4 P_o'''' + \ldots \quad ,$$

where $P_o = P(0)$.

This equation for P may be rearranged as

$$P = P_o + \tfrac{1}{2} P_o''\, \delta^2 \left(1 + \frac{1}{12}\, \frac{P_o''''}{P_o''}\, \delta^2 + \ldots\right).$$

If,

$$1 >> \left(\frac{1}{12} \frac{P_o''''}{P_o''} \delta^2 + \ldots \right) ,$$

an approximate relation of P is then

$$P = P_o + b_1 \delta^2 ,$$

where, $b_1 = \frac{1}{2} P_o''$, a constant.

For a system which is imperfection insensitive ($b_1 > 0$) and has a small imperfection, the above relation may provide an acceptable description of the response for small deflections. An estimate to P_o may then be obtained from a plot of the above equation. The linear plot shown in Figure 22 illustrates how an estimate might be obtained. The value of the intercept on the load axis would be used as the buckling load estimate by this method.

An effort was made to utilize the P vs δ^2 method in the present investigation. Plots of the data obtained did not, however, produce results which could be used because the latitude in the selection of a straight line was too great. This technique was not, therefore, used to obtain buckling load estimates.

Dixon and Strannigan [2] proposed a method for finding upper and lower bound estimates of the critical buckling load from the load vs strain difference curve of a cracked sheet. A typical load vs strain difference curve is shown in Figure 23. Point Q_1 corresponds to a lower bound of the critical load and the point Q_2 corresponds to an

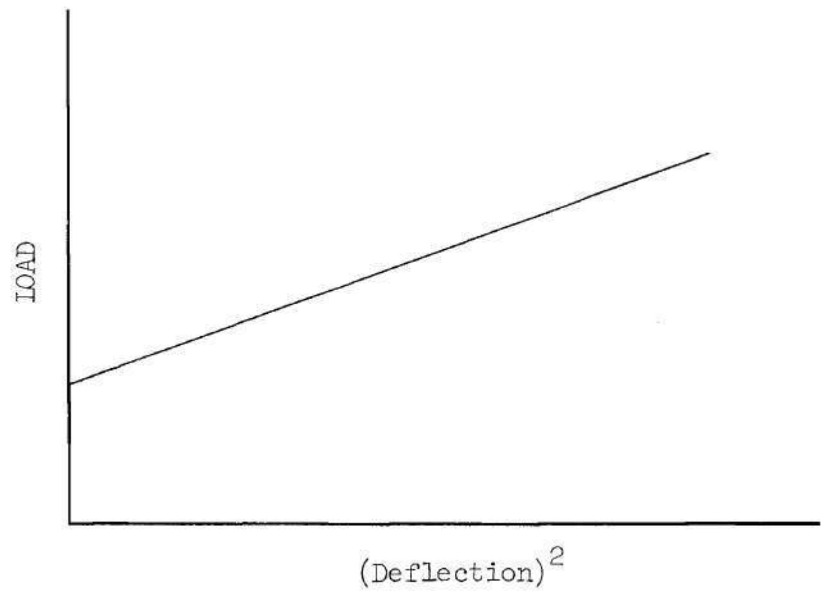

Figure 22. Load vs (Deflection)^2 Plot

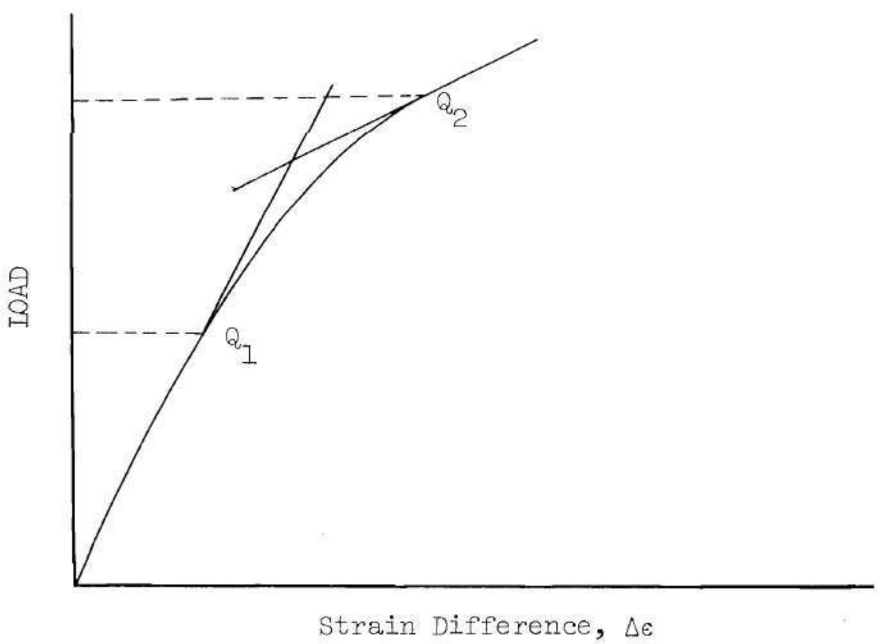

Figure 23. Load vs Strain Difference Plot

upper bound. This method was not used here because it was found to be difficult to select the points Q_1 and Q_2 with confidence. In addition, the range between the bounds is generally quite substantial.

Zielsdorff in his Ph.D. thesis [8] proposed an empirical formula for the buckling stress of a tensioned sheet with a slot cutout. The formula proposed is

$$\sigma_{cr} = E\left(\frac{t}{2H}\right)^2 \left[4.18 + 1.69\left(\frac{R}{H}\right) + 0.02\left(\frac{R}{H}\right)^{\frac{1}{2}}\left(\frac{2H}{t}\right)\right] ,$$

where E is Young's modulus and t is the sheet thickness. The quantities R and H are defined in Figure 24.

Zielsdorff's formula can be used in two ways to obtain buckling stress estimates for the elliptic hole problem. For one estimate the value of the semi-major axis is used for H, and the value of the semi-minor axis is used for R. In this case the ellipse is inscribed in the slot.

For a second estimate the value of the semi-major axis is used for H and the value of the radius of curvature at the end of the major axis is used for R. In this case the slot is inscribed in the ellipse. The buckling stresses estimated by the Lundquist method for all the hole shapes considered are shown in Figure 25. The two estimates for buckling stresses using Zielsdorff's empirical formula for hole shapes ranging between a crack and a circle are also shown in Figure 25. The estimates of the buckling stress form a closed envelope in Figure 25. It may be seen that buckling stress estimates

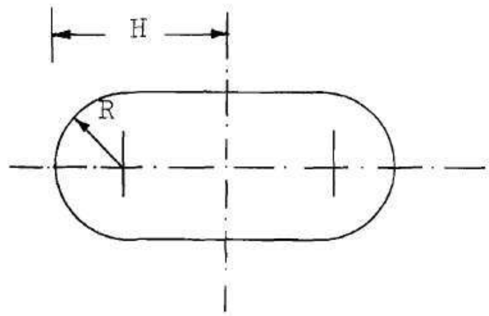

Figure 24. Slot Cutout Geometry

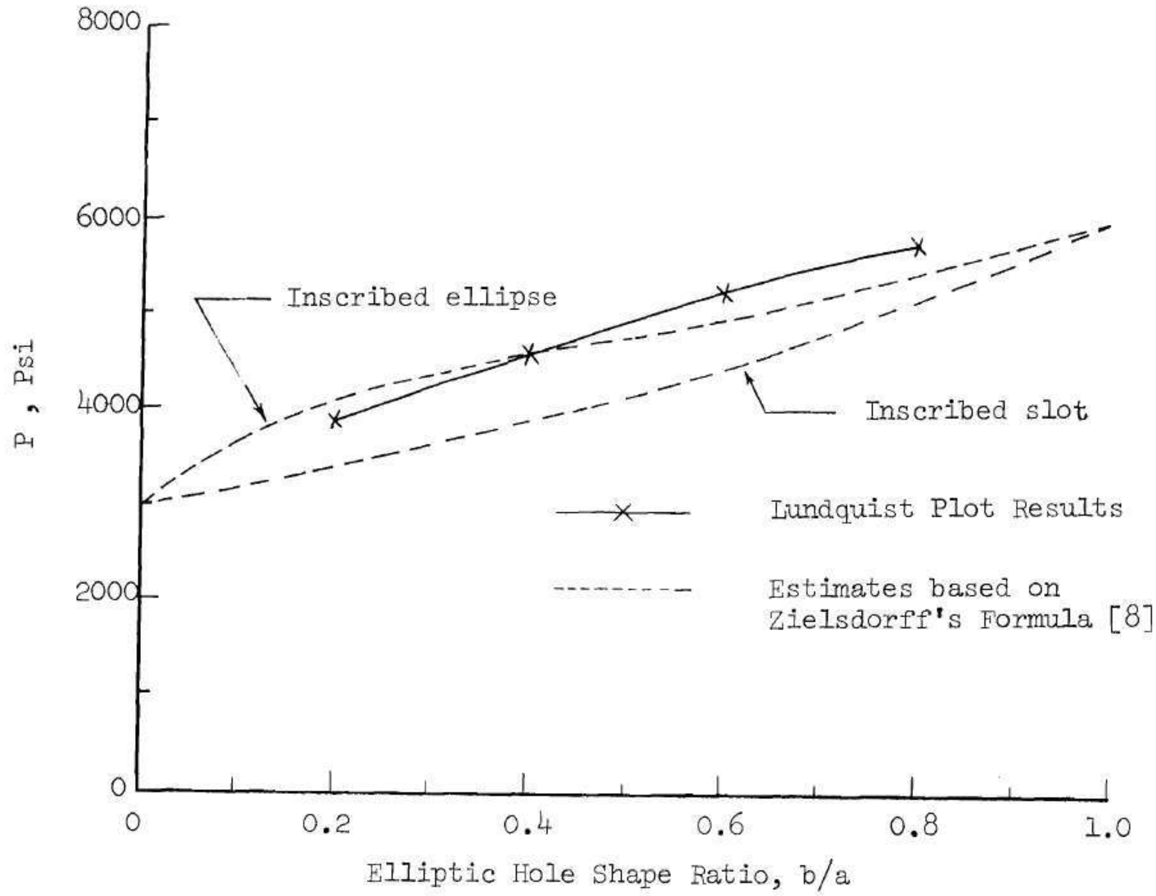

Figure 25. Buckling Stress Estimates

for the cases of b/a = 0.2 and 0.4 using Lundquist method fall within the envelope while the buckling stress estimates for the cases of b/a = 0.6 and 0.8 are above the envelope. It may be concluded from the above results that the upper curve based on Zielsdorff's empirical formula (the case for the ellipse inscribed in the slot) provides a good estimate for the buckling stress for the elliptic holes considered here.

Analytical Results

The buckling stress estimates of a thin tensioned sheet having an elliptic hole were computed using the generalized Galerkin method. A doubly symmetric deflection function in the form of Equation (3) of the previous chapter was chosen for the solution of the eigenvalue problem posed. The results obtained indicated that a small number of exponential terms and a larger number of cosine terms were required for good results. This was particularly true as b/a approaches unity. The convergence for the values of buckling stress was good for the cases of b/a = 0.2 and 0.4. More terms, however, would be required for the cases of b/a = 0.6 and 0.8 to obtain comparable results. Additional terms beyond the fifteen taken for b/a = 0.8 were not used because not only was the total computer time required to obtain a solution large (about 30 minutes), but the data processing time for the estimate was very long (two days). These times would be increased markedly if additional terms had been taken and the time that could practically be devoted would have been exceeded. A review of the experimental and analytical results indicate that useful conclusions can be made without more extensive computations.

The experimental and analytical estimates of buckling stress for all values of b/a ratio considered are shown in Figure 26 for comparison. The points for the analytical solutions in Figure 26 correspond to the largest number of terms taken for the respective hole shapes. It can be seen from Figure 26 that experimental results are consistently higher than the analytical results. The percentage difference for the case of $b/a = 0.2$ is 3%. For the case of $b/a = 0.4$ the difference is 4%. If the experimentally determined estimates were exact, it might be expected that the analytically determined estimates should be equal to or larger than the true value.* Since the expected order appears to be reversed, some discussion of the possible reasons for the observed trend is appropriate.

The buckling stress estimates from the experimental data were obtained using the Lundquist method. It was mentioned earlier in this chapter that the Lundquist plot would give high values of buckling stress if the plotted straight line was influenced by data points beyond point C of Figure 21. This is related to the stiffening characteristics indicated beyond point C in Figure 20. To examine this as a possible effect, the Lundquist plots were carefully reviewed. Particular attention was focused on the location of the point corresponding to point C of Figure 21. The results of this examination indicated that the experimental estimates were not likely to be more than 5% high.

* As used the Gakerkin method is equivalent to a direct use of the total potential energy method.

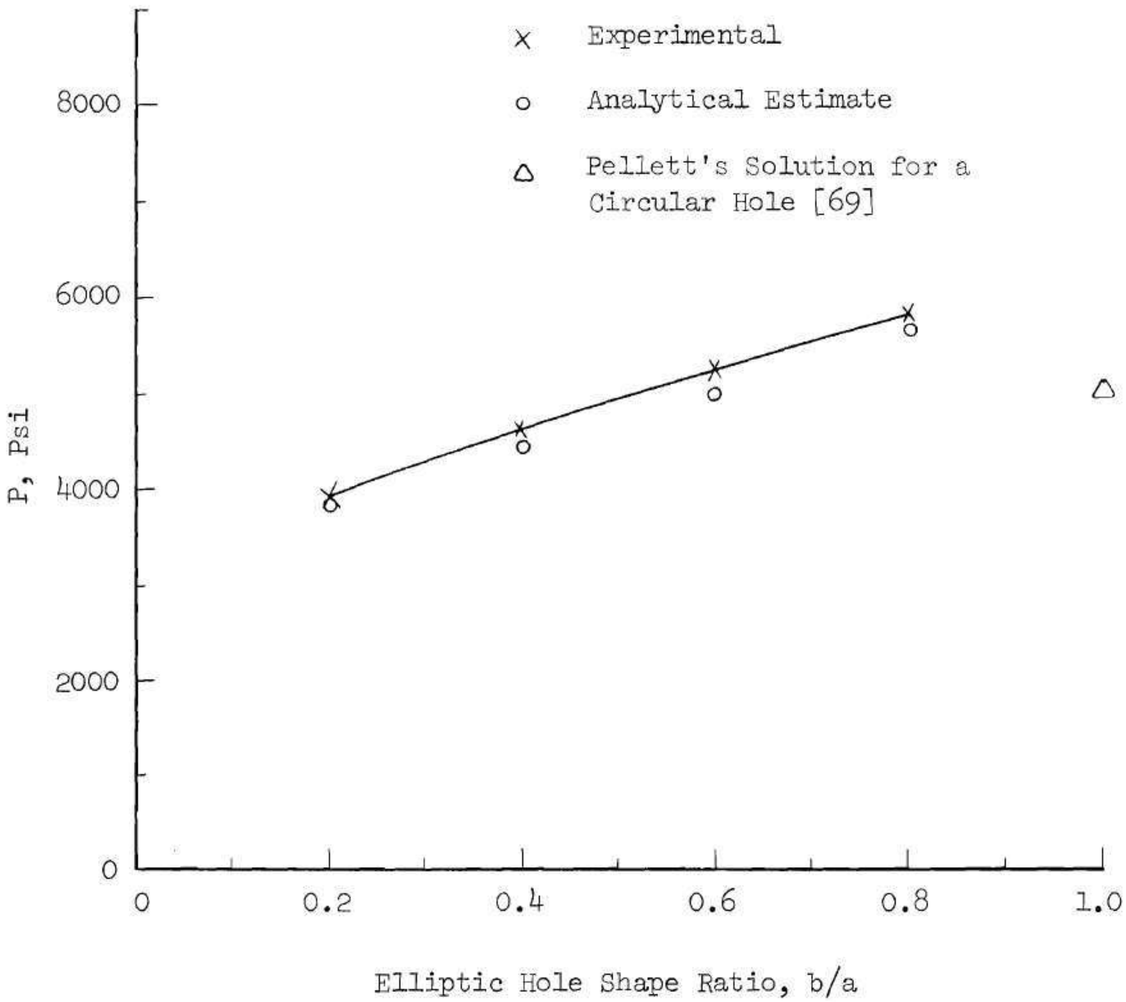

Figure 26. Experimental and Analytical Buckling Stress Estimates

An evaluation of the results obtained should also include a consideration of the extent to which the analytical model exhibits the behavior of the test specimen. The outer boundary of the analytical model was elliptical whereas that of the test specimen was rectangular. Although the in-plane stress states developed could be expected to be very nearly the same, the outer boundary conditions could be considered to be the same only if the out-of-plane deflection behavior is completely confined to a small region adjacent to the opening. Since the degree to which such a behavior can be assumed is not rigorously known, some discussion of this aspect of the results should be included here.

Some insight into the difference between the analytical model and the test specimen can be gained by a comparison of edge conditions. The outer free edges of the test specimen lie within the boundary of the annular region of the analytical model. It follows that along such a line, the analytical model has a greater constraint than the free edge, and this might tend to cause the buckling load for the analytical model to be higher than that for the test specimen. Such a conclusion cannot be accepted as final, however, until the clamped edges of the test specimens are also considered. These edges also are within the annular region of the analytical model, but now, the constraint situation is reversed. That is, the top and bottom edges of the test specimen, being clamped, are more highly constrained than the corresponding lines within the analytical model. This effect, if acting alone, would cause the test specimen to have a higher buckling load than the analytical model.

Since the two effects described are opposite and are considered only in a qualitative sense here it is not known whether or not one is dominant over the other. It is, however clear from the discussion that a comparison of the magnitude of the values obtained should include a recognition of the differences between the analytical and the test model. It might also be concluded that a larger test specimen would be desirable.

Pellett's [69] analytical result for a circular opening is also shown in Figure 26. It is seen from Figure 26 that Pellett's estimate for the circle is below that which could be expected from an extrapolation of results from the present investigation. Pellett indicated that his result was obtained by extrapolating results from a solution using a finite number of terms to a result for an infinite number of terms by use of a least-square procedure. Because of the method of extrapolation, it is not known whether his result is an upper or a lower bound.

The mode shapes corresponding to the case of $b/a = 0.2$ were computed analytically and they are plotted in Figure 27 for the case of:

(1) At $\xi = \xi_o$ for $0 \le \eta \le \pi/2$

(2) At $\eta = 0$ for $\xi \ge \xi_o$

(3) At $\eta = \pi/2$ for $\xi \ge \xi_o$

The space coordinates for the latter two cases have been transformed to the Cartesian coordinates x and y. In Figure 27 w_{max} corresponds to the deflection at $\xi = \xi_o$ and $\eta = \pi/2$. It is seen

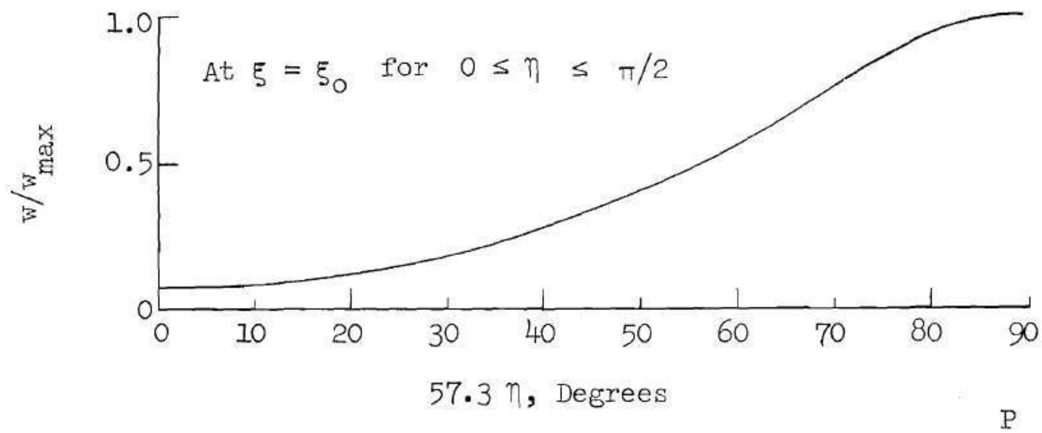

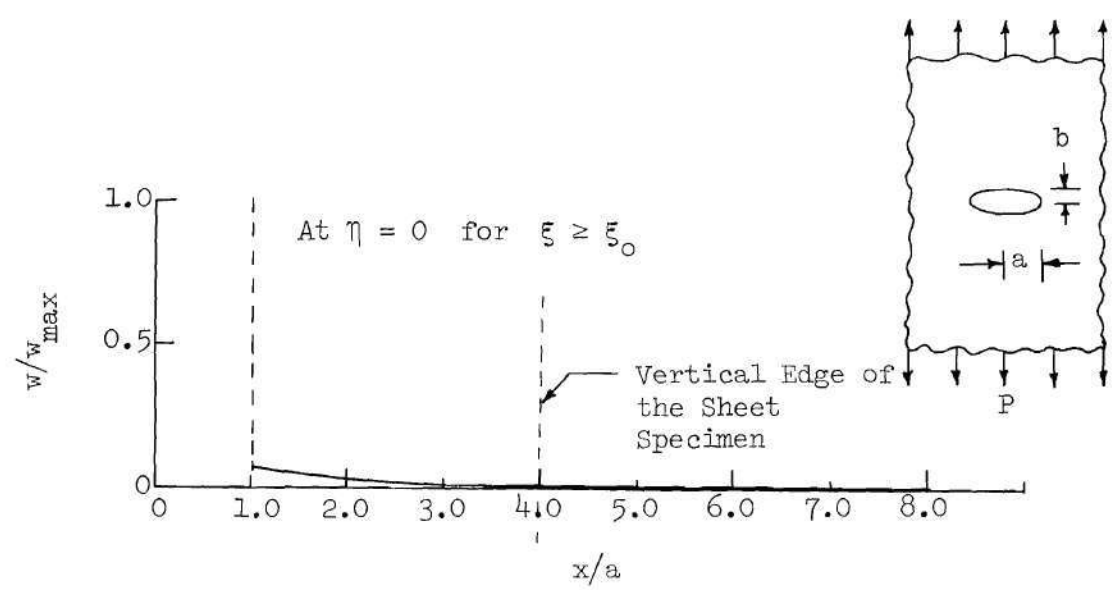

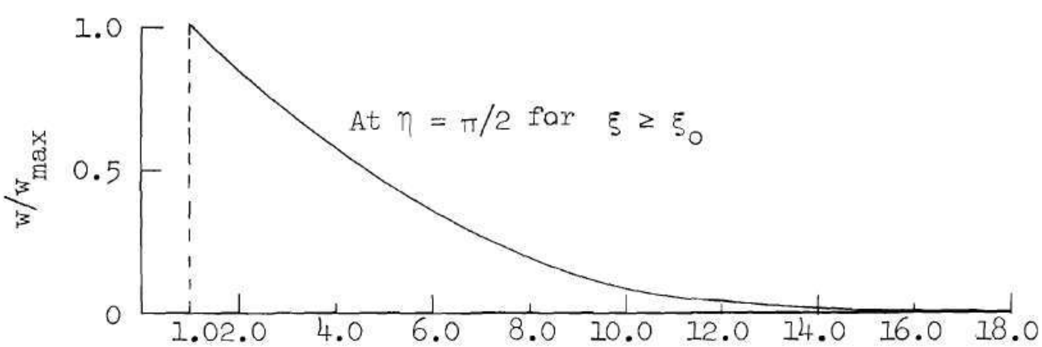

Figure 27. Analytical Transverse Deflection Plots for Buckling with a $b/a = 0.2$

that the deflection becomes small as the distance from the hole becomes large. The plotted mode shapes are consistent with the mode shapes observed visually during the buckling experiments. In the experiments the side edge of the specimen corresponded to a value of $x/a = 4.0$. The top edge of the specimen had a value of $y/b = 36$. An examination of the results of Figure 27 suggests that for $b/a = 0.2$ the length of the specimen was sufficient, but the width of the specimen should have been larger. It is important to emphasize that the conclusions stated apply to the specimens with $b/a = 0.2$. For this specimen the observed region of buckling was relatively compact and localized. As the b/a ratio increased, it was observed that the buckled zone became narrower and elongated in the direction of applied load. It seems likely, then, that the test specimen used may have been too short for the larger b/a ratios tested.

All of the computations cited have been for a doubly symmetric deflection mode. Other types of mode shapes could be considered. For example, a deflection function which is symmetric about the y-axis and antisymmetric about the x-axis may be written as,

$$w_{MN}(\xi,\eta) = \sum_{i=1}^{M} \sum_{j=0}^{N} A_{ij}\, e^{-i\xi} \sin(2j + 1)\eta \ .$$

Using this form of deflection function, a computation was carried out for $b/a = 0.2$ for a 12 term solution. The buckling stress was found to be 8500 psi. The lowest value obtained in this antisymmetric case is substantially higher than the value for the doubly symmetric case. Because of this result, and because of the analytically and experimentally observed deflection behavior indicated a doubly symmetric mode, it may be concluded that the lowest buckling load corresponds to the symmetric mode shape. The remaining possibilities cited in Chapter III were not used for obtaining buckling estimates.

The Vibration Problem

The results of an experimental and analytical investigation of the vibration behavior of a thin tensioned sheet with an elliptic hole were described in Chapter IV. This section is devoted to the discussion of the different aspects of the results obtained.

Experimental Results

The frequency vs applied tensile stress plots of a thin tensioned sheet with an elliptic hole are shown in Figures 17 and 18 of Chapter IV for different values of b/a ratio. Curves which illustrate the main features of the behavior observed are presented in Figures 28 and 29 for the purpose of discussion. It is seen in Figures 17 and 28 that for the b/a ratio of 0.2, the stress vs frequency plot is made up of three distinct regions.

1. The frequency increases with increasing stress (A to B in Figure 28).
2. In the region from B to C of Figure 28 the frequency decreases with the increasing stress.
3. In the region from C to D the frequency again increases with increasing stress.

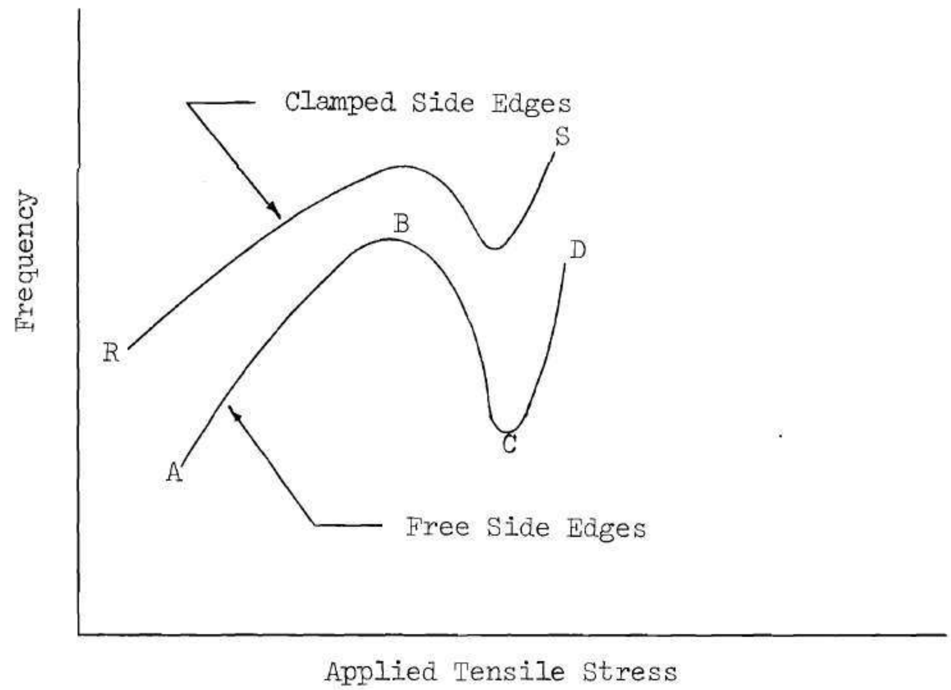

Figure 28. Experimental Stress vs Frequency Plots for $b/a = 0.2$

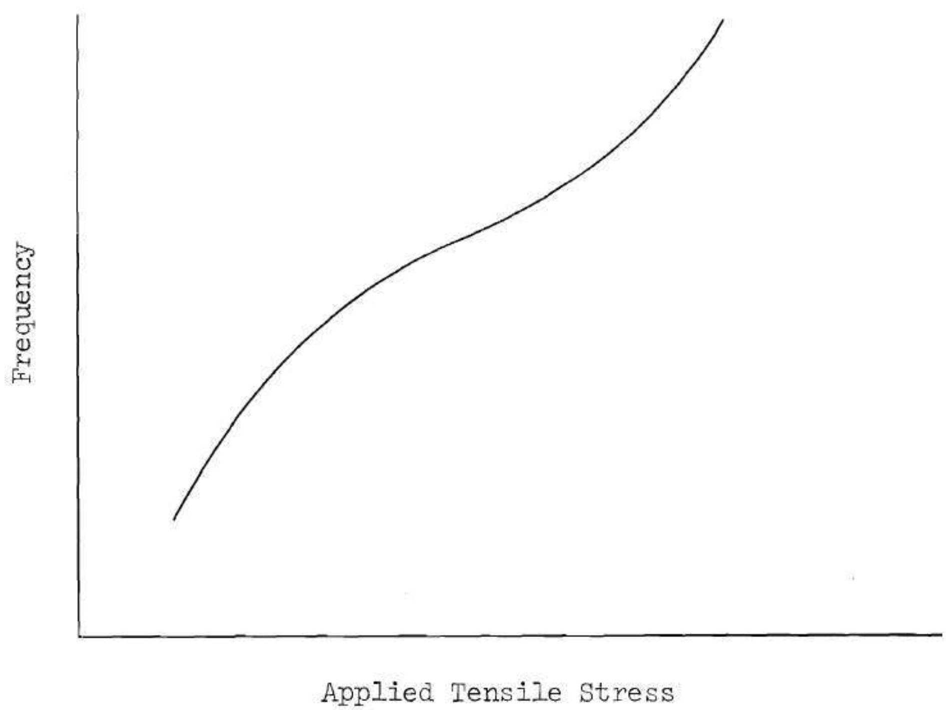

Figure 29. Typical Experimental Stress vs Frequency Plot for $b/a \geq 0.4$

In the first region from A to B the behavior is qualitatively similar to that for a tensioned sheet without a hole. Reference to Figure 18 also indicates that vibration behavior is relatively insensitive to hole shape in this region. The curve for $b/a = 0.2$, 0.4, 0.6, 0.8 tend to merge for values of tensile stress less than 1500 psi. It may be observed that the magnitude of the frequency at a given stress level may be expected to be quite dependent upon specimen size; i.e., length and width. As a consequence, it would follow that for larger specimens, the curve of the first region would be lower since this region corresponds to the overall plate mode.

As the applied tensile load increases, the stress in the compressive zone adjacent to the hole becomes proportionately larger. Although the size of the compressive zone remains unchanged, the local effective stiffness progressively decreases. These factors begin to influence the vibration behavior substantially as the applied tension is increased beyond point B of Figure 28. This results in a region in which the frequency decreases continuously with increasing applied tension.

The plate specimen of Figure 28 is known to be subject to buckling, and a vibration experiment could, therefore, be expected to produce a frequency vs applied stress curve which has a stress axis intercept at the buckling load; i.e., it would be expected that the curve BC would extend downward to the stress axis. The behavior which might be expected is not observed in Figure 28. It does not occur because the equilibrium branch about which oscillation occurs begins to be influenced by the nonlinear effect of middle surface stretching due to bending; i.e., oscillation is about branch CD of Figure 20. Note that if the specimen had been perfect, oscillation would have been about the equilibrium branch OA, and then the frequency vs applied stress curve might have a stress axis intercept. This observation suggests that the behavior observed on BC of Figure 28 is dependent on the specimen imperfection. It is important to note, however, that the nonlinear effect of middle surface stretching must also be present to obtain the observed behavior. If imperfection alone were present, the resistance to bending would tend to zero as the load approached the buckling load, so a zero frequency intercept would have been observed. This would, in essence, correspond to oscillation about the equilibrium branch CE which corresponds to the linearized analysis of the imperfect sheet. Thus, the presence of imperfection is necessary but it is not sufficient to produce the observed behavior.

Ultimately, a third region develops in which the frequency increases with increasing applied tension. In this region the behavior may be characterized as a vibration about the branch CD of Figure 20.

The top curve of Figure 28 is the result of an experiment in which the vertical, free edges of the specimen were constrained by clamping rectangular cross-section bars to the edges. The cross-section of the bars was 1/2" by 1/4". The test procedure followed was first to apply the desired tensile load and then to apply the edge constraint. The objective of this experiment was to determine whether or not the vibration behavior in the region BC of Figure 28 was localized within the outer boundaries of the specimen. If, for example, no transverse motion was occurring when the edges were free, then clamping the edges should not result in a behavior change. As can be seen, however, the frequency curve was raised over the entire range of stress. The vibration behavior clearly was not, therefore, confined to a zone adjacent to the opening in the range BC of Figure 28.

For the b/a ratios of 0.4, 0.6 and 0.8 the observed stress vs frequency behavior (Figure 18) is different from that for b/a = 0.2. The features observed for these cases are illustrated in Figure 29. It is seen that the distinct maximum and minimum behavior of the stress vs frequency curve for b/a = 0.2 is replaced by an inflection point. The region adjacent to the inflection point of Figure 29 represents a point beyond which oscillation is about an equilibrium branch corresponding to the region CD of Figure 20.

In summary it may be concluded that for the specimens tested, the effect of hole shape on the frequency vs applied stress curve is quite marked. The extent to which the differences observed may be modified for larger specimens is not known.

The nature of the mode shape associated with the vibration results has not, up to this point, been specified. Care was, of course, taken to be certain that the frequencies measured were those associated with the first mode. In addition, strain gages were applied on selected specimens to both long edges of the ellipse. By this means it was possible to establish that the mode observed was symmetric with respect to the major axis of the elliptical hole.

Analytical Results

The frequency of vibration of a tensioned, annular sheet having an elliptic hole was computed for $b/a = 0.2$ for different values of the applied load using the generalized Galerkin method. A doubly symmetric deflection function in the form of Equation (3) of Chapter IV was used. An examination of the deflection function used reveals that a localized behavior is being represented due to the rapid decay of the exponential functions. The results obtained by the use of this function are summarized in Figure 19 of Chapter IV. An examination of the results indicates that the frequency decreases with increasing applied load and becomes zero at the buckling load.

In comparing the analytical results with the experimental results, some interesting features may be discerned. Analytically, the frequency is zero at the buckling stress, whereas, the experimental stress vs frequency plot of Figure 28 indicates that in the second region (B to C) a finite minimum (point C) is obtained near the buckling stress. The analytical result represents an oscillation about the linearized solution for the equilibrium branch for a perfect sheet. This means that imperfection and the nonlinear effect of middle surface stretching due to bending are not included in the analysis which produced the results of Figure 19. In the real problem, of course, these effects are present and are manifested in the manner described in a previous section of this Chapter.

A comparison of the experimental and analytical curves of Figure 19 of Chapter IV for $b/a = 0.2$ indicates that in the region in which the local behavior is dominant, the experimentally observed frequency is greater than the computed frequency. Since the computed frequency is for a large but finite annular sheet, it is reasonable to ask whether or not another size plate might more effectively represent the localized behavior observed in the experiments. For example, if a somewhat smaller analytical model were chosen, it would be expected that the computed frequency vs stress curve would be higher than that of Figure 19.

Since the choice of the size of the analytical model used is to some degree arbitrary, it would seem to follow that it would be desirable to develop an analytical model which represents more completely the shape and size of the specimen tested. Analytically, of course, it would also be desirable to then include functions which could also better represent the overall, as opposed to local, vibration behavior of the sheet.

Clarkson and his co-workers [31-36] have studied the behavior of a cracked plate under constant tensile stress subjected to acoustic loads. Their investigation is related to the present study in that the crack is a limiting case of the ellipse. The natural frequency of vibration in Clarkson's work was found to depend on the overall tension of the plate and on the crack length. Their investigation was concerned with basic features of plate vibration; i.e., mode shapes at resonant frequency, and the load vs frequency behavior. The effects of initial stress, over-all noise level, and plate thickness on the rate of crack propagation were also studied.

The stress vs frequency behavior experimentally observed in Clarkson's study is similar to the stress vs frequency behavior for the case of $b/a = 0.2$ in the present investigation. Some analytical work was performed by Clarkson's group. In the model which they adopted the compressive zone above the crack was isolated from the remainder of the sheet. The behavior of the isolated zone was then said to be similar to that of a rectangular plate which was clamped on three edges and free on the edge which corresponded to the crack edge. The actual in-plane stress state was then approximated as a linearly varying, unidirectional stress which acted parallel to the free edge. The stress was compressive and the maximum value occurred at the free edge. The lowest natural frequency of the model was computed by use of the Rayleigh-Ritz procedure and as would be expected, the frequency of the model decreased with increasing stress level. The maximum compressive stress was correlated with the tensile load in the actual sheet specimen. Although these results do reproduce some features of the subject problem, they provide no information about the deflection behavior outside of the compressive zone.

The deflection behavior outside the compressive zone can be examined for the analytical model used here. The mode shapes corresponding to the case of $b/a = 0.2$ were computed and they are plotted in Figure 30. From the bottom graph of Figure 30, it is seen that the maximum deflection occurs at the free edge of the hole, and that it decreases as the distance from the hole becomes large. It may also be seen in the top graph that along the circumference of the hole, the

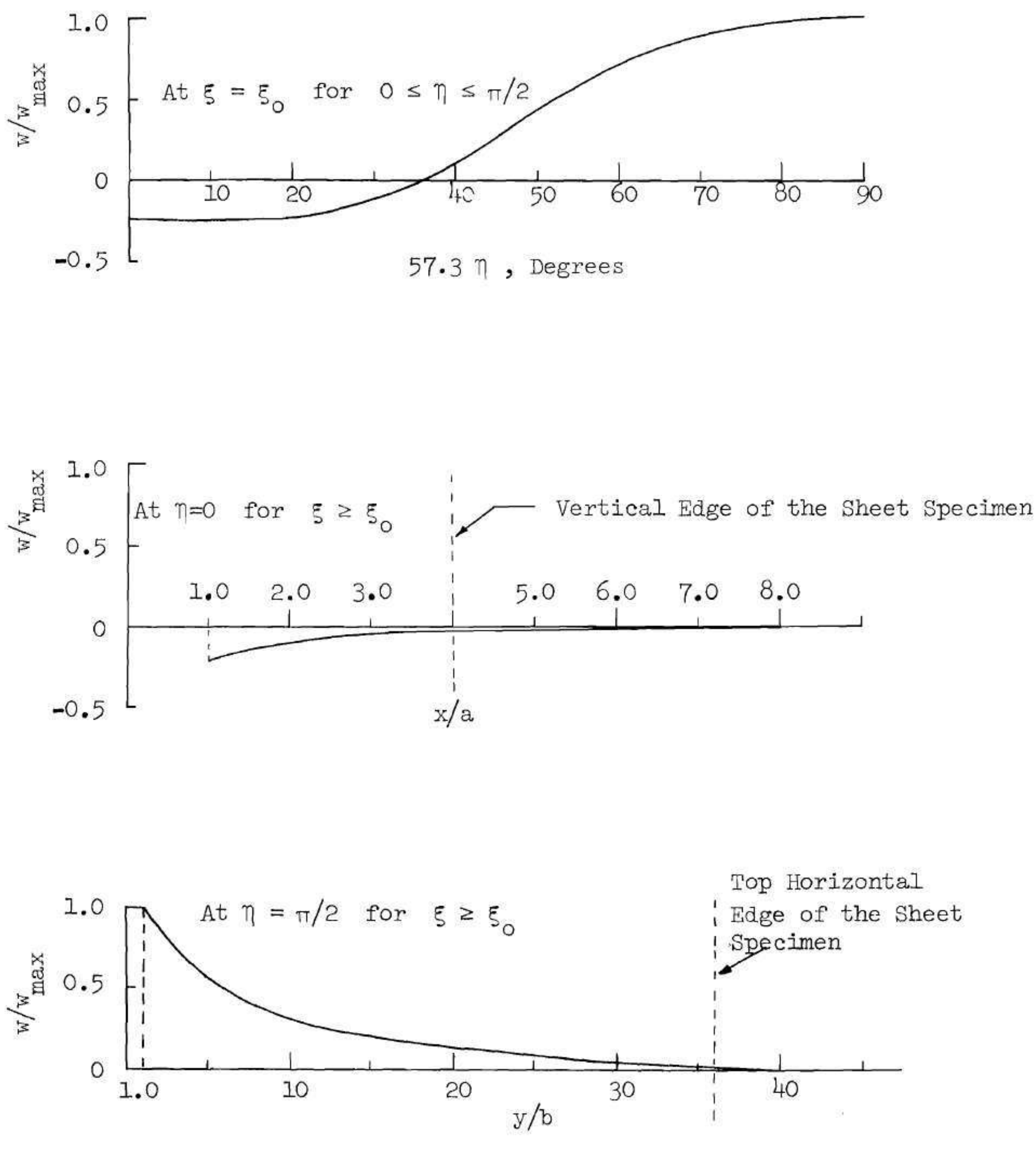

Figure 30. Analytical Transverse Deflection Plots for $b/a = 0.2$

mode shape changes its sign in the range between $\eta = 0$ and $\eta = \pi/2$. It follows that in the region around the hole, one portion of the plate has a positive deflection while another portion has a negative deflection. The nodal line for the mode shape computed is shown in Figure 31. From the middle plot of Figure 30, it may be seen that the deflection at the end of the major axis, though small, is non-zero.

The dashed lines of Figures 30 and 31 indicate the location of the boundary of the sheet specimen which was tested. The top and bottom edges of the test specimen were clamped and the side edges were free. It should be noted that the outer boundary of the analytical model lies outside the plotted graph. In terms of the scale of Figure 31 it would very nearly be a circle whose radius is about 66 inches for $b/a = 0.2$. A comparison of the relative sizes of the test specimen and the analytical model suggests that an improved correlation for the localized type behavior might be achieved by use of a larger test specimen. The other alternative which was noted earlier would be to use an improved analytical model. This latter possibility would probably be preferable in future work.

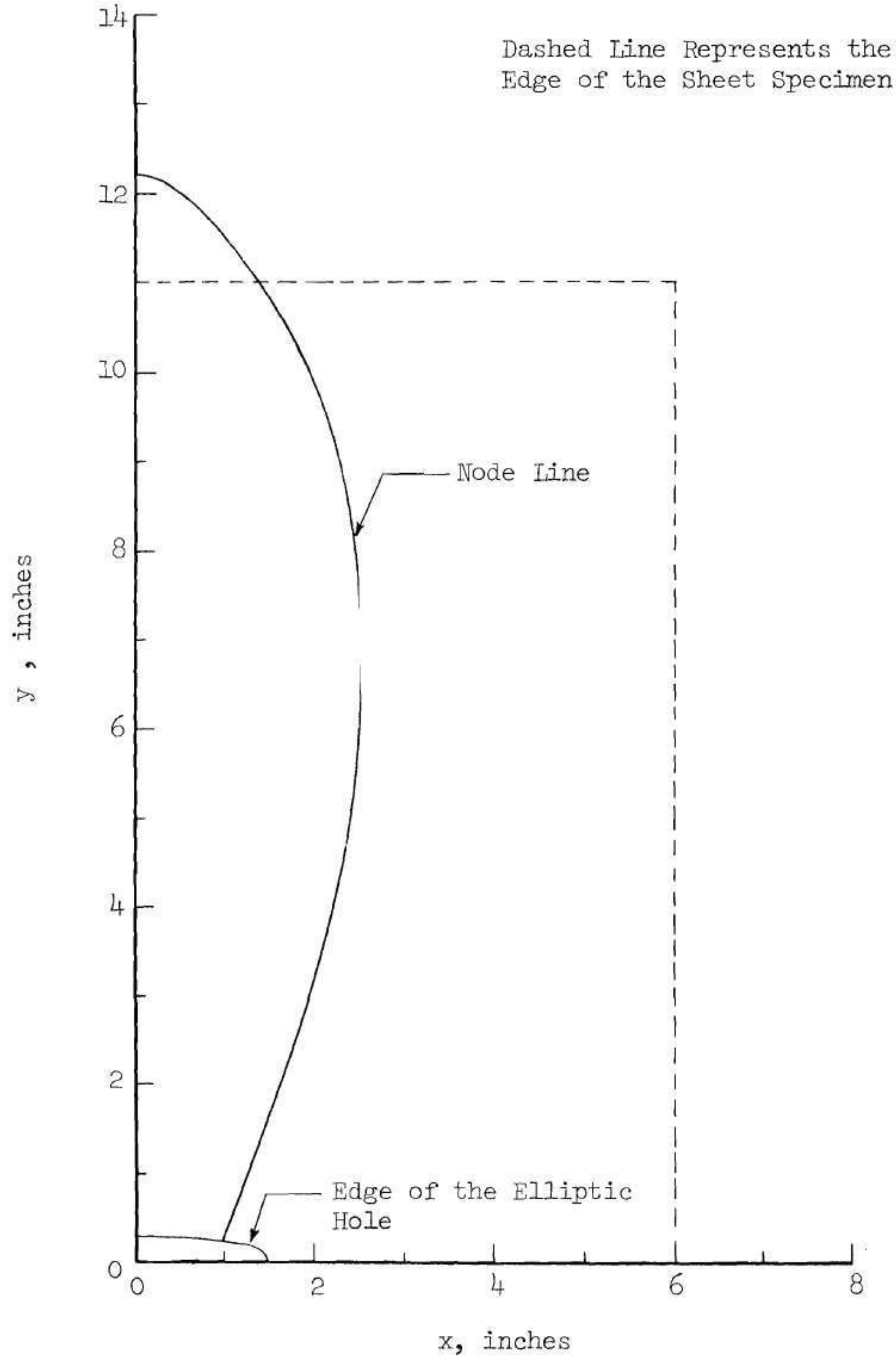

Figure 31. Plot of the Node Line for b/a = 0.2

CHAPTER VI

CONCLUSIONS

An experimental and analytical investigation of the buckling and vibration behavior of a thin tensioned sheet with an elliptic hole was described in the preceding chapters of this dissertation. Conclusions based on the results obtained are summarized in the discussion which follows.

The buckling experiments were conducted on finite sheet specimens with four different hole shapes, and buckling loads were established by use of a modified Southwell method.

A large annular sheet model with elliptic inner and outer boundaries was adopted and analyzed by use of the generalized Galerkin method. Buckling stress estimates were obtained for a range of hole shapes for which the ratio of the minor axis to the major axis of the ellipse varied from 0.2 to 0.8. Mode shapes for the ratio of 0.2 were determined.

Agreement between experimentally and analytically determined buckling stress estimates was good. In view of the agreement observed it may be concluded that for the buckling problem, analytical results based on the sheet model adopted can be used to reproduce the main features of the behavior of the finite specimens tested.

The experimental investigation of the vibration behavior was conducted on finite, tensioned sheet specimens for four values of the ratio of minor axis to major axis. For a ratio value of 0.2 both a local maximum and a local minimum were observed for the frequency vs applied tension curve. For ratio values of 0.4, 0.6, and 0.8 the maximum and minimum observed for the ratio 0.2 is replaced by an inflection point.

The vibration problem of a tensioned annular elliptic sheet with an elliptic hole was solved by use of the generalized Galerkin method. The frequency vs applied tension behavior for a hole ratio of 0.2 was determined for vibration behavior in which the transverse motion is local in character and confined to a region adjacent to the opening. For this case it was found that the frequency is zero at the buckling stress and that the frequency increases with decreasing applied tension.

Some distinct differences were found between the analytical and experimental results. Analytically, the frequency is zero at the buckling stress for the case of $b/a = 0.2$, whereas the experimental stress vs frequency plot exhibits a finite minimum near the buckling stress. This may be traced to the fact that the analytical solution obtained is based on a purely linear formulation for a perfect sheet. Actually, the presence of imperfection and the nonlinear effect of middle surface stretching due to bending begins to be an important factor in the real behavior as the applied tension approaches the buckling stress. This causes the vibration response to deviate markedly from that predicted from the analysis performed.

Although some of the features of the behavior observed in the vibration experiments on finite specimens have been reproduced in the analysis of the large annular elliptic sheet model, an improved correlation might be achieved by use of a larger test specimen. In terms of the usefulness of results which might be obtained from additional work, however, it is believed that it would be preferable to develop an analytical solution of a model which more closely reproduces the features of the test specimen.

CHAPTER VII

RECOMMENDATIONS FOR FUTURE RESEARCH

The buckling and vibration behavior of a thin tensioned sheet with an elliptic hole has been described in this report. In the course of the investigation several interesting features concerning the buckling and vibration behavior have come to light. These features could be more completely explained and further insight into the problem could be developed through extensions of the present research. Recommendations for further research in these areas are presented in the itemized discussion which follows.

1. The analytical solution for the buckling problem in the present research is based on a linearization of the Karman plate equations. When applied loads are near the buckling load in the real problem, the effect of middle surface stretching due to bending cannot be neglected, and the coupled, nonlinear equations (including the effect of imperfection) must be used to describe the plate response. A solution of the indicated nonlinear problem would provide a description not only of the deflection behavior, but also of the redistribution of stress which occurs during loading. The change in the stress concentration factor which accompanies bending and middle surface stretching due to bending is of particular importance with reference to the onset of inelastic behavior. Also, under cyclic loading conditions, the role of the stress concentration factor is well known in the fatigue problem.

2. The model used in the vibration analysis presented here consisted of a large annular sheet with elliptic inner and outer boundaries. Although the model exhibited some features of the finite specimen which was tested, a more complete correspondence between the analytical and the experimental results would be desirable. This could be accomplished by analyzing the specimen tested. The results of this analysis should provide a more complete description of the frequency vs applied tension for the load range from zero up to or near the buckling load.

3. The frequency response of the specimens tested at loads near and above the buckling load differed drastically from that predicted by the analytical results presented in this report. To reproduce the behavior observed, the required analysis would involve oscillation about a static equilibrium branch in which the effect of imperfection is included. Thus, although the vibration analysis could be for simple harmonic motion, the configuration about which small oscillations occur would have to be determined from a solution of the static non-linear Karman equations.

4. Ultimately, the problems discussed here become important in relation to their influence on fatigue behavior. The effect on the stress concentration has been mentioned under item 1. Another effect which may arise would be associated with cases in which the resonant frequency is included in the load vs frequency spectrum. The nucleation of fatigue cracks under such resonant conditions for loads both below and above the buckling load is of basic interest. It is recommended that this problem be investigated in a series of controlled experiments.

APPENDIX A

STRESS COMPUTATION DETAILS

APPENDIX A

STRESS COMPUTATION DETAILS

In Chapter III, the Kolosoff's Equations (5) and (6) are written in the form

$$\sigma_\xi + \sigma_\eta = 2\left[\psi'(z) + \bar{\psi}'(\bar{z})\right] = 4 \text{ Re } \psi'(z),$$

and

$$\sigma_\eta - \sigma_\xi + 2\, i\sigma_{\xi\eta} = 2\, e^{2i\theta}\left[\bar{z}\, \psi''(z) + \chi''(z)\right],$$

where, in elliptic coordinates (see Figures 6 and 7)

$$e^{2i\theta} = \frac{\sinh \Phi}{\sinh \bar{\Phi}},$$

$$\Phi = \xi + i\eta,$$

$$\bar{\Phi} = \xi - i\eta,$$

and $$z = x + iy.$$

ξ and η are nondimensional elliptic coordinates. x and y are Cartesian coordinates in units of length. $\psi(z)$ and $\chi(z)$ are the complex potential functions and they are given in Chapter III. Using the above, we can write

$$\sigma_\xi + \sigma_\eta = P(a_5), \tag{A-1}$$

and

$$\sigma_\eta - \sigma_\xi + 2\, i\sigma_{\xi\eta} = \frac{P}{2}\left(a_{28} + ia_{29}\right), \tag{A-2}$$

where the quantities in the parentheses are tabulated below. Equating real and imaginary parts, we obtain

$$\sigma_\eta - \sigma_\xi = \frac{P}{2}\left(a_{28}\right), \tag{A-3}$$

and

$$\sigma_{\xi\eta} = \frac{P}{4}\left(a_{29}\right). \tag{A-4}$$

From Equations (A-1), (A-3) and (A-4) the stress components in elliptic coordinates may then be written as

$$\sigma_\xi = \frac{P}{2}\left(a_5 - \frac{a_{28}}{2}\right) = P\, f_1(\xi,\eta),$$

$$\sigma_\eta = \frac{P}{2}\left(a_5 + \frac{a_{28}}{2}\right) = P\, f_2(\xi,\eta),$$

and

$$\sigma_{\xi\eta} = \frac{P}{4}\left(a_{29}\right) = P\, f_3(\xi,\eta).$$

From these results we may identify

$$f_1(\xi,\eta) = \frac{1}{2}\left(a_5 - \frac{a_{28}}{2}\right),$$

$$f_2(\xi,\eta) = \frac{1}{2}\left(a_5 + \frac{a_{28}}{2}\right),$$

and

$$f_3(\xi,\eta) = \frac{1}{4}\left(a_{29}\right).$$

Definitions of the a_k quantities are as follows:

$$a_1 = \sinh \xi \cos \eta$$

$$a_2 = \cosh \xi \sin \eta$$

$$a_3 = \frac{a_1^2 - a_2^2}{a_1^2 + a_2^2}$$

$$a_4 = \frac{2a_1 a_2}{a_1^2 + a_2^2}$$

$$a_5 = \left[-e^{2\xi_o} + \left(1 + e^{2\xi_o}\right) \frac{\sinh 2\xi}{(\cosh 2\xi - \cos 2\eta)}\right]$$

$$a_6 = \frac{a_1^3 - 3a_1 a_2^2}{(a_1^3 - 3a_1 a_2^2)^2 + (3a_1^2 a_2 - a_2^3)^2}$$

$$a_7 = \frac{3\ a_1^2 a_2 - a_2^3}{(a_1^3 - 3a_1 a_2^2)^2 + (3a_1^2 a_2 - a_2^3)^2}$$

$$a_8 = a_6 \left(1 + e^{2\xi_o}\right)$$

$$a_9 = a_7 \left(1 + e^{2\xi_o}\right)$$

$$a_{10} = \cosh \xi \ \cos \eta$$

$$a_{11} = \sinh \xi \ \sin \eta$$

$$a_{12} = a_{11} a_9 - a_{10} a_8$$

$$a_{13} = a_{11} a_8 + a_{10} a_9$$

$$a_{14} = \left(\cosh 2\ \xi_o + 1\right)\left(a_{10} a_6 + a_{11} a_7\right)$$

$$a_{15} = \left(\cosh 2\ \xi_o + 1\right)\left(a_{11} a_6 - a_{10} a_7\right)$$

$$a_{16} = \cosh \left(2\ \xi - 2\ \xi_o\right) \cos 2\ \eta e^{2\xi_o}$$

$$a_{17} = \sinh \left(2\ \xi - 2\ \xi_o\right) \sin 2\ \eta e^{2\xi_o}$$

$$a_{18} = a_{16} \left(a_1 a_6 + a_2 a_7\right) - a_{17} \left(a_2 a_6 - a_1 a_7\right)$$

$$a_{19} = a_{17} \left(a_1 a_6 + a_2 a_7\right) + a_{16} \left(a_2 a_6 - a_1 a_7\right)$$

$$a_{20} = \sinh \left(2\ \xi - 2\ \xi_o\right) \cos 2\ \eta e^{2\xi_o}$$

$$a_{21} = \cosh\left(2\,\xi - 2\,\xi_o\right) \sin 2\,\eta e^{2\xi_o}$$

$$a_{22} = a_6\left(a_{20}a_{10} - a_{21}a_{11}\right) + a_7\left(a_{21}a_{10} + a_{20}a_{11}\right)$$

$$a_{23} = a_6\left(a_{21}a_{10} + a_{20}a_{11}\right) - a_7\left(a_{20}a_{10} - a_{21}a_{11}\right)$$

$$a_{24} = a_{14} + 2\,a_{18} - a_{22}$$

$$a_{25} = a_{15} + 2\,a_{19} - a_{23}$$

$$a_{26} = a_{12} + a_{24}$$

$$a_{27} = a_{13} + a_{25}$$

$$a_{28} = a_3a_{26} - a_4a_{27}$$

$$a_{29} = a_4a_{26} + a_3a_{27}$$

To illustrate the application of the preceding results, the nondimensional normal stress on the elliptic boundary and tangential to the edge for different b/a ratios has been computed and is shown in Figure 32. Naturally, in the problems of interest here, the stress state at all points in the field must be computed to perform the required analysis.

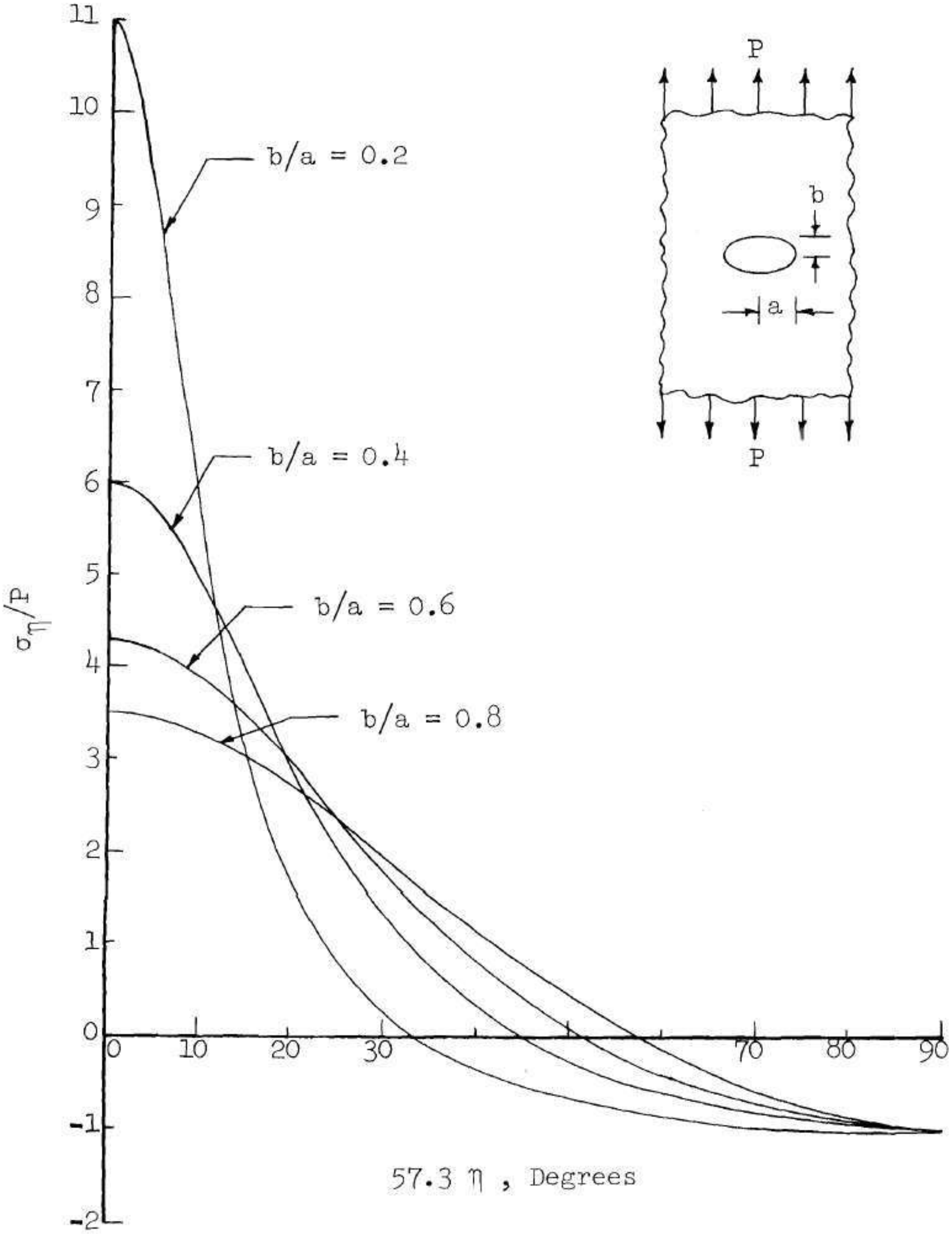

Figure 32. Nondimensional Normal Stress on the Elliptic Hole Boundary

APPENDIX B

PROPERTIES OF THE DEFLECTION FUNCTIONS

APPENDIX B

PROPERTIES OF THE DEFLECTION FUNCTIONS

Definition

The functions $y_1(x)$, $y_2(x)$, ... $y_n(x)$ are linearly independent on an interval I if the only constants c_1, c_2, ..., c_n for which

$$c_1y_1(x) + c_2y_2(x) + \ldots + c_ny_n(x) = 0,$$

are

$$c_1 = c_2 \ldots = c_n = 0.$$

Polynomial Functions

To show that 1, x, ..., x^n are independent over $x_1 \le x \le x_2$ let

$$a_0 + a_1x + a_2x^2 + \ldots + a_nx^n = 0 \qquad \text{(B-1)}$$

when $x_1 \le x \le x_2$. Suppose $a_n \neq 0$. Then, by the fundamental theorem of algebra, the Equation (B-1) can have at most n roots and so the left members can be zero on $x_1 \le x \le x_2$ only a finite number of times. Hence, if we require that Equation (B-1) be satisfied for all x in the interval, we must require that $a_0 = a_1 = a_2 \ldots = a_n = 0$. This result proves that the above set satisfies the conditions for linear independence.

If $x = 1/\xi$, then it also follows that $1, 1/\xi, 1/\xi^2, \ldots, 1/\xi^n$ form a linearly independent set with the stipulation that $\xi \neq 0$ on the interval.

Exponential Functions

To show that $1, e^{-x}, e^{-2x}, \ldots, e^{-nx}$ are linearly independent over $x_1 \le x \le x_2$, an induction proof may be used. The result is clearly valid when $n = 1$, because $1, e^{-x}$ are linearly independent. To begin suppose that the result is valid for a given n. Then consider

$$c_0 + c_1 e^{-x} + c_2 e^{-2x} + \ldots + c_n e^{-nx} + c_{n+1} e^{-(n+1)x} = 0. \quad \text{(B-2)}$$

It is required to show that $c_0 = c_1 = c_2 = \ldots = c_n = c_{n+1} = 0$. First, multiply Equation (B-2) by $e^{(n+1)x}$. Then,

$$c_0 e^{(n+1)x} + c_1 e^{nx} + c_2 e^{(n-1)x} \ldots + c_n e^{x} + c_{n+1} = 0 . \quad \text{(B-3)}$$

Differentiating Equation (B-3) gives

$$c_0(n+1)\ e^{(n+1)x} + c_1(n)\ e^{nx} + c_2(n-1)\ e^{(n-1)x} + \ldots + c_n e^{x} = 0. \quad \text{(B-4)}$$

Multiplying Equation (B-4) by $e^{-(n+1)x}$ gives

$$c_0(n+1) + c_1(n)e^{-x} + c_2(n-1)e^{-2x} + \ldots + c_n e^{-nx} = 0. \quad \text{(B-5)}$$

Therefore, according to the given assumption

$$c_0(n+1) = c_1(n) = \ldots = c_n = 0$$

and hence

$$c_0 = c_1 = \dots = c_n = 0.$$

It then follows from Equation (B-3) that $c_{n+1} = 0$. Thus, it is proved that if the result is valid for a given n, it is also valid for $n+1$. Hence, $1, e^{-x}, e^{-2x}, \dots, e^{-nx}$ form a linearly independent set.

APPENDIX C

LOAD-BENDING STRAIN DATA

Table C-1. Load-Bending Strain Data for b/a = 0.2

LOAD (pounds)	BENDING STRAIN (micro-inch/inch)	LOAD (pounds)	BENDING STRAIN (micro-inch/inch)
0	0	1150	575
100	-37	1200	675
200	-37	1250	770
300	-33	1300	859
350	-30	1350	945
400	-25	1400	1035
450	-19	1450	1120
500	-10	1500	1200
550	- 2	1550	1278
600	5	1600	1356
650	20	1650	1433
700	35	1700	1510
750	55	1750	1580
800	80	1800	1646
850	120	1850	1722
900	165	1900	1785
950	229	1950	1850
1000	301	2000	1920
1050	402		
1100	485		

Table C-2. Load-Bending Strain Data for b/a = 0.4

LOAD (pounds)	BENDING STRAIN (micro-inch/inch)	LOAD (pounds)	BENDING STRAIN (micro-inch/inch)
0	0	1200	355
100	- 7	1250	437
200	-10	1300	525
300	-10	1350	615
400	- 4	1400	710
500	5	1450	805
600	15	1500	895
700	33	1550	990
750	45	1600	1075
800	55	1650	1165
850	73	1700	1250
900	92	1750	1326
950	116	1800	1410
1000	145	1850	1495
1050	185	1900	1566
1100	230	1950	1641
1150	285	2000	1720

Table C-3. Load-Bending Strain Data for b/a = 0.6

LOAD (pounds)	BENDING STRAIN (micro-inch/inch)	LOAD (pounds)	BENDING STRAIN (micro-inch/inch)
0	0	1450	150
100	23	1500	185
200	32	1550	235
300	37	1600	320
400	40	1650	433
500	40	1700	575
600	45	1750	705
700	47	1800	835
800	49	1850	955
900	51	1900	1055
1000	57	1950	1165
1050	61	2000	1265
1100	65	2050	1360
1150	70	2100	1455
1200	75	2150	1545
1250	81	2200	1625
1300	93	2250	1720
1350	105	2300	1780
1400	120	2350	1860
		2400	1940

Table C-4. Load-Bending Strain Data for $b/a = 0.8$

LOAD (pounds)	BENDING STRAIN (micro-inch/inch)	LOAD (pounds)	BENDING STRAIN (micro-inch/inch)
0	0	1700	868
100	-22	1750	958
200	- 6	1800	1048
300	11	1850	1133
400	25	1900	1223
500	38	1950	1328
600	58	2000	1423
700	77	2050	1508
750	88	2100	1603
800	98	2150	1683
850	113	2200	1778
900	128	2250	1873
950	143	2300	1948
1000	160	2350	2036
1050	182	2400	2113
1100	203	2450	2195
1150	231	2500	2273
1200	261	2550	2348
1250	293	2600	2433
1300	339	2650	2507
1350	378	2700	2587
1400	428	2750	2647
1450	479	2800	2724
1500	549	2850	2793
1550	635	2900	2863
1600	713	2950	2938
1650	788	3000	3008

REFERENCES

1. Mansfield, E. H., "On Theoretical Plasticity and Crack Propagation," ARC-CP-688, Aeronautical Research Council, London, 1961.

2. Dixon, J. R. and Strannigan, J. S., "Stress Distribution and Buckling in Thin Sheets with Central Slits," Proceedings of the 2nd International Conference on Fracture, Chapman and Hall, London, 1969, pp. 10/1-10/14.

3. Cherepanov, G. P., "On the Buckling Under Tension of a Membrane Containing Holes," Applied Mathematics and Mechanics (Translation of PMM), Vol. 27, No. 2, 1963, p. 405.

4. Cherepanov, G. P., "On the Solution of Certain Problems with an Unknown Boundary in the Theory of Elasticity and Plasticity," Applied Mathematics and Mechanics (Translation of PMM), Vol. 28, No. 1, 1964, p. 162.

5. Carlson, R. L., Zielsdorff, G., and Harrison, J., "Buckling in Cracked Thin Sheets," Proceedings of the Air Force Conference on Fatigue and Fracture of Aircraft Structures and Materials, AFFDL-TR-70-144, 1970.

6. Forman, R. G., "Experimental Program to Determine Effect of Crack Buckling and Specimen Dimensions on Fracture Toughness of Thin Sheet Materials," AFFDL-TR-65-146, 1965.

7. Walker, E. K., "A Study of the Influence of Geometry on the Strength of Fatigue Cracked Panels," AFFDL-TR-66-92, 1966.

8. Zielsdorff, G., "An Investigation of the Out-of-Plane Deflection Behavior of Thin Sheets with Cutouts in a Tensile Field," Ph.D. Thesis, School of Aerospace Engineering, Georgia Institute of Technology, June 1971.

9. Griffith, A. A., "The Phenomena of Rupture and Flow in Solids," Philosophical Transactions of the Royal Society of London, England, Vol. A221, 1921, p. 165-166.

10. Yoffe, E. H., "The Moving Griffith Crack," Philosophical Magazine, Series 7, Vol. 42, 1951, p. 739.

11. Craggs, J. W., "On the Propagation of a Crack in an Elastic Brittle Material," Journal of the Mechanics and Physics of Solids, Vol. 8, 1960, pp. 66-75.

12. Maue, A. W., "Die entspannungswelle bei plotzlishem einschnitt eines gespannten elastischen korpers," Zeitschrift fur Angewandte Mathematik und Mechanik, Band 34, 1954, pp. 1-12.

13. Ang, D. D., "Some Radiation Problems in Elastodynamics," Dissertation, California Institute of Technology, 1958.

14. Baker, B. R., "Dynamic Stresses Created by a Moving Crack," Journal of Applied Mechanics, Vol. 29, Trans. ASME, Series E, Vol. 84, 1962, pp. 449-454.

15. Wells, A. A. and Post, D., "The Dynamic Stress Distribution Surrounding a Running Crack - a Photoelastic Analysis," Naval Research Laboratory, NRL-4935, Washington, D.C., April 23, 1957.

16. Clebsch, A. and B. de Saint Venant, "Theorie de l'elasticite des corps solides," 1883, p. 689.

17. Biot, M. A., "Increase of Torsional Stiffness of a Prismatical Bar Due to Axial Tension," Journal of Applied Physics, Vol. 10, 1939, pp. 860-864.

18. Goodier, J. N., "Elastic Torsion in the Presence of Initial Axial Stress," Journal of Applied Mechanics, Paper No. 50-APM-4.

19. Biot, M. A., "The Influence of Initial Stress on Elastic Waves," Journal of Applied Physics, Vol. 11, 1940, pp. 522-530.

20. Herrmann, G., "Influence of Initial Stress on the Dynamic Behavior of Elastic and Viscoelastic Plates," Publication of the International Assn. for Bridge and Structural Engineering, Vol. 16, 1956, pp. 275-294.

21. Herrmann, George and Armenakas, A. E., "Vibrations and Stability of Plates Under Initial Stress," Journal of the Engineering Mechanics Division of Proc. of the American Society of Civil Engineers, June 1960, EM3, pp. 65-93.

22. Warburton, G. B., "The Vibration of Rectangular Plates," Proceedings of the Institute of Mechanical Engineers, Vol. 168, 1954, p. 371.

23. Walker, A. C., "Flat Rectangular Plates Subjected to a Linearly Varying Edge Compressive Loading," Thin-walled Structures, edited by A. H. Chilver, John Wiley and Sons, 1967, pp. 208-247.

24. Bolotin, V. V., The Dynamic Stability of Elastic Systems, published by Holden-Day Inc. (Translated from Russian), 1964, pp. 398-400.

25. Washizu, K., "Variational Methods Applied to Free Lateral Vibration of a Plate with Initial Stress," Transactions of Japan Soc. Aeronaut. Space Science, 6, 9, pp. 36-42, 1963.

26. Herrmann, George and Shaw, John, "Vibration of Thin Shells Under Initial Stress," Journal of the Engineering Mechanics Division, Proceedings of the American Society of Civil Engineers. EM5, October, 1965, pp. 37-59.

27. Herrmann, G. and Armenakas, A. E., "Dynamic Behavior on Cylindrical Shells Under Initial Stress," Proceedings, 4th U. S. National Congress of Applied Mechanics, University of California, Berkeley, Calif., 1962, pp. 203-213.

28. Armenakas, A. E., "Influence of Initial Stress on the Vibrations of Simply Supported Circular Cylindrical Shells," AIAA Journal American Institute of Aeronautics and Astronautics, Vol. 2, No. 9, September 1964, pp. 1607-1612.

29. Modi, V. J., "Vibration of a Cylinder with Temperature Gradient Across the Thickness," Canadian Aeronautics and Space Journal, Vol. II, November 7, 1965, pp. 227-233.

30. Ong, C. C. and Herrmann, G., "Vibration of Thin Cylindrical Shells with Initial Stresses Due to Thermal Loadings," AIAA Paper No. 69-59.

31. Pietrusewicz, S.A., "Behavior of a Cracked Plate Under Constant Tensile Stress Subjected to High Intensity Noise," Ph.D. Thesis, University of Southampton, 1963.

32. Clarkson, B. L. and Pietrusewicz, S. A., "The Propagation of Fatigue Cracks by Random Pressures in a Turbulent Boundary Layer," Inst. Sound Vib. Memo. ISAV 104, 1964.

33. Clarkson, B. L., "The Propagation of Fatigue Cracks in a Tensioned Plate Subject to Acoustic Loads," Acoustical Fatigue in Aerospace Structures (ed. W. H. Trapp and D. M. Forney), Syracuse University Press, 1965, pp. 361.

34. Pietrusewicz, S. A., "Further Notes on the Behavior of Plates Under Constant Stress Subjected to High Intensity Noise," Bath University of Technology, Report No. 150, 1969.

35. Pietrusewicz, S.A., "Notes on Further Experiments on Crack Propagation in Tensioned Plates Subjected to High Intensity Noise," Journal of Sound and Vibration, 11, (2), 1970, pp. 235-250.

36. Petyt, M., "The Vibration Characteristics of a Tensioned Plate Containing a Fatigue Crack," Journal of Sound and Vibration, 8, pp. 377, 1968.

37. Jost, G. S., "Combined Stress Crack Propagation in Thin Panels," Proceedings of the 2nd International Conference on Fracture, Brighton, England, April 1969. Reprinted from Fracture, 1969, pp. 745-753.

38. Jost, G. S., "Thin Panel Fracture Surface Striations Formed Under Acoustic Loading," University of Southampton Institute of Sound and Vibration Research Report ISVR-TR-7, July 1968.

39. Jost, G. S., "Fatigue Crack Growth Under Random Combined Stress Conditions," Ph.D. Thesis, University of Southampton, June 1969.

40. Mills, D., "Acoustically Propagated Cracks in Biaxially Tensioned Plates," Ph.D. Thesis, University of Southampton, March 1970.

41. Griffith, A. A., "The Phenomena of Rupture and Flow in Solids," Philosophical Transactions of the Royal Society of London, England, Vol. A221, 1921, pp. 167-171.

42. Irwin, G. R., "Fracture and Fracture Mechanics," University of Illinois, Theoretical and Applied Mechanics Report 202 (1961).

43. Irwin, G. R., "Relation of Stresses Near a Crack to the Crack Extension Force," in 9th International Congress of Applied Mechanics, University of Brussels, Vol. 8, p. 245, 1957.

44. Irwin, G. R. and Kies, J. A., "Fracture and Fracture Dynamics," The Welding Journal, Vol. 31, No. 2, Research Supplement (1952).

45. Irwin, G. R., "Analysis of Stresses and Strains Near the End of a Crack Traversing a Plate," Journal of Applied Mechanics, Vol. 24, Trans. ASME, Vol. 79, 1957, pp. 361-364.

46. Orowan, E., J. West Scot. Iron Steel Inst., 45, 1947, Conference on Fatigue and Fracture of Metals, MIT, June 1950.

47. Felbeck, D. K. and Orowan, E., Welding Journal, New York, Research Supplement, 34, 570S, 1955.

48. Westergaard, H. M., "Bearing Pressures and Cracks," Journal of Applied Mechanics, Vol. 6, June 1939, pp. A49-A53.

49. Paris, P. C., Unpublished Fracture Mechanics notes. (Presented as a short course at the Boeing Airplane Company, Jan-March, 1960).

50. Paris, P. C., Gomez, M. P., and Anderson, W. E., "A Rational Analytical Theory of Fatigue," The Trend in Engineering, Vol. 13, No. 1, pp. 9-14, University of Washington, January 1961.

51. Paris, P. C. and Erdogan, F., "A Critical Analysis of Crack Propagation Laws," Journal of Basic Engineering, Transactions ASME, Series D, Vol. 85, 1963, pp. 528-534.

52. Washizu, Kyuichiro, Variational Methods in Elasticity and Plasticity, Pergamon Press, 1968, pp. 329.

53. Novozhilov, V. V,, The Theory of Thin Shells, Translated by P. G. Lowe, Edited by J.R.M. Radok, Noordhoff Ltd. The Netherlands, 1959, Chap. I.

54. Fung, Y. C., Foundations of Solid Mechanics, Prentice-Hall, Inc. 1965, pp. 338-339.

55. Parkus, Heinz, Thermoelasticity, Blaisdell Publishing Company, 1968, pp. 63-64.

56. Muskhelishvili, N. I., Some Basic Problems of the Mathematical Theory of Elasticity, (Translation by J.R.M. Radok) P. Noordhoff Ltd., Groningen, Holland, 1953.

57. Kolosoff, G. V., "On an Application of Complex Function Theory to a Plane Problem of the Mathematical Theory of Elasticity," (in Russian). Yuriev, 1909.

58. Durelli, A. J., Parks, V. J. and Feng, H. C., "Stresses Around an Elliptical Hole in an Infinite Plate Subjected to Axial Loadings," Journal of Applied Mechanics, Vol. 33, p. 192, 1966. ASME.

59. Milne-Thomson, L. M., Plane Elastic Systems, Springer, Berklin, 1960.

60. Sokolnikoff, I. S., Mathematical Theory of Elasticity, 2nd Edition, McGraw-Hill Book Company, Inc., 1957, Chapter 5.

61. Timoshenko, S. P., Goodier, J. N., Theory of Elasticity, 3rd Edition, McGraw-Hill Book Company, 1970, Chapter 7.

62. Hilderbrand, F. B., Methods of Applied Mathematics, 2nd Edition, Prentice-Hall, Inc., 1965, Section 1.28.

63. Courant, R. and Hilbert, D., Methods of Mathematical Physics, Interscience Publishers, Inc., New York, 1953, pp. 51-54.

64. Agnew, R. P., Differential Equations, 2nd Edition, McGraw-Hill Book Company, Inc., 1960, Section 6.1.

65. Mikhlin, S. G., Approximate Methods for Solution of Differential and Integral Equations, American Elsevier, New York, 1967.

66. Meirovitch, L., Analytical Methods in Vibrations, Macmillan Co., New York, 1967, Chapter 4.

67. Carlson, R. L. and Datta, P. K., "On the Analysis of Plate Stability Experiments," Proceedings of the XIV South American Conference of Structural Engineering and IV Pan American Symposium of Structures, October 1970, Vol. III, pp. 1-33, Buenos Aires, Argentina.

68. Lundquist, E. E., "Generalized Analysis of Experimental Observations in Problems of Elastic Stability," NACA TN-658, 1938.

69. Pellett, D. A., Costello, R. G. and Brock, J. E., "Buckling of a Tension Panel Containing a Circular Hole," AIAA Journal Vol. 6, No. 10, pp. 2012-2014, October 1968.

70. Agnew, R. P., loc. cit. Ref. 64, Section 6.1.

VITA

Prosun Kumar Datta was born in Calcutta, West Bengal, India on March 21, 1947. He attended South Suburban School (Main), Calcutta and graduated with first division in 1963.

He entered Indian Institute of Technology, Kharagpur in 1963 and was awarded the degree of Bachelor of Technology in Aeronautical Engineering with first class honors in 1968.

In September, 1968, Mr. Datta came to the United States of America to enroll in the Graduate Division of the Georgia Institute of Technology, Atlanta, Georgia and was awarded a graduate research assistantship in the School of Aerospace Engineering. He received the degree of Master of Science in Aerospace Engineering in September 1969 and continued his education at the Georgia Institute of Technology by enrolling as a Ph.D. student in the School of Aerospace Engineering.

Mr. Datta co-authored a paper "Analysis of Plate Experiments" published in the proceedings of the XIV South American Conference of Structural Engineers and IV Pan American Symposium of Structures at Buenos Aires, Argentina. He worked extensively in the field of structural stability and structural dynamics while he was employed as a graduate research assistant in the School of Aerospace Engineering. Mr. Datta plans to work as a research and development engineer in the field of Aerospace Engineering.

APPLICATION OF FINITE-STATE INFLOW TO FLAP-LAG-TORSION DAMPING IN HOVER

A THESIS

Presented to

The Faculty of the Division of Graduate Studies

by

Donizeti de Andrade

In Partial Fulfillment

of the Requirements for the Degree of

Doctor of Philosophy

in the School of Aerospace Engineering

Georgia Institute of Technology

May 8, 1992